

A large, abstract sculpture made of stacked, angular, metallic-looking plates or sheets of material. The plates are arranged in a way that suggests a spiral or a series of steps, with some plates pointing upwards and others downwards. The sculpture is set against a bright blue sky with scattered white and grey clouds. The lighting creates strong highlights and shadows on the metallic surfaces, emphasizing their texture and form.

Towards personalized therapy for metastatic prostate cancer: technical validation of [^{18}F] fluoromethylcholine

Daniela-Elena Oprea-Lager

Towards personalized therapy for metastatic prostate cancer: technical validation of [¹⁸F]fluoromethylcholine

Daniela-Elena Oprea-Lager

© 2016 Daniela-Elena Oprea-Lager

ISBN: 978-90-6464-956-1

The printing of this thesis was financially supported by Bayer HealthCare B.V., Sanofi Nederland and BV Cyclotron VU.

Lay-out: Ferdinand van Nispen tot Pannerden Citroenvlinder D.T.P & Vormgeving,
my-thesis.nl, Bilthoven

Printed by: GVO drukkers en vormgevers B.V., Ede

VRIJE UNIVERSITEIT

**Towards personalized therapy
for metastatic prostate cancer:
technical validation of [¹⁸F]fluoromethylcholine**

ACADEMISCH PROEFSCHRIFT

ter verkrijging van de graad Doctor aan
de Vrije Universiteit Amsterdam,
op gezag van de rector magnificus
prof.dr. V. Subramaniam,
in het openbaar te verdedigen
ten overstaan van de promotiecommissie
van de Faculteit der Geneeskunde
op dinsdag 16 februari 2016 om 13.45 uur
in de aula van de universiteit,
De Boelelaan 1105

door

Daniela-Elena Oprea-Lager

geboren te Brasov, Roemenië

promotoren: prof.dr. O.S. Hoekstra
prof.dr. R.J.A. van Moorselaar

leescommisie: prof.dr. J.J.J.M. van der Hoeven
prof.dr. I.J. de Jong
prof.dr. J.J.M.C.H. de la Rosette
prof.dr. P.L. Jager
dr. C.W. Menke-van der Houven van Oordt
dr. W.V. Vogel

paranimfen: drs. J. van Dodewaard-de Jong
drs. K.M. Duvivier

Aan mijn ouders (Parintilor mei)

CONTENTS

CHAPTER 1	Introduction and outline	11
CHAPTER 2	Dual-phase PET/CT to differentiate [¹⁸ F]fluoromethylcholine uptake in reactive and malignant lymph nodes in patients with prostate cancer PLoS One. 2012;7(10):e48430	25
CHAPTER 3	[¹⁸ F]fluoromethylcholine as a chemotherapy response read-out in prostate cancer cells Mol Imaging Biol. 2015;17(3):319–327	45
CHAPTER 4	Quantification of [¹⁸ F]fluoromethylcholine kinetics in patients with prostate cancer J Nucl Med. 2015;56(3):365–371	63
CHAPTER 5	Repeatability of quantitative [¹⁸ F]fluoromethylcholine PET/CT measurements in prostate cancer Manuscript accepted for publication in J Nucl Med	87
CHAPTER 6	A clinical and experimental comparison of time of flight PET/ MRI and PET/CT systems Mol Imaging Biol. 2015;17(5):714–725	111
CHAPTER 7	General discussion, synthesis and perspectives	137
ADDENDUM	List of abbreviations	152
	Dutch summary – Nederlandse samenvatting	155
	Acknowledgments – Dankwoord	163
	Curriculum vitae	173
	List of publications	175



CHAPTER 1

Introduction and outline of the thesis

Prostate cancer

Prostate cancer (PC) is the second most common cancer in men worldwide [1]. The disease presents itself mostly in men above the age of 50 and the incidence increases with age. The clinical behavior of PC is very diverse. Some tumors are indolent, do not cause any symptoms and arise as microscopic, well-differentiated foci that may never become clinically manifest. However, a significant proportion of PC patients presents with or will develop aggressive tumors that lead to morbidity, metastases and ultimately to death. The estimated incidence of PC in Europe in 2012 was 417,000, with 92,000 death reported. [2]. Recurrence in patients with PC is common during the first decade after treatment with curative intent, including radical prostatectomy (RP), brachytherapy or external radiotherapy. Cancer specific survival (CSS) at 10-years follow-up after RP is 84-90%, while post external radiotherapy the CSS vary between 77-95% [3].

The initial systemic treatment in metastatic PC is based on androgen deprivation. Nevertheless, after an initial response to anti-hormonal therapy, the majority of PC patients will ultimately progress and reach a castration-resistant (CR) state. Progression towards castration-resistant prostate cancer (CRPC) is common within 18-36 months [3]. In these patients, chemotherapy has proven to slow down androgen independent tumor growth. In particular, docetaxel, a registered agent from the taxane class, was introduced as first-line chemotherapy [4]. Its effect is largely based on interaction with microtubules [5]. Docetaxel plus estramustine or prednisone was found to significantly reduce the prostate-specific antigen (PSA) value and improve overall survival when compared to mitoxantrone-prednisone therapy. In combination with prednisone, docetaxel also appeared to be useful in achieving significant improvement of pain palliation and quality of life [4, 6]. These clinical results have resulted in the regimen of docetaxel and prednisone once every three weeks becoming the current recognized standard chemotherapeutic treatment of CRPC [6].

Although these successes with docetaxel have improved clinical outcome of PC, the progressive development of chemotherapy resistance in PC remains a major problem and new chemotherapeutic agents that circumvent resistance are urgently needed. Cabazitaxel is found to be such an agent, being accepted as the second-line cytotoxic modality in metastatic CRPC. Its role is based on the possibility of exerting antitumor activity on docetaxel-resistant neoplasms [7, 8]. Clinical studies, including

the phase III trial on the treatment of hormone-refractory metastatic PC previously treated with docetaxel-containing regimen (TROPIC study), demonstrated a 30% reduced risk of death, associated with a prolonged survival up to 2.4 months [7, 9], in favor of cabazitaxel-prednisone versus mitoxantrone-prednisone. Currently, cabazitaxel-prednisone is the only chemotherapeutic option with demonstrated survival advantage for the treatment of patients with metastatic CRPC who have progressed under docetaxel-based chemotherapy [9, 10].

In the beginning of this decennium, molecular profiling studies have improved the knowledge about the heterogeneous biological behavior of PC. It was found that even in the presence of a castrate range <1.7 nmol/L of testosterone in the blood of CRPC patients, a proportion of these tumors remains dependent on androgen-receptor (AR) signaling for growth [11]. Five potential mechanisms of development of CRPC were described, based on ligand and AR dependence [12]. Series of progressive changes in intracellular AR signaling in CRPC in comparison to newly diagnosed (untreated) tumors were identified and validated, with AR overexpression being the most frequently identified phenotype [11]. Based on these observations, a multitude of therapeutic options against CRPC was recently proposed, including agents that interfere with androgenic stimulation of tumor growth (e.g., abiraterone, enzalutamide) [13–16] in as well as pre- or post- chemotherapy settings, immunotherapy (sipuleucel-T) [17], and bone-seeking radiopharmaceuticals (e.g., Radium-223 [18]). An example of a patient with metastatic CRPC, demonstrating AR overexpression and a good response on Enzalutamide is presented in Figure 1.

Abiraterone acetate inhibits androgen biosynthesis by irreversibly blocking CYP17, an essential enzyme in testosterone and estrogen synthesis [13]. When combined with low-dose prednisone, Abiraterone improves survival of patients with CRPC [13, 14]. Enzalutamide is an antiandrogen agent with demonstrated potential to inhibit nuclear translocation of the AR and DNA binding. Double-blind, phase III studies have demonstrated Enzalutamide to significantly prolong the survival of men with metastatic CRPC after chemotherapy [15], but also to significantly decrease the risk of disease progression and death, and to delay the initiation of chemotherapy in men with metastatic PC [16]. Sipuleucel-T is an active cellular immunotherapeutic which prolongs survival among men with asymptomatic or minimally symptomatic metastatic CRPC [17]. Radium-223 dichloride is an alpha emitter which selectively binds to areas of increased bone turnover in metastatic lesions. The emitted high-

energy alpha particles with short range radiation induce double-stranded DNA breaks, resulting in a highly localized cytotoxic effect in the target areas [18].

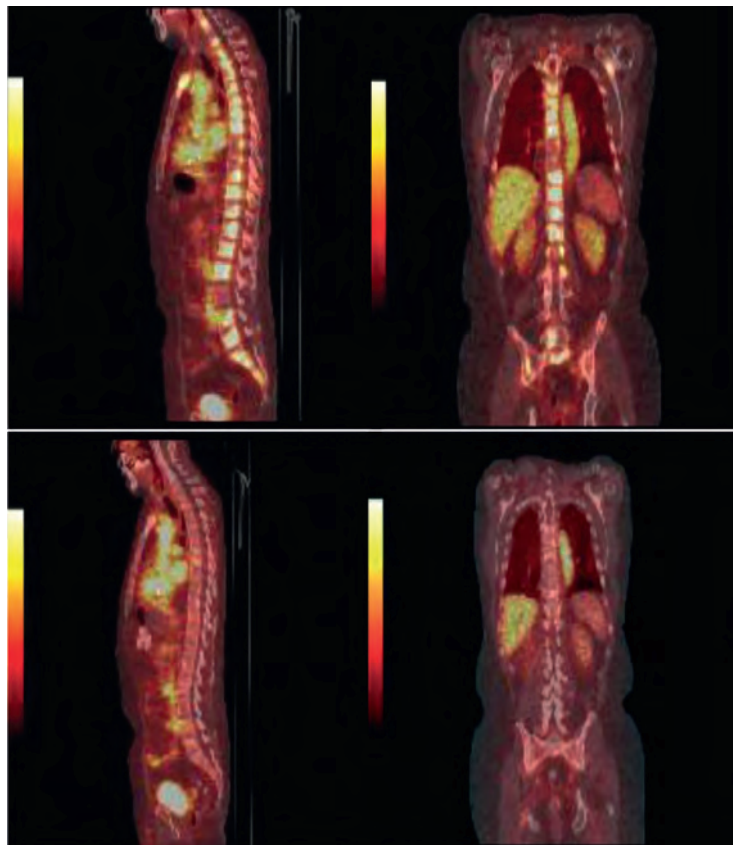


Figure 1. Patient with CRPC, before and after therapy with Enzalutamide (MDV3100). (Illustration reproduced with permission from Scher et al., Ref. 11).

Sagittal and coronal views of two PET scans, 1 h after administration of 16β -18F-fluoro-5 α -dihydrotestosterone (FDHT), in the same patient with CRPC, are presented. The top row shows the fused PET/CT images at baseline and the bottom row the fused PET/CT scan 4 weeks after treatment with Enzalutamide. Both the sagittal and coronal images, at baseline and 4 weeks after start of Enzalutamide therapy, show a reduction in FDHT accumulation in the tumor within the vertebrae, compared with the cardiac and aortic blood pool, in which FDHT metabolites circulate bound to serum proteins.

However, despite the variety of therapeutic options, proper sequencing (e.g., modality, timing) in individual patients with PC is unclear. Furthermore, the economic impact of these therapies has to be taken into account, due to the relatively high costs. To this end, it is essential, both from an ethical and an economical perspective, to opt for tailored therapies. This means developing “instruments” able to identify which phenotype

is predominant within individual PC patients and timely evaluating the response to therapy, thus avoiding futile costly and toxic treatments.

Role of imaging in prostate cancer

Accurate diagnostic “instruments” in PC are essential, since therapeutic options vary greatly with stage and grade of the disease, specific patterns of metastatic spread (i.e., hematogeneous and/ or lymphatic) and dominant phenotype [19, 20]. Conventional imaging techniques, including transrectal ultrasound, computed tomography (CT) and magnetic resonance imaging (MRI), are used routinely in PC, but their diagnostic accuracy is suboptimal [21]. Multimodality imaging has improved patient care over the past decade. Non-invasive, integrated positron emission tomography/ computed tomography (PET/CT) has proven to be a valuable diagnostic tool by combining *in vivo* metabolic and anatomic information [22]. PET/CT is used extensively in oncology for diagnosis, initial staging, restaging, therapy planning, and response monitoring of a variety of malignancies [23, 24].

PET is a functional imaging technique based on the detection of coincident photons originating from the annihilation of emitted positrons with electrons from adjacent tissues. PET uses radiotracers, which are biomolecules labeled with neutron-deficient nuclei (i.e., positron emitters). Before and upon intravenous administration of a standard dose radiotracer to the patient, the radioisotope decays, emitting a positron. After traveling a short path (1-2 mm) in tissue, the positron will annihilate with an electron, generating two 511 keV photons, which are emitted in opposite direction. PET detectors register the annihilation photons in coincidence. The spatial distribution of the radiotracer is obtained through the acquisition, storage, corrections (e.g., for the attenuation, scatter, normalization) and finally reconstruction of the emission images [25].

In an attempt to achieve accurate registration of the anatomical and functional images, the first combined PET/CT imaging system was introduced in 1998. The dual modality offers several potential advantages above the conventional imaging techniques. First of all, it fulfills a supplementary and complementary role. PET allows visualization of increased uptake of the tracer in areas which are (in)compatible with physiological biodistribution. CT, on the other hand, enables the exact localization of these areas

and helps to increase the specificity of PET, by identifying benign causes for enhanced tracer uptake. Secondly, the (low-dose) CT data generate an attenuation map to correct PET data, thus improving the visual quality and quantitative accuracy of the correlated acquisitions. Nowadays, fully three-dimensional PET/CT systems are state of the art, with time-of-flight (TOF) capability (i.e., high resolution allowing the exact calculation of the location of the photon's events) which improves the signal to noise ratio [26].

PET is an extremely sensitive imaging modality for which only small amounts of radiolabelled molecules (tracers, ~nM) need to be injected. The measurement of the tracer distribution allows for quantitative assessment of tissue function without affecting the underlying physiology [27]. Appropriate quantification of a new radiopharmaceutical requires kinetic modeling. This implies dynamic PET scanning starting at injection of the tracer and arterial blood sampling (to acquire the arterial input function and to measure potential tracer metabolites). With current PET scanners, the field of view of such dynamic scans is limited to about 15-25 cm. However, hybrid imaging techniques (e.g., PET/CT, PET/MRI) using new specific tracers might enable a quantitative assessment of response in metastatic sites (e.g., in lymph nodes and bone), using a single, non-invasive scan procedure, in a whole body (WB) setting. Acquisitions in WB setting are essential in the context of malignancy, since these allow characterizing all possible metastatic lesions in the body.

The quantitative approach, although reliable, is technically demanding. For clinical practice it is important to develop simple and accurate quantitative methods, which are complementary to visual image interpretation, thus minimizing the interobserver variability [28]. PET data analysis methods can be divided in three major groups:

1. qualitative analysis or visual assessment,
2. semi-quantitative analysis, including standardized uptake value (SUV) and lesion-to-background ratio, and
3. absolute quantitative analysis, including (a) nonlinear regression (NLR), (b) Patlak graphical analysis and (c) simplified quantitative methods.

Visual, qualitative assessment of the attenuated and non-attenuated PET images is the basis of any PET study interpretation. A pathological [¹⁸F]fluoromethylcholine ([¹⁸F]FCH) avid lesion is defined as a focus with higher choline uptake than the surrounding background, incompatible with accumulation in a physiological site. The major concern regarding this assessment is the significant inter- and intra-observer variability of PET image interpretation [28].

SUV is the most popular PET semi-quantitative index in the Nuclear Medicine field [28]. It provides a measure of radiotracer metabolism and is defined as the tissue concentration of tracer, as measured by PET, divided by the injected dose, normalized to patient weight, multiplied by a decay factor. SUV estimation is a semi-automated procedure, being readily calculated with current software available by the PET scanners. Moreover, SUV is a function of several factors such as: time interval between intravenous administration of the tracer and image acquisition, residual activity in the syringe/ infusion system, decay of the injected dose and partial volume effects [31]. However, standardization of procedures is required and yet only available for [¹⁸F]fluorodeoxyglucose ([¹⁸F]FDG) [29].

NLR analysis employs the estimation of the net rate of tracer influx (Ki) from dynamic PET data and a standard two or more tissue compartment models, based on arterial input function. It represents a quantitative method with the advantage of being independent of uptake period, by also providing insight into various rate constants [28].

Patlak graphical analysis expresses the regional concentration of a tracer at time t after injection. It is more robust than NLR method, but has the same disadvantage of dynamic scanning, which makes its implementation complex for clinical practice.

Simplified kinetic method requires a single static scan and few venous blood samples during the scan acquisition. The samples are further needed to scale a population – derived average plasma curve. The method has the advantage of estimating tracer metabolism without dynamic scanning and with a reduced blood sampling protocol. However, it implies validation in a large patient population sample [28].

Only a decade after the successful implementation of PET/CT, integration of PET with magnetic resonance imaging (PET/MRI) was introduced as the next hybrid imaging option. Strengths of MRI include its high soft tissue contrast, high spatial resolution, and lack of exposure to ionizing radiation. Since these two modalities (i.e., PET and MRI) are not easily combined in a single scanner, the design has taken years of technical research. Several hybrid PET/MRI systems are currently available clinically: an integrated system housing both components in a single gantry, or a geometrically separated PET and MRI on either side of a rotating table [30]. The former has the obvious advantage of truly simultaneous image acquisition, and the latter does not require any concession for either component, being also equipped with time of flight (TF) capability.

Whilst in the case of PET/CT, the merged modality quickly found its way in routine daily practice, PET/MRI is facing a number of technical challenges (e.g., presence of well-controlled magnetic and radio frequency fields; accurate MR-based attenuation correction maps) that never were an issue for PET/CT [27]. These issues require a high level of multidisciplinary collaboration in order to capitalize the full multiparametric potential of PET/MRI. However, the current challenge is to make PET/MRI suitable for clinical practice. Current clinical applications with PET/MRI are still in their infancy.

Radiolabeled choline

The complex and heterogeneous biology of PC poses major challenges and opportunities. The implementation of performant PET hard- and soft-ware, together with the advances in the molecular biology of PC, offer possibility for development of new imaging biomarkers and promising radiotracers. For multimodality imaging techniques (e.g., PET/CT, PET/MRI) several radiopharmaceuticals are available to detect and quantitate physiologic and metabolic pathways. The most commonly used oncological PET tracer, $[^{18}\text{F}]$ FDG, shows limited sensitivity for the detection of androgen dependent PC [31]. In contrast, encouraging results have been reported on the use of both ^{11}C and ^{18}F labeled choline derivates as PET tracers for PC [32–36].

The amino acid choline is an important precursor for the biosynthesis of phosphatidylcholine, a key component of the cell membrane phospholipids. Following transport into the cell, choline is phosphorylated by choline kinase to phosphocholine and trapped within the cell [37]. Most types of cancer, including PC, are characterized by increased choline transport and over-expression of choline kinase, in response to enhanced demand of phosphatidylcholine in highly proliferating cells [21, 38]. Because of its longer half-life (110 versus 20 minutes) and better spatial resolution due to the shorter positron range of ^{18}F , $[^{18}\text{F}]$ FCH seems to be more convenient for routine clinical use than ^{11}C -labeled choline [39]. Normal biodistribution of $[^{18}\text{F}]$ FCH shows relatively high uptake in the salivary glands, pancreas, liver, spleen, and kidneys; variable uptake in the bowel; and excretion into urine [40].

Since the uptake of $[^{18}\text{F}]$ FCH overlaps among normal, benign, and malignant prostate tissues [41], there are mixed results, with the potential utility of this radiotracer in the diagnosis and staging of primary PC [42]. At present, $[^{18}\text{F}]$ FCH is used mainly for

restaging of PC in case of biochemical relapse, with a diagnostic performance that appears to improve with increasing PSA level, although it is not recommended for routine use when the PSA level is less than 1 ng/mL [36]. A systematic review and meta-analysis [43] on the role of choline PET or PET/CT by biochemical relapse of PC showed a pooled sensitivity and specificity to identify all recurrent/ metastatic localizations (prostatic region, bone, or lymph node) of 86% (95% CI 83–88%) and 93% (95% CI 90–95%), respectively.

If uptake of radiolabeled choline would reflect viable tumor tissue, changes over time of the choline signal might serve as a measure of response to therapy. For monitoring response to systemic treatment in metastasized PC, however, accurate quantification is required. To date, [¹⁸F]FCH biodistribution and radiation dosimetry have been studied [40, 44–46], but full kinetic analysis has not yet been reported.

Response evaluation and prediction in prostate cancer

The actual response to (chemo)therapeutic regimens in individual PC patients is variable. It is important to monitor therapeutic (in)efficacy in time, to prevent patients from undergoing futile and expensive therapy for too long, since alternative and potentially effective drugs are available. Presently, monitoring of progression is based on a response metrics construct requiring various diagnostic tests, including PSA measurement, CT and bone scintigraphy [47]. The limitations of the current approach are related to the heterogeneity of metastasized PC (i.e., coexistence of androgen sensitive and insensitive components with different impact on e.g., PSA [48]) and to its skeletal predominance (with bone- and CT-scans having difficulties in timely and accurately detecting response). Therefore, there is a clear need for alternative and more accurate response monitoring methods [49–51].

With each new radiopharmaceutical the challenge is to validate reliable simplified quantitative procedures, applicable in daily clinical practice, in WB setting. Whether [¹⁸F]FCH could also be employed in monitoring treatment response in PC patients receiving docetaxel and cabazitaxel therapy is unclear. Definitive data from clinical studies have not yet become available. Nevertheless, experiments in-vitro have shown promising results on the use of PET tracers to monitor anti-androgen treatment or chemotherapy [52, 53].

Summarizing, PET imaging is a promising approach, both in clinical and research applications. PET allows for quantitative measurements with high sensitivity, yielding non-invasive information about biological processes through the body. Standard methods of PET quantification are difficult to implement in daily clinical practice. Simplified methods of quantification are available but should be validated versus the standard methods. To distinguish biological change from noise, repeatability of a tracer should be known. Due to the increasing role of [¹⁸F]FCH PET in PC, clinically feasible protocols, based on reliable and repeatable indices characterizing tumor activity, are essential for monitoring response to therapy. Complex quantitative analysis methods are likely to become widely available in clinical setting. This enhances the potential of radiolabeled choline PET to “tailor” treatment by timely evaluating the effectiveness of therapy, thus avoiding ineffective, costly or risky treatments.

Outline of this thesis

The aim of the present thesis was to investigate the role of [¹⁸F]FCH as a potential response evaluation tool in patients with prostate cancer.

In **chapter two** we studied the diagnostic role of dual-phase [¹⁸F]FCH PET/CT in a clinical setting. Therefore, we analyzed whether time-trends of enhanced [¹⁸F]FCH in lymph nodes of PC patients can help to discriminate reactive from malignant ones, and whether single time point SUV measurements may also suffice.

In **chapter three** we studied an alternative potential application of [¹⁸F]FCH in metastatic PC. In this context, we investigated whether uptake of [¹⁸F]FCH, in comparison with [¹⁸F]FDG, accurately reflects chemotherapy efficacy at the tumor cell level in PC.

In **chapter four** we investigated how [¹⁸F]FCH can be reliably measured in a routine clinical setting. For this purpose, pharmacokinetic modeling of dynamic PET data in combination with arterial blood sampling was used to determine the appropriate plasma input compartment model for [¹⁸F]FCH. In addition, the validity of using simplified methods for quantification of [¹⁸F]FCH was assessed.

In **chapter five** we investigated whether the simplified methods for [¹⁸F]FCH uptake measuring, as proposed in chapter four, are repeatable in daily practice. For this purpose, we assessed repeatability of various quantitative [¹⁸F]FCH parameters in PC, also including metabolic tumor volume and total lesion choline uptake.

In **chapter six** we performed a clinical and technical validation of [¹⁸F]FCH in PC. Therefore, we compared image quality and quantitative accuracy of PET/MRI and PET/CT systems with identical TF PET gantries, using phantom and clinical studies.

In **chapter seven** results are generally discussed and summarized, including the perspectives.

REFERENCES

1. Jemal A, Bray F, Center MM, et al. Global cancer statistics. *CA Cancer J Clin.* 2011;61:69–90
2. Ferlay J, Steliarova-Foucher, Lortet-Tieulent J, et al. Cancer incidence and mortality patterns in Europe: estimates of 40 countries in 2012. *Eur J Cancer.* 2013;49:1374–1403
3. Mottet N, Bellmunt J, Briers E, et al. EAU guidelines on prostate cancer. 2015; http://uroweb.org/wp-content/uploads/09-Prostate-Cancer_LR.pdf
4. Petrylak DP, Tangen CM, Hussain MH, et al. Docetaxel and estramustine compared with mitoxantrone and prednisone for advanced refractory prostate cancer. *N Engl J Med.* 2004;351:1513–1520
5. Michielsen DP, Braeckman JG and Denis L. Cabazitaxel for the treatment of prostate cancer. *Expert Opin Pharmacother.* 2011;12:977–982
6. Tannock IF, De Wit R, Berry WR, et al. Docetaxel plus prednisone or mitoxantrone plus prednisone for advanced prostate cancer. *N Engl J Med.* 2004;351:1502–1512
7. de Bono JS, Oudard S, Ozguroglu M, et al. Prednisone plus cabazitaxel or mitoxantrone for metastatic castration-resistant prostate cancer progressing after docetaxel treatment: a randomised open-label trial. *Lancet.* 2010;376:1147–1154
8. Paller CJ and Antonarakis ES. Cabazitaxel: A novel second-line treatment for metastatic castration-resistant prostate cancer. *Drug Des Devel Ther.* 2011;5:117–124
9. Parente P, Parnis F and Curney H. Emerging and second line therapies for the management of metastatic castration-resistant prostate cancer: The Australian perspective. *Asia-Pac J Clin Oncol.* 2012;8:31–42
10. Higano CS and Crawford ED. New and emerging agents for the treatment of castration-resistant prostate cancer. *Urol Oncol.* 2011;29(6 Suppl):S1–S8
11. Scher HI, Beer TM, Higano CS, et al. Antitumour activity of MDV3100 in castration-resistant prostate cancer: a phase 1–2 study. *Lancet.* 2010;75:1437–1446
12. Feldman BJ and Feldman D. The development of androgen-independent prostate cancer. *Nature Rev Cancer.* 2001;1:34–45
13. Fizazi K, Scher HI, Molina A, et al. Abiraterone acetate for treatment of metastatic castration-resistant prostate cancer: final overall survival analysis of the COU-AA-301 randomised, double-blind, placebo-controlled phase 3 study. *Lancet Oncol.* 2012;13:983–992
14. Ryan CJ, Smith MR, de Bono JS, et al. Abiraterone in metastatic prostate cancer without previous chemotherapy. *N Engl J Med.* 2013;368:138–148
15. Scher HI, Fizazi K, Saad F, et al. Increased survival with enzalutamide in prostate cancer after chemotherapy. *N Engl J Med.* 2012;367:1187–1197
16. Beer TM, Armstrong AJ, Rathkoph DE, et al. Enzalutamide in metastatic prostate cancer before chemotherapy. *N Engl J Med.* 2014;371:424–433
17. Kantoff PW, Higano CS, Shore ND, et al. Sipuleucel-T immunotherapy for castration-resistant prostate cancer. *N Engl J Med.* 2010;363:411–422
18. Parker C, Nilsson S, Heinrich D, et al. Alpha emitter radium-223 and survival in metastatic prostate cancer. *N Engl J Med.* 2013;369:213–223
19. Bray F, Lortet-Tieulent J, Ferlay J, et al. Prostate cancer incidence and mortality trends in 37 European countries: an overview. *Eur J Cancer.* 2010;46:3040–3052
20. Heidenreich A, Bastian PJ, Bellmunt J, et al. EAU guidelines on prostate cancer. Part 1: screening, diagnosis, and local treatment with curative intent-update 2013. *Eur Urol.* 2014;65:124–137
21. Schwarzenböck S, Souvatzoglou M and Krause BJ. Choline PET and PET/CT in primary diagnosis and staging of prostate cancer. *Theranostics.* 2012;2:318–330
22. Schiepers C and Dahlbom M. Molecular imaging in oncology: the acceptance of PET/CT and the emergence of MR/PET imaging. *Eur Radiol.* 2011;21:548–554
23. Fletcher JW, Djulbegovic B, Soares HP, et al. Recommendations on the use of ¹⁸F-FDG PET in oncology. *J Nucl Med.* 2008;49:480–508
24. Juweid ME, Stroobants S, Hoekstra OS, et al. Use of positron emission tomography for response assessment of lymphoma: consensus of the Imaging Subcommittee of International Harmonization Project in Lymphoma. *J Clin Oncol.* 2007;25:571–578
25. Lonsdale MN and Beyer T. Dual-modality PET/CT instrumentation – Today and tomorrow. *Eur J Radiol.* 2010;73:452–460
26. Zaidi H and Alavi A. Current trends in PET and combined (PET/CT and PET/MR) systems design. *PET Clin.* 2007;109–123

27. Yaqub M, Oprea-Lager DE, Hofman M and Boellaard R. Methodological aspects of PET/MR imaging. *Tijdschr v Nucl Geneesk.* 2013;35:1153–1159

28. Basu S, Zaidi H and Alavi A. Clinical and research applications of quantitative PET imaging. *PET Clin.* 2007;161–172

29. Boellaard R, Delgado-Bolton R, Oyen WJ, et al. FDG PET/CT: EANM procedure guidelines for tumour imaging: version 2.0. *Eur J Nucl Med Mol Imaging.* 2015; 42:328–354

30. Jadvar H and Colletti PM. Competitive advantage of PET/MRI. *Eur J Radiol.* 2013;doi:10.1016/j.ejrad.2013.05.028

31. Price DT, Coleman RE, Liao RP, et al. Comparison of [¹⁸F]fluorocholine and [¹⁸F]fluorodeoxyglucose for positron emission tomography of androgen dependent and androgen independent prostate cancer. *J Urol.* 2002;168:273–280

32. Bauman G, Belhocine T, Kovacs M, et al. ¹⁸F-fluorocholine for prostate cancer imaging: a systematic review of the literature. *Prostate Cancer Prostatic Dis.* 2012;15:45–55

33. DeGrado TR, Baldwin SW, Wang S, et al. Synthesis and evaluation of (¹⁸F)-labeled choline analogs as oncologic PET tracers. *J Nucl Med.* 2001;42:1805–1814

34. Fuccio C, Rubello D, Castellucci P, et al. Choline PET/CT for prostate cancer: main clinical applications. *Eur J Radiol.* 2011;80:e50–e56

35. Picchio M, Briganti A, Fanti S, et al. The role of choline positron emission tomography/computed tomography in the management of patients with prostate-specific antigen progression after radical treatment of prostate cancer. *Eur Urol.* 2011;59:51–60

36. Reske SN, Blumstein NM, Neumaier B, et al. Imaging prostate cancer with ¹¹C-choline PET/CT. *J Nucl Med.* 2006;47:1249–1254

37. Roivainen A, Forsback S, Gronroos T, et al. Blood metabolism of [methyl-¹¹C]choline; implications for in vivo imaging with positron emission tomography. *Eur J Nucl Med.* 2000;27:25–32

38. Sutinen E, Nurmi M, Roivainen A, et al. Kinetics of [¹¹C]choline uptake in prostate cancer: a PET study. *Eur J Nucl Med Mol Imaging.* 2004;31:317–324

39. Jadvar H. Prostate cancer: PET with ¹⁸F-FDG, ¹⁸F- or ¹¹C-acetate, and ¹⁸F- or ¹¹C-choline. *J Nucl Med.* 2011;52:81–89

40. Uusijarvi H, Nilsson LE, Bjartell A and Mattsson S. Biokinetics of ¹⁸F-choline studied in four prostate cancer patients. *Radiat Prot Dosimetry.* 2010;139:240–244

41. Igerc I, Kohlfürst S, Gallowitsch HJ, et al. The value of ¹⁸F-choline PET/CT in patients with elevated PSA-level and negative prostate needle biopsy for localization of prostate cancer. *Eur J Nucl Med Mol Imaging.* 2008;35:976–983

42. Kwee SA, Coel MN, Lim J and Ko JP. Prostate cancer localization with ¹⁸fluorine fluorocholine positron emission tomography. *J Urol.* 2005;173:252–255

43. Evangelista L, Zattoni F, Guttilla A, et al. Choline PET or PET/CT and biochemical relapse of prostate cancer—a systematic review and meta-analysis. *Clin Nucl Med.* 2013;38:305–314

44. DeGrado TR, Reiman RE, Price DT, et al. Pharmacokinetics and radiation dosimetry of ¹⁸F-fluorocholine. *J Nucl Med.* 2002;43:92–96

45. Verwer EE, Oprea-Lager DE, van den Eertwegh AJ, et al. Quantification of ¹⁸F-fluorocholine kinetics in patients with prostate cancer. *J Nucl Med.* 2015;56:365–371

46. Tavola F, Janzen T, Giussani A, et al. Nonlinear compartmental model of ¹⁸F-choline. *Nucl Med Biol.* 2012;39:261–268

47. Scher HI, Morris MJ, Basch E and Heller G. End points and outcomes in castration-resistant prostate cancer: from clinical trials to clinical practice. *J Clin Oncol.* 2011;29:3695–3704

48. Lilja H, Ulmert D and Vickers AJ. Prostate-specific antigen and prostate cancer: prediction, detection and monitoring. *Nat Rev Cancer.* 2008;8:268–278

49. Wahl RL, Jacene H, Kasamon Y and Lodge MA. From RECIST to PERCIST: Evolving Considerations for PET response criteria in solid tumors. *J Nucl Med.* 2009;50 (Suppl 1):122S–150S

50. Costelloe CM, Chuang HH, Madewell JE and Ueno NT. Cancer response criteria and bone metastases: RECIST 1.1, MDA and PERCIST. *J Cancer.* 2010;1:80–92

51. Wallace TJ, Torre T, Grob M, et al. Current approaches, challenges and future directions for monitoring treatment response in prostate cancer. *J Cancer.* 2014;5:3–24

52. Müller SA, Holzapfel K, Seidl C, et al. Characterization of choline uptake in prostate cancer cells following bicalutamide and docetaxel treatment. *Eur J Nucl Med Mol Imaging.* 2009;36:1434–1442

53. Oprea-Lager DE, van Kanten MP, van Moorselaar RJ, et al. [¹⁸F]fluoromethylcholine as a chemotherapy response read-out in prostate cancer cells. *Mol Imaging Biol.* 2015;17:319–327



CHAPTER 2

Dual-phase PET/CT to differentiate [¹⁸F]fluoromethylcholine uptake in reactive and malignant lymph nodes in patients with prostate cancer

Daniela E. Oprea-Lager¹

Andrew D. Vincent²

Reindert J.A. van Moorselaar³

Winald R. Gerritsen^{4,5}

Alfons J.M. van den Eertwegh⁵

Jonas Eriksson^{1,6}

Ronald Boellaard¹

Otto S. Hoekstra¹

¹Department of Radiology and Nuclear Medicine, VU University Medical Center, Amsterdam, the Netherlands

²Department of Biometrics, Antoni van Leeuwenhoek Hospital, The Netherlands Cancer Institute, Amsterdam, the Netherlands

³Department of Urology, VU University Medical Center, Amsterdam, the Netherlands

⁴ Department of Oncology, St Radboud University Medical Center, Nijmegen, the Netherlands

⁵Department of Medical Oncology, VU University Medical Center, Amsterdam, the Netherlands

⁶ Department of Medicinal Chemistry, Organic Pharmaceutical Chemistry, Uppsala University, P.O. Box 256, SE-751 05 Uppsala, Sweden

ABSTRACT

PURPOSE

The purpose of this study was to investigate whether time-trends of enhanced [¹⁸F]fluoromethylcholine ([¹⁸F]FCH) in lymph nodes (LN) of prostate cancer (PC) patients can help to discriminate reactive from malignant ones, and whether single time point standardized uptake value (SUV) measurements also suffice.

METHODS

25 PC patients with inguinal (presumed benign) and enlarged pelvic LN (presumed malignant) showing enhanced [¹⁸F]FCH uptake at dual-phase PET/CT were analyzed. Associations between LN status (benign versus malignant) and SUV_{max} and $SUV_{meanA50}$, determined at 2 min (early) and 30 min (late) post injection (p.i.), were assessed. We considered two time-trends of [¹⁸F]FCH uptake: type A ($SUV_{early} > SUV_{late}$) and type B ($SUV_{late} \geq SUV_{early}$). Histopathology and/or follow-up were used to confirm the assumption that LN with type A pattern are benign, and LN with type B pattern malignant.

RESULTS

Analysis of 54 nodes showed that LN status, time-trends, and 'late' (30 min p.i.) SUV_{max} and $SUV_{meanA50}$ parameters were strongly associated ($P < 0.0001$). SUV_{max} relative difference was the best LN status predictor. All but one inguinal LN showed a decreasing [¹⁸F]FCH uptake over time (pattern A), while 95% of the pelvic nodes presented a stable or increasing uptake (pattern B) type.

CONCLUSION

Time-trends of enhanced [¹⁸F]FCH uptake can help to characterize lymph nodes in prostate cancer patients. Single time-point SUV measurements, 30 min p.i., may be a reasonable alternative for predicting benign versus malignant status of lymph nodes, but this remains to be validated in non-enlarged pelvic lymph nodes.

INTRODUCTION

Choline-based PET has proven value in several neoplasms, and especially in prostate cancer (PC) [1, 2]. [¹⁸F]FCH PET/CT seems to become a useful imaging tool to solve the clinical problem of rising serum prostate-specific antigen (PSA) after initially treated PC [3-5], with PET/CT sensitivity being proportionally related to the PSA level [6, 7].

Choline is the precursor of phosphatidylcholine, an essential phospholipid of cell membranes. The phosphorylation process is catalyzed by choline kinase (CK) [2]. In PC, enhanced choline uptake is explained by both increased mitogenic activity as well as up regulation of CK [8]. However, the signal is not tumor specific [9, 10]. Since biopsy of presumed regional lymph node metastases is often not trivial due to their localization in PC, false positive readings may induce serious problems in the clinical context.

Both [¹⁸F] and [¹¹C]-labeled choline derivates have been developed and studied as possible metabolic imaging tools in the detection of primary PC, regional LN and distant metastases [11, 12]. The main advantages of [¹⁸F] over [¹¹C]-labeled tracers are the longer half-life (110 min versus 20 min) and a better spatial resolution due to the shorter positron range of ¹⁸F. However, [¹⁸F]choline is excreted in urine [13] and this can compromise the interpretation of the pelvic area. Since [¹⁸F]FCH is rapidly cleared from the blood pool, acquisition protocols have been designed with imaging of the pelvis prior to bladder filling (within minutes after injection), followed by a whole body scan after e.g., 30 min [1, 14-16] – the dual-phase protocol. Patterns of tracer uptake as a function of time have shown to be helpful in discriminating intraprostatic tracer uptake [8, 15] as well as sites of suspected haematogeneous metastases [17].

It was suggested that increasing or stable [¹⁸F]FCH uptake over time (3-7 min versus 30-60 min after injection) was compatible with malignancy, while a decreasing tracer uptake is associated with benign status [8, 15, 17]. For lymph node assessment this hypothesis has not been validated. Beheshti et al. [8] described an interesting early [¹⁸F]FCH wash-out pattern of false-positive LN in the preoperative setting of 130 patients with high and intermediate risk for disseminated PC. This phenomenon was deemed highly important for the differentiation of malignant versus benign nodes. However, the study could not support this finding with a statistically relevant number of lesions.

In the present study we investigated whether time-trends of enhanced [¹⁸F]FCH uptake in lymph nodes can help to discriminate between benign and malignant sites, and we explored whether single time point SUV measurements may also suffice.

MATERIALS AND METHODS

Patients

Formal ethical approval for performing this retrospective study was obtained from the Medical Ethics Committee of the VU University Medical Center, Amsterdam, the Netherlands (approval date June 2012, reference 2012/254). This approval states that written informed consent from participants is wavered since the study does not fall within the scope of the Medical Research Involving Human Subjects Act (section 16.2 WMO, 26th February 1998).

We retrospectively studied [¹⁸F]FCH PET/CT scans of 66 consecutive patients with prostate cancer (median age, 63 years; range, 50-80 years), performed at the VU University Medical Center, Amsterdam, The Netherlands, between January 2009 and March 2011. Three main clinical indications (I) for PET/CT were: I₁, PSA relapse in previously treated PC (n=39); I₂, newly diagnosed PC (n=16) and I₃, staging of patients with suspected oligometastases (typically skeletal, identified with other imaging modalities), in newly diagnosed or already treated PC (n=11).

Patient characteristics [age, Gleason score (G1), serum PSA at diagnosis and at the time of performing the PET/CT] were gathered, including the date and the type of previous therapy [e.g., radical prostatectomy (RP), external-beam radiation therapy (EBRT), brachytherapy (BT), pelvic lymph node dissection (PLND), anti-androgen therapy (ADT) or the combination of these].

Inclusion criteria were: dual-phase [¹⁸F]FCH PET/CT performed in patients with histopathologically proven PC; enhanced [¹⁸F]FCH uptake in any inguinal nodes and in pelvic LN with a short axis diameter \geq 8 mm, visible at early and/ or late PET scan. Patients with multiple malignancies (e.g., one or more other types of carcinoma apart from the PC) were excluded.

PSA relapse, suspected to be associated with residual or recurrent disease, was defined as a serum concentration level above 0.2 ng/ml, after RP and after the combination of RP with other types of therapy. A rising PSA level > 2 ng/ml above the nadir value in patients treated by means of EBRT was considered suspect for persistent or recurrent disease [18]. Increased serum PSA was confirmed by two consecutive exams for all patients. The maximal time interval between performing the PET/CT scan and the last PSA determination was 14 days.

Based on histology, the primary PC was classified as low (Gl <7), intermediate (Gl = 7) and high grade (Gl > 7), according to the modified Gleason Grading System [19].

Lymph node classification

We classified lymph nodes as benign or malignant using the following approach: inguinal lymph nodes with enhanced [¹⁸F]FCH uptake were considered benign since the prostatic lymph node drainage pattern does not include inguinal nodes [20–22]. Pelvic nodes with a short axis diameter ≥ 8 mm were classified as malignant [23]. Additional confirmation was obtained using histopathology (whenever feasible), and with clinical follow-up of 6–12 months in all patients. Follow-up consisted of PSA measurements over time (as above mentioned) and/or evaluation of other imaging (i.e., contrast-enhanced abdominopelvic CT, pelvic MRI). We applied the following radiological criteria to classify change [24]: an increase by 30% versus initial size as progression, a decrease by 30% as regression, and intermediate values or no change in size as stable.

Therefore, malignancy was defined as a positive histopathological result; radiologically confirmed progression in size of the pertaining lymph nodes; decrease or normalization of serum PSA and radiological response after therapy, providing these were the only abnormal findings on the initial PET/CT scan; decrease or normalization of serum PSA with nodal regression after RT, with the RT field including the site of the suspected LN.

Synthesis of [¹⁸F]FCH

[¹⁸F]FCH was synthesized according to the methods proposed by DeGrado et al. [1, 25] and Iwata et al. [26], with minor modifications and by use of automated modules built in-house [27]. In short, cyclotron produced [¹⁸F]fluoride was reacted with dibromomethane, the formed [¹⁸F]fluorobromomethane was purified and used in the alkylation of 2-(dimethylamino)ethanol to obtain 2.6 ± 0.9 GBq [¹⁸F]FCH after semi-preparative high performance liquid chromatography (HPLC) purification, reformulation in aqueous 0.9% NaCl and sterile filtration.

The radiochemical purity was > 99.5% and no chemical impurities were detected as assessed by analytical radio/ultra-violet-HPLC (UV-HPLC). Residual concentrations of dibromomethane (0-8 ppm) and 2-(dimethylamino)ethanol (95±40 ppm) were determined by flame ionization detector - gas chromatography (FID-GC). Absence of bacterial endotoxins in the product was confirmed by an Endosafe portable test system (PTS) reader (Charles River) and all samples were tested for sterility.

PET/CT Imaging

All studies were performed on a Gemini TF-64 PET/CT scanner (Philips Medical Systems, Best, the Netherlands) with an axial field per view of 18 cm. Low-dose CT (LD-CT) was collected using a beam current of 30 to 50 mAs at 120 keV. CT was reconstructed using an image matrix size of 512x512 resulting in voxel sizes of 1.17x1.17 mm and a slice thickness of 5 mm. For PET, data were reconstructed by means of a raw action ordered subset expectation maximization algorithm using default reconstruction parameters. Time of flight (TF) information was used during reconstruction. Reconstructed images had an image matrix size of 144x144, a voxel size of 4x4 mm and a slice thickness of 5 mm.

All patients underwent the standard [¹⁸F]FCH image acquisition protocol at our institution: following the LD-CT, 'early' PET image acquisition started 2 min after intravenous injection of 4 MBq/kg [¹⁸F]FCH, using a 35 cm scan trajectory over the pelvic region (2 min/bed position); patients were asked to void 20 min post injection (p.i.), and at 30 min p.i. a 'late' whole body PET sequence was started, from mid-thigh to the skull vertex, again using 2 min acquisitions/ bed position. Patient preparation was similar to that required for FDG PET [28].

PET/CT data analysis

PET/CT images were evaluated by an experienced nuclear medicine specialist who first identified all lymph nodes with enhanced FCH uptake versus their direct background (on early and/ or late scan time points) within the field of view of the early scan trajectory. Lymph node diameters were measured using the CT component of the PET/CT scanner, and standard CT and MRI, where available.

PET and LD-CT images were converted to ECAT 7 format and regions of interest (ROIs) were semi-automatically drawn around every pelvic LN that met the inclusion criteria mentioned above, using in-house developed software, as previously described [29, 30].

For lesion delineation, we used the adaptive threshold of 50% of maximum voxel value within tumor, the 3D volume of interest A50 (VOI_{A50}). This method is similar to the fixed threshold method, except that it adapts the threshold relative to the local average background, thereby correcting for the contrast between tumor and local background. For example, the A50 contour value corresponds to a value at 50% of the sum of the maximum voxel value and the local background value. The latter value is derived from 'background' voxels that are identified as those voxels located on a single voxel thick shell at 2.5 cm from the edge of a 70% of maximum pixel value isocontour, excluding all voxels with an SUV larger than 2.5.

SUV's were normalized for body weight. For data-analysis, we used early (2 min p.i.) and late (30 min p.i.) SUV_{max} and SUV_{mean} , as well as their absolute [$SUV_{late} - SUV_{early}$] and relative differences [$(SUV_{late} - SUV_{early}) / SUV_{early}$].

Furthermore, based on literature [8], we considered two possible time-trends of [¹⁸F]FCH uptake by comparing the SUV early and the SUV late: type A pattern (decreasing over time) if the SUV early > the SUV late and type B pattern (stable/ increasing over time) if the SUV late was equal or exceeded the SUV early. Equality of SUV's was decided using the 2nd decimal. In the present context, accuracy measures relate to the ability of time-trends (2 versus 30 min p.i.) of tracer uptake to discriminate malignant and benign lymph nodes with enhanced [¹⁸F]FCH uptake.

Statistical Analysis

The two sample Mann-Whitney tests were performed to determine a shift in the median values for benign and malignant tumors. Linear mixed-effects models were constructed to determine the relation between SUV_{max} and SUV_{mean} . Included in this model were tumor status (benign versus malignant) and post injection scan time (2 min versus 30 min) as fixed effects, as well as random slopes per patient and per lesion (nested within patient). The residuals were assumed to be exponential related to SUV_{mean} , and pairwise interactions between SUV_{mean} and both tumor status and scan time were also tested. An identical linear regression model ignoring repeated measures and heteroscedasticity was used to provide an R^2 . Receiver Operating Characteristic (ROC) curves were constructed to determine the thresholds maximizing specificity and sensitivity. The binomial distribution is used to determine 95% confidence intervals of the sensitivity and specificity estimates for the optimal thresholds. To ensure that these results are not influenced by within-patient correlations in uptake, a Monty

Carlo process is performed where ROC curves are produced for 500 datasets randomly generated so that each patient has only one lesion. The range of the sensitivities and specificities of the optimal thresholds from these ROC curves were visually compared with the sensitivities and specificities calculated using all observations.

RESULTS

We identified 25 eligible patients who had 54 lymph nodes with enhanced [¹⁸F]FCH uptake that met our inclusion criteria. In 13/25 (52%) patients the PET/CT had been performed because of PSA relapse (I₁), and in 9/25 (36%) for staging at presentation (I₂); the remaining three patients had been referred for restaging in the context of presumed oligometastases (I₃). The mean interval between the primary therapy and the time of referral to [¹⁸F]FCH PET/CT was 23 months (range: 3-48 months). In 17 patients (pelvic group; median age: 63 years; range: 50-80 years) we found 34 enlarged pelvic nodes (classified as malignant, see methods), and there were 7 patients (inguinal group; median age: 63 years; range: 57-68 years) with 15 [¹⁸F]FCH positive inguinal LN, classified as benign. One patient had enhanced [¹⁸F]FCH uptake in both two inguinal and three enlarged pelvic nodes. In either group the median number of eligible lymph nodes per patient was 2 (range: 1-6). Patient characteristics are presented in Table 1.

Table 1. Patient characteristics.

Total patients (N=25)	Pelvic group (N=17)	Combined pelvic & inguinal (N=1)	Inguinal group (N=7)
Mean age (years)	63 (range: 50-80)	63	63 (range: 57-68)
Mean serum PSA (ng/ml) at diagnosis	51	27	18
Mean serum PSA (ng/ml) at PET time	38	37	17
Gleason score (number of patients)			
<7	4	-	2
7	7	-	4
>7	6	1	1
Previous therapy: number of patients (indication)			
EBRT (±ADT ±PLND)	5 (3×I ₁ + 2×I ₃)	-	2 (2×I ₁)
EBRT + RP	2 (2×I ₁)	-	1 (I ₂)
RP	1 (I ₁)	-	2 (2×I ₁)
ADT	1 (I ₁)	-	1 (I ₃)
BT	1 (I ₁)	-	-
NA	7 (7×I ₁)	1 (I ₃)	1 (I ₂)

N number, EBRT external -beam radiation therapy, ADT anti-androgen therapy, PLND pelvic lymph node dissection, RP radical prostatectomy, BT brachytherapy, NA not applicable, I₁: PSA relapse after therapy, I₂: newly diagnosed prostate cancer, I₃: staging patients with suspected oligometastases from prostate cancer

All LN showed enhanced FCH uptake at early (2 min p.i.) as well as late (30 min p.i.) time points (Table 2). The long axes of the inguinal and pelvic lymph nodes were similar (11 \pm 2, and 12 \pm 3 mm, respectively); short axis diameters were slightly smaller in the former group (8 \pm 1 vs. 10 \pm 2 mm, respectively; $P < 0.001$).

Table 2. SUV metrics of lymph nodes as a function of time.

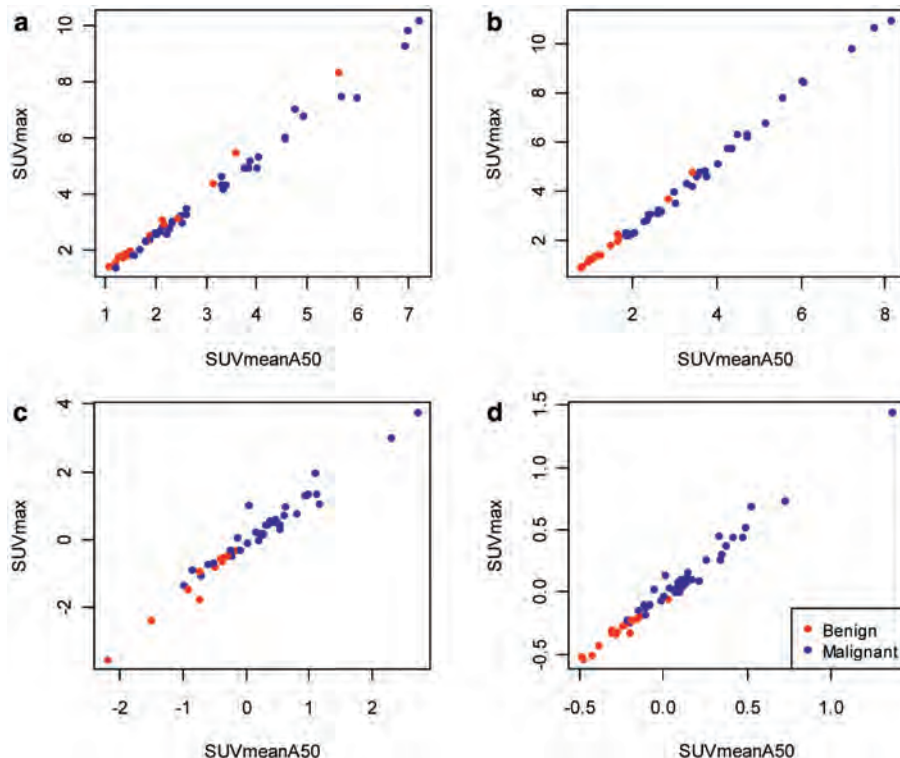
Standard Uptake Value (SUV)	Benign N = 17	Malignant N = 37	Total N = 54
Maximum			
Early (2 min p.i.)			
Median	2	3.5	3
(Range)	(1.4–8.4)	(1.4–10)	(1.4–10)
Late (30 min p.i.)			
Median	1.4	4.3	3.2
(Range)	(0.95–4.8)	(2.2–11)	(0.95–11)
Difference			
Median	-0.64	0.44	0
(Range)	(-3.6–0.08)	(-1.4–3.8)	(-3.6–3.8)
Relative Difference			
Median	-0.32	0.084	0
(Range)	(-0.54–0.055)	(-0.25–1.4)	(-0.54–1.4)
Mean_{A50}			
Early (2 min p.i.)			
Median	1.5	2.6	2.3
(Range)	(1.1–5.6)	(1.2–7.2)	(1.1–7.2)
Late (30 min p.i.)			
Median	1.1	3.4	2.6
(Range)	(0.75–3.4)	(1.8–8.1)	(0.75–8.1)
Difference			
Median	-0.42	0.31	0.03
(Range)	(-2.2–0.02)	(-1–2.7)	(-2.2–2.7)
Relative Difference			
Median	-0.29	0.11	0.013
(Range)	(-0.49–0.019)	(-0.22–1.4)	(-0.49–1.4)

$$\text{Difference} = \text{SUV}_{\text{late}} - \text{SUV}_{\text{early}}$$

$$\text{Relative difference} = (\text{SUV}_{\text{late}} - \text{SUV}_{\text{early}}) / \text{SUV}_{\text{early}}$$

We found highly significant associations between the LN status (inguinal/ benign vs. enlarged pelvic/ malignant) and the SUV_{max} and SUV_{mean_{A50}} 30 min p.i., and their absolute and relative differences ($P < 0.0001$). The correlation between the mean and max SUV metrics was near-perfect (Figure 1; the linear regression model resulted in an almost identical relation and an adjusted R^2 of 0.99).

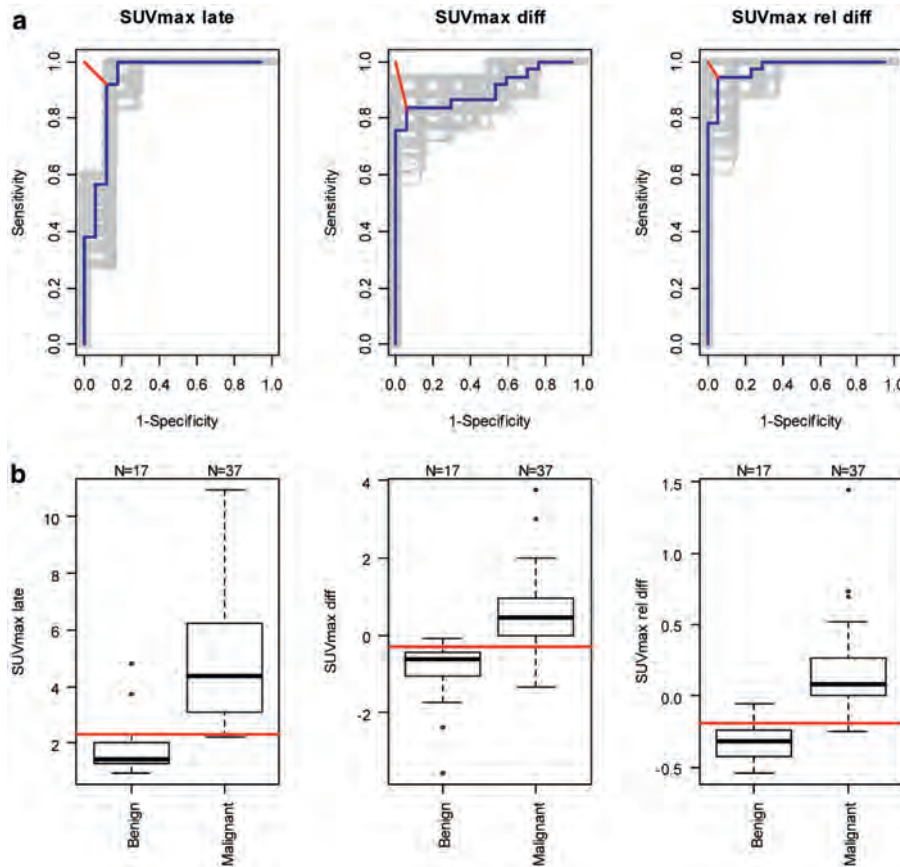
Figure 1. Comparison of SUV_{max} and $SUV_{meanA50}$. a. Early = 2 min p.i.; b. Late = 30 min p.i.; c. Difference = $SUV_{late} - SUV_{early}$; d. Relative difference = $(SUV_{late} - SUV_{early}) / SUV_{early}$. At the early scan time point, $SUV_{max} = 1.40 * SUV_{mean} - 0.07$ (Benign) – 0.27 (Malignant); versus a reduction of -0.07 in the intercept at the late (30 min p.i.) assessment.



For further analyses we focused on the SUV_{max} . The number of LN with a $[^{18}\text{F}]$ FCH uptake pattern type A ($SUV_{early} > SUV_{late}$) or B ($SUV_{early} \leq SUV_{late}$), in the benign and malignant group for the above mentioned thresholds are included in Table 3. Based on the SUV_{max} relative difference, all but one LN in the benign group showed a type A, decreasing uptake over time, while in the malignant group 95% (35/37) of the nodes presented a type B pattern uptake. From the 54 LN, only 3 nodes were found to have a stable uptake over time: one from the inguinal and two from the pelvic group, respectively.

ROC analyses of uptake trends over time and of SUV's at either time-point (Figure 2) showed that the SUV_{max} relative difference was the best predictor of the lymph node status, followed by the SUV_{max} late and the SUV_{max} absolute difference [see also Table 3 for the areas under the ROC curve (AUC)].

Figure 2. ROC analyses and Threshold boxplots. a. ROC analyses of SUV_{max} 30min p.i. assessment (late), difference ($\text{SUV}_{\text{late}} - \text{SUV}_{\text{early}}$) and relative difference ($(\text{SUV}_{\text{late}} - \text{SUV}_{\text{early}})/\text{SUV}_{\text{early}}$). The grey lines represent the 500 ROC curves for randomly generated datasets in which only one lesion is included for each patient; the blue lines are the ROC curves for all 54 lesions; the red lines indicate the shortest distance to the top left hand corner; b. Threshold boxplots. Thresholds associated with the shortest distance to the top left hand corner in the ROC curves are indicated in the boxplots by the horizontal red lines.



The threshold of SUV_{max} relative difference that maximized both sensitivity and specificity was -0.19, for a sensitivity of 95% (95%CI 82-99) and a specificity of 94% (95%CI 71-100), versus a SUV_{max} late threshold of 2.3, for a sensitivity of 92% (95%CI 78-98) and a specificity of 88% (95%CI 64-99).

Table 3. Optimal thresholds for different SUV measures.

Standard Uptake Value (SUV)	Threshold	Pattern type	Ben	Mal	Sensitivity (95% CI)	Specificity (95% CI)	AUC (95% QR)
SUV_{max}							
Late (30 min p.i.)	2.32	A	15	3	92 (78-98)	88 (64-99)	0.93 (0.88-0.94)
		B	2	34			
Difference	-0.31	A	16	6	84 (68-94)	94 (71-100)	0.90 (0.87-0.97)
		B	1	31			
Relative Difference	-0.19	A	16	2	95 (82-99)	94 (71-100)	0.98 (0.95-0.99)
		B	1	35			
SUV_{meanA50}							
Late (30 min p.i.)	1.66	A	15	0	100 (91-100)	88 (64-99)	0.95 (0.91-0.95)
		B	2	37			
Difference	-0.18	A	16	7	81 (65-92)	94 (71-100)	0.89 (0.84-0.98)
		B	1	30			
Relative Difference	-0.15	A	16	3	92 (78-98)	94 (71-100)	0.97 (0.92-0.99)
		B	1	34			

Pattern type: A = SUVearly > SUVlate; B = SUVearly ≤ SUVlate

Ben benign, Mal malignant, CI confidence interval, AUC area under the ROC curve, QR quartile range

Difference = SUVlate – SUVearly

Relative difference = (SUVlate – SUVearly) / SUVearly

In the 17 patients with 34 enlarged [¹⁸F]FCH positive pelvic nodes, histopathological confirmation was obtained in 4 (11 LN); all had type B time trends at [¹⁸F]FCH PET/CT. During follow-up, 3 patients (6 LN) had radiological nodal progression; from these five LN had a type B pattern and one LN proved to be false negative: type A trend and radiological progression. In 3 other patients, with only pathologically enlarged pelvic lymph nodes (6 LN) to explain an elevated PSA and with a type B pattern, PSA normalized upon therapy, accompanied by shrinkage of these nodes. PSA decrease and disappearance of a solitary (type B) pelvic node was observed in another patient who was treated with pelvic radiotherapy that focused on a suspected recurrence in prostate and this lymph node.

Six other patients (with 9 type B and 1 type A pelvic lymph nodes) were treated with systemic therapy, because of local recurrence and/ or skeletal metastases. Finally, the patient with both 2 inguinal and 3 pelvic LN (type A in the inguinal and type B in the pelvic nodes) was treated with RT (prostate) and ADT because of confirmed bone oligometastases at presentation. In these 7 patients, PSA decreased over time and radiological regression of all 13 enlarged pelvic nodes together with stable dimensions of the inguinal nodes were recorded, as well. However, this did not unequivocally confirm the LN status due to the use of systemic therapy for coexistent bone metastases.

Of the inguinal nodes (14 type A and 1 type B with stable uptake over time) none showed signs of malignancy during follow-up; of these, in one patient a lymph node biopsy was tumor negative. One patient (2 LN) opted for watchful waiting policy (otherwise negative PET), and his PSA was stable at 0.4 ng/ml for the follow-up of 12 months. In another patient (type A LN) a local recurrence was treated with HIFU with good clinical response (PSA) and no signs of progression.

DISCUSSION

In our referral-based spectrum of patients with enhanced [¹⁸F]FCH uptake in pelvic and inguinal lymph nodes, decreasing [¹⁸F]FCH uptake over time seems to be a reliable tool to differentiate benign and malignant nodes. Together with similar findings by others to classify radioactive choline positive lesions suspected to represent hematogeneous metastases, our results are relevant for clinical decision making and simplification of diagnostic procedures, e.g., in patients with elevated PSA and positive [¹⁸F]FCH PET findings. Moreover, the results underline the relevance of a sequential PET imaging protocol after a single injection of [¹⁸F]FCH to account for the time-trend of tracer uptake.

We classified disease-status as *malignant* for enlarged pelvic nodes, and as *benign* for inguinal nodes of any size. Our criterion of benignity was based on the typical prostate drainage pattern which does not include inguinal nodes, as described by Inoue et al. [20]. They identified by using fluorescence navigation 3 lymphatic drainage pathways, comprising the obturator, the external and internal iliac nodes. Similar drainage patterns were found by Tokuda et al. [21] in 125 patients with LN metastases. Weckermann et al. [22] performed both sentinel lymph node dissection and radical prostatectomy in 1055 patients with PC. Despite a high percentage (> 50%) of positive nodes identified outside the standard lymphadenectomy borders, none of them were found in the inguinal region. In our study we also never encountered occurrences of malignancy in inguinal nodes (histological analysis, clinical radiological follow-up).

We considered pelvic nodes with a short axis diameter equal or exceeding 8 mm as being malignant. This threshold was chosen based on the study of Jager et al. [23] who reported a 98% specificity for MRI using this dimension. In their meta-analysis, Hövels et al. [31] found that false positivity of CT / MRI (similar performance for either

technique) at thresholds of 8-10 mm is only 7%. In an attempt to reduce the remaining uncertainty, a standard of reference method was used. This approach, as extensively described in the "Materials and Methods" section, consisted of the combination of histopathological examination (whenever available) and the results obtained by clinical or radiological follow-up. This is a commonly used procedure [32-37] to account for the limitations of retrospective studies. In difficult cases, biopsy of the proper radioactive choline avid lymph nodes was improved and verified by using a dedicated gamma-probe [38]. Confirmation seemed feasible in 65% of these pelvic LN (24/37). In 7 patients treated with ADT and/or chemotherapy for coexisting bone metastases, decreases of nodal diameter could not be interpreted since such changes are not necessarily compatible with a 'malignant tissue' response to treatment.

Note that in our present context 'sensitivity' and 'specificity' should not be confused with 'the accuracy of [¹⁸F]FCH PET/CT to diagnose metastatic lymph nodes in prostate cancer'. The results pertain to the ability of tracer uptake time-trends to classify lymph nodes with enhanced [¹⁸F]FCH uptake.

The relevance of uptake time-trends to characterize [¹⁸F]FCH foci has been demonstrated in malignant bone metastases, in recurrent PC, and in malignant zones of the prostate in preoperative setting [8, 15, 17]. Our findings corroborate and extend those of Beheshti et al. [8] who reported on 18 malignant lymph nodes showing stable or increasing uptake over time. The imaging protocol consisted of a dynamic PET/CT scan of the pelvic region for 8 min, starting 1 min p.i., followed by whole body (WB) images 10 min after [¹⁸F]FCH injection and optional supplementary delayed WB acquisitions, 90-120 min p.i., when abnormalities were detected. However, since that study comprised only 4 [¹⁸F]FCH positive reactive lymph nodes (with decreasing uptake over time) they urged for validation of these patterns in a larger study.

In our study, all but one inguinal nodes showed decreasing [¹⁸F]FCH uptake over time (Figure 3), versus 95% (35/37) of the pelvic category demonstrating stable or increasing uptake (Figure 4).

Figure 3. Example of decreasing [¹⁸F]FCH uptake over time in a right inguinal lymph node (red arrow; SUV_{max} early: 4.41; SUV_{max} late: 2.03) of a patient with newly diagnosed prostate cancer. This lymph node was classified as benign. Transversal sections of the Low-dose CT, PET and fused PET/CT images: a, b and c – early phase; d, e and f – late phase. [¹⁸F]FCH uptake in the prostate is also visible.

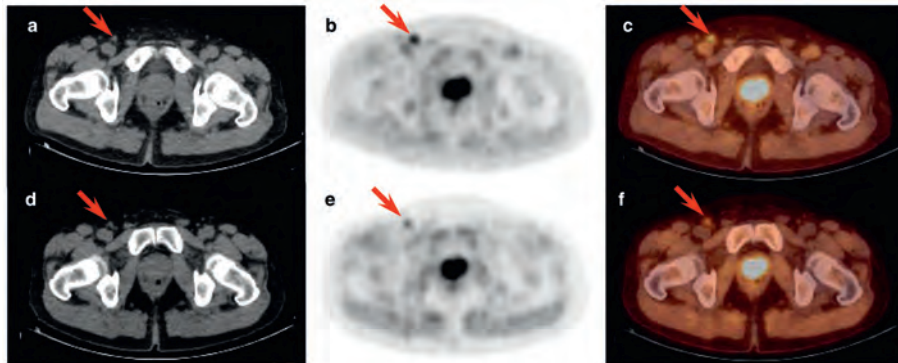
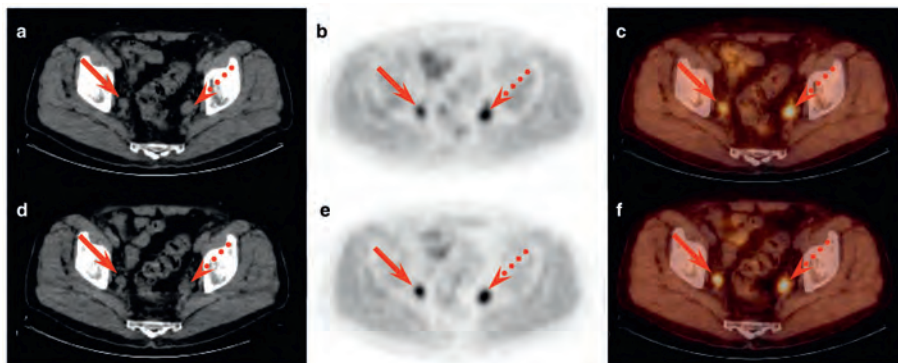


Figure 4. Example of increasing [¹⁸F]FCH uptake over time in a right para-iliac lymph node (red solid arrow; SUV_{max} early: 3.02; SUV_{max} late: 4.35) and a left para-iliac node (red dotted arrow; SUV_{max} early: 3.47; SUV_{max} late: 4.79) of a patient with biological relapse after initially treated prostate cancer. These lymph nodes were classified as malignant. Transversal sections of the Low-dose CT, PET and fused PET/CT images: a, b and c – early phase; d, e and f – late phase.



Kwee et al. [15] suggested as a possible explanation for the tracer decrease over time in benign zones the dephosphorylation of [¹⁸F]FCH by prostatic acid phosphatase while a trapping mechanism of the tracer in the malignant cells was responsible for the increased uptake in PC. This can only be validated with full kinetic modeling.

Our results are at variance with those of Cimitan et al. [15] who reported no significant late/early [¹⁸F]FCH uptake ratios in proven local recurrent prostatic disease or abdominopelvic LN, when performing a dual phase [¹⁸F]FCH PET/CT in 43 patients

with PSA relapse. However, their dual-phase PET/CT protocol included WB scans with variable early and late acquisitions, 5 to 15 min p.i. and 65 to 200 min p.i., respectively. The discrepancy may be explained by the rapid clearance of the [¹⁸F]FCH after administration [14, 16], which implies that timing of the early acquisitions is crucial and should be done using a strict imaging protocol.

The prevalence of patients with inguinal lymph nodes showing enhanced [¹⁸F]FCH uptake was 12% (8/66 patients). Our finding that reactive nodes remained detectable over time (i.e., for 30 min after injection) seems being inconsistent with the observation of Price et al. [16] who found persistent uptake at the late, 45 min p.i., images in only 1 of 4 patients with initially enhanced inguinal node uptake. We content that this variance results from improved signal to noise ratios with the current TF scanner generations.

Our data suggest that the type B pattern is a strong indication for malignancy, the PPV being 97% (35/36; see Table 3, for the best LN status predictor: SUVmax Relative Difference). The fact that the PPV is not 100% implies in clinical practice that, e.g. in case of multiple potentially malignant [¹⁸F]FCH positive LN, the ones with type B patterns should be the primary biopsy candidates.

Our results also suggest that a single point measurement in the context of a whole body scan, starting in caudocranial direction, 30 min after injection, is a reasonable alternative for relative change to differentiate reactive from malignant LN in patients with PC. Obviously, omitting the early scan would simplify the scan procedure. However, compared to measuring relative changes, the use of absolute SUV's is more demanding at the level of standardization. Evidently, the present results pertain to lymph nodes with enhanced [¹⁸F]FCH uptake and ≥ 8 mm short axis. Ascertaining the single time-point approach requires validation versus histopathology.

CONCLUSION

Time-trends of enhanced [¹⁸F]FCH uptake in lymph nodes of prostate cancer patients seem to help discriminate benign from malignant localizations. Single time-point SUV measurements, 30 min p.i., may be a reasonable alternative for predicting the nodal status, but this remains to be validated in non-enlarged pelvic lymph nodes.

REFERENCES

1. DeGrado TR, Baldwin SW, Wang S, Orr MD, Liao RP, et al. Synthesis and evaluation of ¹⁸F-labeled choline analogs as oncologic PET tracers. *J Nucl Med.* 2001;42:1805-1814
2. Kwee SA, DeGrado TR, Talbot JN, Gutman F and Coel MN. Cancer imaging with fluorine-18-labeled choline derivatives. *Semin Nucl Med.* 2007;37:420-428
3. Fuccio C, Rubello D, Castellucci P, Marzola MC and Fanti S. Choline PET/CT for prostate cancer: main clinical applications. *Eur J Radiol.* 2011;80:e50-56
4. Heinisch M, Dirisamer A, Loidl W, Stoiber F, Gruy B, et al. Positron emission tomography/computed tomography with F-18-fluorocholine for restaging of prostate cancer patients: meaningful at PSA < 5 ng/ml? *Mol Imaging Biol.* 2006;8:43-48
5. Picchio M, Briganti A, Fanti S, Heidenreich A, Krause BJ, et al. The role of choline positron emission tomography/computed tomography in the management of patients with prostate-specific antigen progression after radical treatment of prostate cancer. *Eur Urol.* 2011;59:51-60
6. Jadvar H. Prostate cancer: PET with ¹⁸F-FDG, ¹⁸F- or ¹¹C-acetate and ¹⁸F- or ¹¹C-choline. *J Nucl Med.* 2011;52:81-89
7. Pelosi E, Arena V, Skanjeti A, Pirro V, Douroukas A, et al. Role of whole-body ¹⁸F-choline PET/CT in disease detection in patients with biochemical relapse after radical treatment for prostate cancer. *Radiol Med.* 2008;113:895-904
8. Beheshti M, Imamovic L, Broigner G, Vali R, Waldenberger P, et al. ¹⁸F choline PET/CT in the preoperative staging of prostate cancer in patients with intermediate or high risk of extracapsular disease: a prospective study of 130 patients. *Radiology.* 2010;254:925-933
9. Hara T, Kosaka N and Kishi H. PET imaging of prostate cancer using carbon-11-choline. *J Nucl Med.* 1998;39:990-995
10. Igerc I, Kohlfürst S, Gallowitsch HJ, Matschnig S, Kresnik E, et al. The value of ¹⁸F-choline PET/CT in patients with elevated PSA-level and negative prostate needle biopsy for localisation of prostate cancer. *Eur J Nucl Med Mol Imaging.* 2008;35:976-983
11. Bauman G, Belhocine T, Kovacs M, Ward A, Beheshti M, et al. ¹⁸F-fluorocholine for prostate cancer imaging: a systematic review of the literature. *Prostate Cancer Prostatic Dis.* 2012;15(1):45-55
12. Reske SN, Blumstein NM, Neumaier B, Gottfried HW, Finsterbusch F, et al. Imaging prostate cancer with ¹¹C-choline. *J Nucl Med.* 2006;47(8):1249-1254
13. Schillaci O, Calabria F, Tavolozza M, Ciccìò C, Carlanì M, et al. ¹⁸F-choline PET/CT physiological distribution and pitfalls in image interpretation: experience in 80 patients with prostate cancer. *Nucl Med Commun.* 2010;31:39-45
14. DeGrado TR, Reiman RE, Price DT, Wang S and Coleman RE. Pharmacokinetics and radiation dosimetry of ¹⁸F-fluorocholine. *J Nucl Med.* 2002;43:92-96
15. Kwee SA, Wei H, Sesterhenn I, Yun D and Coel MN. Localization of primary prostate cancer with dual-phase ¹⁸F-fluorocholine PET. *J Nucl Med.* 2006;47:262-269
16. Price DT, Coleman RE, Liao RP, Robertson CN, Polascik TJ, et al. Comparison of [¹⁸F]Fluorocholine and [¹⁸F]fluorodeoxyglucose for positron emission tomography of androgen dependent and androgen independent prostate cancer. *J Urol.* 2002;168:273-280
17. Cimitan M, Bortolus R, Morassut S, Canzonieri V, Garbeglio A, et al. [¹⁸F]-fluorocholine PET/CT imaging for the detection of recurrent prostate cancer at PSA relapse: experience in 100 consecutive patients. *Eur J Nucl Med Mol Imaging.* 2006;33:1387-1398
18. Heidenreich A, Bellmunt J, Bolla M, Joniau S, Mason M, et al. EAU guidelines on prostate cancer. Part1: screening, diagnosis, and treatment of clinically localised disease. *Eur Urol.* 2011;59(1):61-71
19. Egevad L, Mazzucchelli R and Montironi R. Implications of the International Society of Urological Pathology Modified Gleason Grading System. *Arch Pathol Lab Med.* 2012;136(4):426-434
20. Inoue S, Shiina H, Arichi N, Mitsui Y, Hiraoka T, et al. Identification of lymphatic pathway involved in the spreading of prostate cancer by fluorescence navigation approach with intraoperatively injected indocyanine green. *Can Urol Assoc J.* 2011;5:254-259
21. Tokuda Y, Carlino LJ, Gopalan A, Tickoo SK, Kaag MG, et al. Prostate cancer topography and patterns of lymph node metastasis. *Am J Surg Pathol.* 2010;34:1862-1867

22. Weckermann D, Dorn R, Trefz M, Wagner T, Wawroschek F, et al. Sentinel lymph node dissection for prostate cancer: experience with more than 1000 patients. *J Urol.* 2007;177:916–920
23. Jager GJ, Barentsz JO, Oosterhof GO, Witjes JA and Ruijs SJ. Pelvic adenopathy in prostatic and urinary bladder carcinoma: MR imaging with a three-dimensional T1-weighted magnetization-prepared-rapid gradient-echo sequence. *AJR Am J Roentgenol.* 1996;167:1503–1507
24. Beer AJ, Eiber M, Souvatzoglou M, Holzapfel K, Ganter C, et al. Restricted water diffusibility as measured by diffusion-weighted MR imaging and choline uptake in (¹¹C)choline PET/CT are correlated in pelvic lymph nodes in patients with prostate cancer. *Mol Imaging Biol.* 2011;13(2):352–361
25. DeGrado TR, Coleman RE, Wang S, Baldwin SW, Orr MD, et al. Synthesis and evaluation of ¹⁸F-labeled choline as an oncologic tracer for positron emission tomography: initial findings in prostate cancer. *Cancer Res.* 2001;61:110–117
26. Iwata R, Pascali C, Bogni A, Furumoto S, Terasaki K, et al. [¹⁸F]fluoromethyl triflate, a novel and reactive [¹⁸F] fluoromethylating agent: preparation and application to the on-column preparation of [¹⁸F]fluorocholine. *Appl Radiat Isot.* 2002;57:347–352
27. Windhorst AD, ter Linden T, de Nooij A, Keus JF, Buijs FL, et al. A complete, multipurpose, low cost, fully automated and GMP compliant radiosynthesis system. *J Labelled Cpd Radiopharm.* 2001;44:1052–1054
28. Boellaard R, O'Doherty MJ, Weber WA, Mottaghy FM, Lonsdale MN, et al. FDG PET and PET/CT: EANM procedure guidelines for tumour PET imaging: version 1.0. *Eur J Nucl Med Mol Imaging.* 2010;37:181–200
29. Cheeseman P, van Velden FH, Yaqub M, Frings V, de Langen AJ, et al. Effects of image characteristics on performance of tumor delineation methods: a test-retest assessment. *J Nucl Med.* 2011;52:1550–1558
30. Frings V, de Langen AJ, Smit EF, van Velden FH, Hoekstra OS, et al. Repeatability of metabolically active volume measurements with ¹⁸F-FDG and ¹⁸F-FLT PET in non-small cell lung cancer. *J Nucl Med.* 2010;51:1870–1877
31. Hövels AM, Heesakkers RA, Adang EM, Jager GJ, Strum S, et al. The diagnostic accuracy of CT and MRI in the staging of pelvic lymph nodes in patients with prostate cancer: a meta-analysis. *Clin Radiol.* 2008;63:387–395
32. Castellucci P, Fuccio C, Nanni C, Santi I, Rizzello A, et al. Influence of trigger PSA and PSA kinetics on ¹¹C-choline PET/CT detection rate in patients with biochemical relapse after radical prostatectomy. *J Nucl Med.* 2009;50:1394–1400
33. Krause BJ, Souvatzoglou M, Tuncel M, Herrmann K, Buck AK, et al. The detection rate of [¹¹C]Choline- PET/CT depends on the serum PSA value in patients with biochemical recurrence of prostate cancer. *Eur J Nucl Med Mol Imaging.* 2008;35:18–23
34. Fuccio C, Castellucci P, Schiavina R, Santi I, Allegri V, et al. Role of ¹¹C-choline PET/CT in the restaging of prostate cancer patients showing a single lesion on bone scintigraphy. *Ann Nucl Med.* 2010;24:485–492
35. Breeuwsma AJ, Pruim J, van den Bergh AC, Leliveld AM, Nijman RJ, et al. Detection of local, regional, and distant recurrence in patients with PSA relapse after external-beam radiotherapy using ¹¹C-choline positron emission tomography. *Int J Radiat Oncol Biol Phys.* 2010;77:60–64
36. Rinnab L, Mottaghy FM, Blumstein NM, Reske SN, Hautmann RE, et al. Evaluation of [¹¹C]-choline positron-emission/computed tomography in patients with increasing prostate-specific antigen levels after primary treatment for prostate cancer. *BJU Int.* 2007;100:786–793
37. Scher B, Seitz M, Albinger W, Tiling R, Scherr M, et al. Value of ¹¹C-choline PET and PET/CT in patients with suspected prostate cancer. *Eur J Nucl Med Mol Imaging.* 2007;34:45–53
38. Hartemink KJ, Muller S, Smulders YM, Petrouskja van den Tol M and Comans EF. Fluorodeoxyglucose F18(FDG)-probe guided biopsy. *Ned Tijdschr Geneeskd.* 2010;154:A1884



CHAPTER 3

[¹⁸F]fluoromethylcholine as a chemotherapy response read-out in prostate cancer cells

Daniela E. Oprea-Lager¹

Mitchell P. van Kanten¹

Reindert J.A. van Moorselaar²

Alfons J.M. van den Eertwegh³

Peter M. van de Ven⁴

Irene V. Bijnsdorp²

Otto S. Hoekstra¹

Albert A. Geldof^{1,2}

¹Department of Radiology and Nuclear Medicine, VU University Medical Center, Amsterdam, the Netherlands

²Department of Urology, VU University Medical Center, Amsterdam, the Netherlands

³Department of Medical Oncology, VU University Medical Center, Amsterdam, the Netherlands

⁴ Department of Epidemiology and Biostatistics, VU University Medical Center, Amsterdam, the Netherlands

ABSTRACT

PURPOSE

The objective of the present study is to determine whether uptake of [¹⁸F]fluoromethylcholine ([¹⁸F]FCH) in comparison with 2-deoxy-2-[¹⁸F]-fluoro-D-glucose ([¹⁸F]FDG) accurately reflects chemotherapy efficacy at the tumor cell level in prostate cancer (PC).

METHODS

The effects of docetaxel and cabazitaxel on viable tumor cell number were explored in four PC cell lines. Cellular uptake of [¹⁸F]FDG and [¹⁸F]FCH, was compared with the effects measured using sulforhodamine B (SRB) assay, cell counting and colony formation assay (CFA), as proximators of viable tumor cell number. Agreement between uptake and cell numbers was assessed by Bland-Altman plots.

RESULTS

[¹⁸F]FCH uptake in all PC cell lines significantly correlated to the cell numbers surviving the respective drug concentrations. Bland-Altman analysis showed that [¹⁸F]FDG uptake resulted in signal overestimation and higher variability after chemotherapy.

CONCLUSION

[¹⁸F]FCH uptake correlates well with viable tumor cell numbers remaining after docetaxel and cabazitaxel exposure. Radiolabeled choline is a potential response monitoring biomarker after chemotherapy for PC.

INTRODUCTION

Prostate cancer (PC) is the second most common cancer in males worldwide [1]. The disease presents itself mostly in men above the age of 50 and the incidence increases with age. The clinical behavior of PC is very diverse. Some tumors are indolent, do not cause any symptoms and arise as microscopic, well-differentiated foci that may never become clinically manifest. However, a significant proportion of PC patients presents with or will develop aggressive tumors that lead to morbidity, metastases and ultimately to death.

The initial systemic treatment in metastatic PC is based on androgen deprivation. Nevertheless, the majority of PC patients will ultimately progress and reach a castration resistant PC (CRPC) status after starting the anti-hormone treatment. Therapeutic options against CRPC include agents that interfere with androgenic stimulation of tumor growth (e.g., abiraterone, enzalutamide) [2–4], immunotherapy (sipuleucel-T) [5], chemotherapy (docetaxel, cabazitaxel) [6, 7] and bone-seeking radiopharmaceuticals (e.g., Radium-223) [8]. Abiraterone acetate inhibits androgen biosynthesis by irreversibly blocking the CYP17, an essential enzyme in testosterone and estrogen synthesis [2]. When combined with low-dose prednisone, Abiraterone improves survival of patients with CRPC [3]. Enzalutamide is an antiandrogen agent with demonstrated potential to inhibit nuclear translocation of the androgen receptor and DNA binding, inducing tumor volume reduction in xenograft models [4]. Sipuleucel-T is an active cellular immunotherapeutic which prolongs survival among men with asymptomatic or minimally symptomatic metastatic CRPC [5]. Docetaxel and cabazitaxel are chemotherapeutic drugs from the Taxane class. Their principal mechanism of action is disruption of microtubule function, resulting in cell death [6, 7]. Radium-223 dichloride (radium-223) is an alpha emitter which selectively binds to areas of increased bone turnover in metastatic lesions. The emitted high-energy alpha particles with short range radiation induce double-stranded DNA breaks, resulting in a highly localized cytotoxic effect in the target areas [8].

However, despite the variety of therapeutic options available, the proper sequencing (e.g., modality, timing) in individual patients is unclear. When chemotherapy is indicated the initial regimen is docetaxel combined with prednisone [9, 10]. It has been shown that this combination significantly prolongs overall survival, compared to mitoxantrone [6]. For patients progressing after docetaxel, treatment with another

taxane, cabazitaxel, is an option. This drug significantly increases overall survival compared with mitoxantrone plus prednisone in men whose disease progressed on docetaxel [7].

However, the actual response to chemotherapeutic regimens in individual patients is variable. It is important to monitor therapeutic (in)efficacy in time, to prevent patients from undergoing futile therapy for too long, since alternative and potentially effective drugs are available. Presently, monitoring of progression is based on a response metrics construct requiring various diagnostic tests, including serum prostate-specific antigen (PSA) measurement and bone scintigraphy [11]. The limitations of the current approach are related to the heterogeneity of metastasized PC (i.e., coexistence of androgen sensitive and insensitive components with different impact on e.g., PSA [12]) and to its skeletal predominance (with bone- and computed tomography-scans having difficulties in timely and accurately detecting response). There is thus a clear need for alternative and more accurate response monitoring methods [13–15]. New specific tracers using Positron Emission Tomography (PET) in whole body setting might enable a quantitative assessment of response in metastatic sites (e.g., in lymph nodes and bone), using a single, non-invasive scan procedure.

2-deoxy-2- [¹⁸F]-fluoro-D-glucose ([¹⁸F]FDG) is a potential tracer in the monitoring of antimicrotubule therapy effects in PC, but its clinical use thus far has been limited, because [¹⁸F]FDG uptake is highly variable and mostly confined to aggressive PC cells [16, 17]. Therefore, other tracers are being evaluated to describe tumor physiology as response to treatment [18–21]. [¹⁸F]fluoromethylcholine ([¹⁸F]FCH) PET [22] has shown promising results in the localization of locally recurrent or metastatic disease in men with biochemical failure [23–25] as well as in the early detection of bone metastases [26, 27].

Whether [¹⁸F]FCH could also be employed in monitoring treatment response in patients receiving docetaxel and cabazitaxel therapy is unclear. Definitive data from clinical studies have not yet become available. Nevertheless, experiments in-vitro have shown promising results on the use of PET tracers to monitor anti-androgen treatment or chemotherapy [28]. The objective of the present study is to assess whether changes of [¹⁸F]FCH and/or [¹⁸F]FDG uptake in PC cells appropriately reflect chemotherapy induced cytotoxicity.

MATERIALS AND METHODS

Cell lines

PC3, DU 145 and LNCaP (-FGC clone) human PC cell lines were originally obtained from the American Type Culture Collection, Rockville, Md., USA (ATCC# CRL 1435; HTB-81; CRL 1740 respectively). R3327- MATLyLu (MLL) rat prostate tumor variant was established in cell culture as described earlier [29, 30]. Cell lines were cultured in RPMI-1640 culture medium (Gibco BRL, Life technologies Europe BV, Bleiswijk, The Netherlands), supplemented with 10% Fetal Calf Serum (Cambrex Fetal Calf Serum EU Standard, #14-801F, Lonza Verviers, Belgium), 100U/mL penicillin/streptomycin (Gibco BRL), 1 mM sodium Pyruvate and Insulin/Transferrin/Selenite medium Supplement (Sigma-Aldrich Chemicals, St. Louis MO, USA) at 37° C in a humidified atmosphere of 5% CO₂/95% air. Semi-annual screening demonstrated the cultures to be mycoplasma free.

Drug incubations

Docetaxel was obtained from Sigma-Aldrich chemicals (Zwijndrecht, the Netherlands) and was dissolved in dimethylsulfoxide to stock concentrations of 10 nM. Cabazitaxel was obtained from Sanofi-Aventis (Aventis Pharma, Antony Cedex, France) and was dissolved in Phosphate Buffered Salt Solution (10nM). All stock solutions were stored in aliquots at -20°C until use. For the drug incubations the respective cell lines were seeded into tissue culture flasks (25 cm, #690160; Greiner Bio-One, Alphen a/d Rijn, The Netherlands) in cell densities of 300.000 (PC-3; DU145), 500.000 (LNCaP) or 30.000 (R3327-MATLyLu), respectively. After 24 hours drugs were added in the desired concentrations. After 3 days of drug incubation the remaining cell numbers were determined using a CASY cell counter (Casy TT, Roche Diagnostics, Almere, The Netherlands) and parallel cultures were either worked up for Colony Formation Assay (CFA) or incubated with ¹⁸F-radiolabeled choline and deoxyglucose. All experiments were performed in triplicate and were repeated at least three times.

Sulforhodamine B (SRB) assay

Evaluation of drug cytotoxic effects using the sulforhodamine B (SRB)- assay was performed as described earlier [31]. In short: 3500 PC3 cells, 3500 DU145 cells, 5000 LNCaP cells or 1500 MLL cells were seeded in each well of 96-well plates (Cellstar #655180; Greiner BioOne, Frickenhausen, Germany). After 24 hours drugs were added in increasing concentrations and cells were incubated for 3 days. After this incubation

time, wells were fixed with trichloroacetic acid (1 hour at 4°C) and stained using SRB solution (0.4% SRB in 1% acetic acid). The optical density was measured at 492 nm after reconstitution of the dye in 150 µL 10 mM Tris buffer. The values were normalized to cell density of control cultures (100%) and were corrected for the optical density values at t=0 (0%). Subsequently, inhibitory concentrations were calculated resulting in 10%, 50% and 90% reduction in cell numbers compared to control: IC_{10} , IC_{50} and IC_{90} respectively (all from 3 experiments in triplicate; means \pm SEM).

Colony Formation Assay (CFA)

Cells were exposed to IC_{10} , IC_{50} and IC_{90} concentrations of either cabazitaxel or docetaxel for 3 days. Subsequently, 200 cells were seeded in each well of 6-well plates for colony formation, as described previously [32]. After seven to ten days the colonies were fixed using 4% PBS buffered formaldehyde. The colonies were then stained with Giemsa-solution and counted using a Leica stereomicroscope. All experiments were performed in triplicate and repeated at least three times.

To facilitate the colony formation of LNCaP cells, conditioned medium (RPMI-1640 medium exposed for 24-48 hours to growing LNCaP cultures) was added (60:40). This allowed for autocrine stimulation of cell proliferation in this specific cell line. For R3327-MATLyLu cells, a modification of the CFA technique was used in order to account for the low efficient adherence of these cells to culture flask surfaces, as described earlier [29]. Briefly, after drug exposure, MLL cells were seeded in 0.25% agar (in PBS) which was layered on top of semisolid agar (0.375%).

Choline and Deoxyglucose labeling

[¹⁸F]FCH and [¹⁸F]FDG were prepared in the radiochemistry unit of the department of Radiology and Nuclear Medicine of the VU University Medical Center, Amsterdam, the Netherlands. Addition of the label (around 2 MBq) was performed 1 hour after replenishment of the growing cultures with fresh medium (in the case of [¹⁸F]FDG labeling, glucose-free RPMI 1640 medium was used for this replenishment). After incubation with the radiopharmaceutical for 1 hour, the cultures were washed twice using sterile phosphate-buffered salt solution and the uptake of the radiotracer in cells after trypsinization was measured using a gamma counter. The activity was calculated in percentage of total counts added and corrected for the cell number. All experiments were performed in triplicate and repeated at least three times.

Western Blotting

Western blotting was performed as described previously [31]. In brief, cells were exposed to either cabazitaxel or docetaxel for 3 days, washed with PBS and scraped in lysis buffer (Cell Signaling Technology Inc., supplemented with 0.04% protease inhibitor cocktail). Protein amounts in the supernatants were determined by the Bio-Rad assay (Bio-Rad Laboratories, Veenendaal, the Netherlands); 40 µg of protein was separated on a 10% SDS-PAGE and electroblotted onto polyvinylidene difluoride (PVDF) membranes (Millipore ImmobilonTM –FL PVDF, 0.45 µm). Subsequently, the membranes were blocked and incubated overnight at 4°C with the primary antibody anti-GLUT-1 (polyclonal # ab15309; dilution 1:1000; Abcam, Cambridge, UK) or alternatively with anti-β actin (#A5441; 1:10,000; Sigma Aldrich Chemicals, Deisenhofer, Germany) as loading control. Subsequently, the membranes were incubated with the secondary antibody against mouse (goat-δ-mouse-IRDye (680; #926-32220), Westburg, Leusden, The Netherlands). The bands were scanned using an Odyssey Infrared Imager (Westburg) at high quality, and expression levels were quantified with the Odyssey software program LI-COR Biosciences.

Cell volume determinations

Using CASY TT electronic cell counter, the effects of drug incubations of docetaxel and cabazitaxel (at IC₅₀ concentration level) on average cell volume were determined after 3 days of incubation for all cell lines. Average volume is reported in the results in femtoliter (fl).

Analysis and statistics

Agreement between uptake of radiolabeled [¹⁸F]FCH and [¹⁸F]FDG in the four PC cell lines and cell number was assessed by means of Bland-Altman plots, in which the differences between uptake of the tracer (%) and cell number (%) were plotted against the averages of these values [33, 34].

RESULTS

Effect of cabazitaxel and docetaxel on prostate cancer cell viability

The drug induced effects on the four PC cell lines after an incubation of 3 days were assessed using the SRB assay. In Table 1, the IC₁₀, IC₅₀ and IC₉₀ values were taken to delineate a representative and differential range of drug effect levels to be used to

compare [¹⁸F]FCH / [¹⁸F]FDG uptake with measures of viable cell numbers after drug incubation. The sensitivity of the various cell lines was reflected in their differential pattern of sensitivity towards docetaxel and cabazitaxel.

Subsequently, the chosen concentrations (IC_{10} , IC_{50} and IC_{90}) of docetaxel and cabazitaxel, aimed at reflecting low, medium and highly effective treatment results, respectively, were used in a 3-day incubation scheme with cells from the four PC lines to delineate efficacy on colony forming capacity. The colony forming ability at the IC_{10} and IC_{90} dose levels of both drugs decreased in a dose-dependent manner and analogously to the SRB-derived survival values, for all cell lines (Figure 1).

Effect of treatment on [¹⁸F]FCH and [¹⁸F]FDG signal

To evaluate the effect of docetaxel and cabazitaxel on [¹⁸F]FCH and [¹⁸F]FDG uptake, cells were exposed for 3 days to IC_{10} , IC_{50} and IC_{90} concentrations of the drugs, after which the cellular uptake of the radiotracer was measured. In all four cell lines, a clear relation was observed between actual cell numbers counted after treatment and level of [¹⁸F]FCH and [¹⁸F]FDG uptake. Using Bland-Altman plots we analyzed the degree to which the [¹⁸F]FCH / [¹⁸F]FDG uptake co-varied with viable cell numbers, in response to drug concentration in cells from the respective cell lines (Figure 2).

Table 1. Drug concentration (nM) ranges selected on the base of sulforhodamine B (SRB) assay-measured IC_{10} , IC_{50} and IC_{90} values, in prostate cancer cell lines PC3, DU145, LNCaP and MLL.

	Docetaxel			Cabazitaxel		
	IC_{10}	IC_{50}	IC_{90}	IC_{10}	IC_{50}	IC_{90}
PC3	0.5	1.0	10	0.5	1	10
DU145	0.5	1.0	5	0.5	2	5
LNCaP	0.5	2	10	1	5	50
MLL	2	10	50	0.5	2	10

Figure 1. CFA-determined treatment effects of docetaxel and cabazitaxel on proliferation of prostate cancer cells correlated to SRB-determined toxicity levels (IC_{10} , IC_{50} , IC_{90} are drug concentrations resulting in 10, 50 and 90% reduction in cell numbers compared to control value, respectively). Surviving fractions are given in percentage compared to control \pm standard deviation, carried out in triplicate using prostate cancer cell lines PC3, DU145, LNCaP and MLL. a effect of docetaxel. b effect of cabazitaxel. Left bar: IC_{10} , middle bar IC_{50} , right bar IC_{90} .

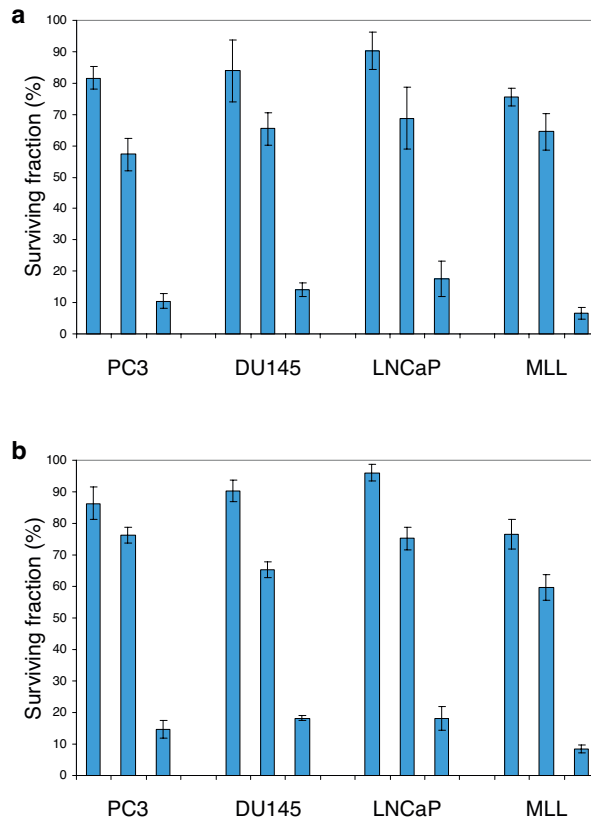
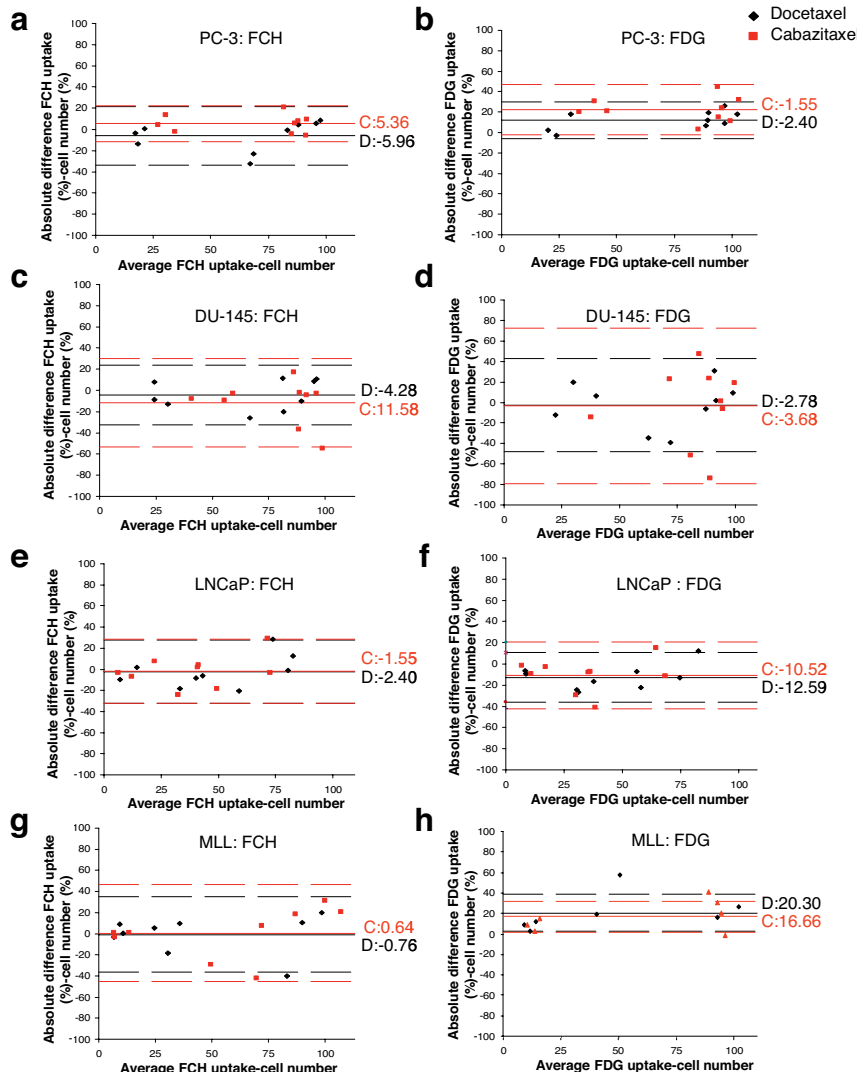


Figure 2. Bland-Altman plots for cellular [^{18}F]FCH uptake in four prostate tumor cell lines (a PC-3, c DU145, e LNCaP, g MLL) and [^{18}F]FDG uptake (b PC-3, d DU145, f LNCaP, h MLL), after docetaxel and cabazitaxel treatment. The x-axis shows the average between cell number percent and uptake percent and the y-axis shows the absolute difference between cell number percent and uptake percent. The straight lines indicate the average uptake after incubation with docetaxel (black) and cabazitaxel (red). The dotted lines indicate the limits of agreement for uptake after incubation with docetaxel (black) and cabazitaxel (red).



Average difference between tracer uptake and cell number was closer to 0 for [¹⁸F]FCH compared to [¹⁸F]FDG with the exception of DU145 cell line after treatment with cabazitaxel. [¹⁸F]FDG uptake overestimated the numbers of cells remaining after docetaxel and cabazitaxel treatment in PC3 and MLL cell lines (Table 2). Furthermore, agreement between uptake and cell numbers was generally worse for [¹⁸F]FDG when compared to [¹⁸F]FCH as can be seen from the increased limits of agreement (determined as 1.96 times standard deviation of the difference between tracer uptake and cell number) for the Bland-Altman analyses (Table 2).

Table 2. Comprehensive results of Bland-Altman analyses for [¹⁸F]FCH and [¹⁸F]FDG uptake compared to cell numbers after docetaxel (doc) and cabazitaxel (cab) treatment of prostate cancer cell lines PC3, DU145, LNCaP and MLL. The average difference between uptake of docetaxel (and cabazitaxel) and cell number in the Bland-Altman plots is given in this table (mean difference \pm limits of agreement, both in percent).

	[¹⁸ F]FCH		[¹⁸ F]FDG	
	Docetaxel	Cabazitaxel	Docetaxel	Cabazitaxel
PC3	-5.96 \pm 27.79	5.63 \pm 16.83	12.08 \pm 18.07	22.42 \pm 24.42
DU145	-4.28 \pm 28.14	-11.58 \pm 41.66	-2.78 \pm 45.53	-3.68 \pm 75.81
LNCaP	-2.40 \pm 29.92	-1.55 \pm 30.30	-12.59 \pm 23.44	-10.52 \pm 31.73
MLL	-0.76 \pm 35.90	0.64 \pm 46.07	34.15 \pm 62.17	29.79 \pm 58.65

To explain the increased [¹⁸F]FDG uptake by PC cells after incubation with docetaxel and cabazitaxel, we measured the expression of glut-1 glucose transporters using Western blot after incubation at IC₉₀ drug concentrations. The glut-1 transporter protein expression appeared not to be upregulated by treatment with either docetaxel or cabazitaxel (Figure 3).

Since taxane exposure may lead to increase in cell volume through stabilization of microtubules and inadequate cell division, an effect on radiotracer uptake on a per cell basis may result. Therefore, the mean volume of PC cells from the four different cell lines was determined after 3 days of incubation with IC₉₀ concentrations of docetaxel or cabazitaxel. The mean cell volume increased with a factor about 2 or 3 times for all four cell lines after incubation with each of the two chemotherapeutic drugs, most notably for PC3 and MLL (Figure 4).

Figure 3. a Western blot displaying stained antibody incubations using anti-glut-1 antibody on cell homogenates of four prostate cancer cell lines PC3, MLL, DU145 and LNCaP, after treatment with IC₉₀ concentrations of docetaxel and cabazitaxel. Anti- β actin was used as a loading control. b Expression levels were quantified with the Odyssey software.

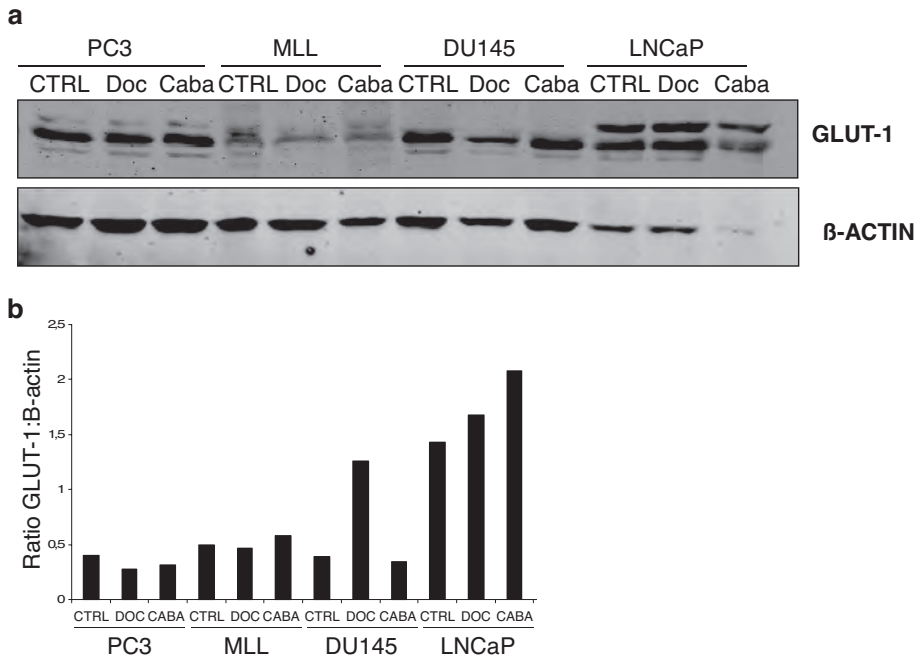
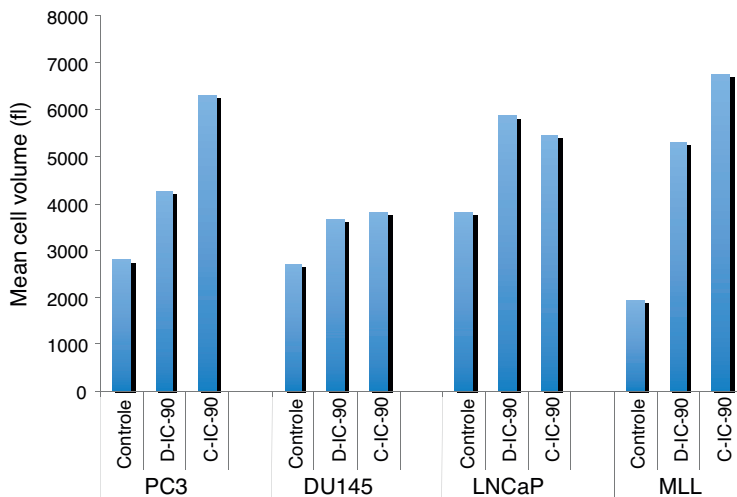


Figure 4. Mean cell volume (in fl) of prostate cancer cells, measured after incubation during 3 days with concentrations of docetaxel and cabazitaxel aimed at 90% inhibitory effect in four prostate cancer cell lines LNCaP, PC3, DU145 and MLL.



DISCUSSION

In the present study we compared the reduction in cellular uptake of radioactive [¹⁸F]FCH in prostate tumor cells in vitro under different burdens of docetaxel and cabazitaxel, with parameters of cell viability. The radiotracer uptake was proportional to the number of cells counted after therapy and these cell numbers correlated to clonogenic capacity as an additional sign of (reproductive) viability of the cells surviving the treatment. From this comparison we conclude [¹⁸F]FCH to be an adequate read-out parameter for response to treatment. [¹⁸F]FDG, on the other hand, showed in the case of PC3 and MLL an overestimation of the viable cell numbers remaining after therapy. This could lead to misinterpretation of the treatment outcome.

Non-invasive and timely therapy monitoring using PET would enable to quickly evaluate treatment efficacy in individual cancer patients thereby tailoring therapy, improving healthcare and quality of life, while offering economic benefits. Therefore we examined the possibility to use [¹⁸F]FCH as a novel readout for chemotherapy response monitoring in PC cells after treatment with either docetaxel or cabazitaxel, which are presently the drugs of choice in clinical PC chemotherapy.

A panel of different prostatic tumor cell lines was used, comprising both androgen-sensitive (LNCaP) as well as androgen-insensitive cell lines (PC-3; DU145 and R3327 MAT-LyLu). An influence of PC differentiation in patients on the level of [¹⁸F]FDG uptake has been described by Schwarzenböck et al. [35]. It has been shown that the grade of differentiation of PC cells is inversely proportional to the level of [¹⁸F]FDG uptake. In our experiments the relative sensitivity of treatment effects as evidenced by [¹⁸F]FCH and [¹⁸F]FDG uptake was investigated. The observed differential sensitivity of the various cell lines for the respective drugs is thought to reflect differences in expression of drug transporters like ABCC4 [30, 36]. All four cell lines investigated were [¹⁸F]FCH and [¹⁸F]FDG avid and the relative changes of tracer uptake and viable cell numbers upon exposure to docetaxel and cabazitaxel were closely related. Whether the efficacy of chemotherapy in PC *in vivo* will also be reflected by such a proportional decrease of the [¹⁸F]FCH signal, remains to be determined. However, in animal experiments employing PC xenografts, a reduced uptake of [¹⁴C]Choline compared to muscle tissue was shown within a week after docetaxel therapy and thereby confirm our present conclusions [37, 38]. In the present, comparative study we have explored four different PC cell lines, two radiotracers (¹⁸F- radiolabeled choline and - FDG) and two chemotherapeutic drugs in a range of three concentrations.

Although we did not measure [¹⁸F]FCH and [¹⁸F]FDG levels before and after drug treatment, the radiotracers were supplied in excess and are therefore not supposed to be a limiting factor. Docetaxel/ cabazitaxel may contribute to an effect on the cellular uptake of [¹⁸F]FCH signal through a modulation of choline metabolism [39]. Choline transporters mediate the cellular uptake and the transport is the rate limiting step for the synthesis of phosphocholine which is enhanced in malignant transformation. Choline transporters of high and low affinity have been found in normal prostate tissue and are increased in PC [40]. Expression of choline transporters - and therefore choline uptake rate - have been described to be influenced by anticancer drugs [28, 41]. Such an effect could become visible in a decreased choline uptake per cell. Nevertheless, in the present study the choline uptake signal was correlated closely to the surviving cell numbers after treatment with docetaxel and cabazitaxel. Therefore, we conclude that interference with choline metabolism is not a confounder in the present observations.

At present, it is unknown how the increased [¹⁸F]FDG uptake after treatment in some cell lines is brought about. Especially, the overestimation of viable cell numbers by the [¹⁸F]FDG signal after chemotherapy deserves attention as it may result in a false negative interpretation of treatment efficacy. Possible explanations for an observed disjointed relationship of [¹⁸F]FDG response from viable cell numbers after chemotherapy may relate to differential effects on hexokinase and glut-1 expression [42], but mostly these effects result in decreased [¹⁸F]FDG uptake rather than the opposite. Moreover, in our present *in vitro* study we did not observe changes of glut-1 expression to explain increased [¹⁸F]FDG uptake after drug treatment. However, a very different cause for this effect in our experiments may have been found in the observed increase of cell volume after docetaxel or cabazitaxel treatment. The increased volume of such swollen cells after therapy may result in increased [¹⁸F]FDG signal per cell. The absence of these effects in the case of [¹⁸F]FCH may be related to different metabolic pathways, but this aspect has to be further investigated. Interestingly, other authors have also found increased levels of radiotracer uptake after therapy [28, 43]. Cellular stress resulting in increased cellular metabolism or otherwise increased cell permeability have been given as an explanation for a flare at 10 minutes after start of treatment [28]. A transient increase in FDG uptake has been described by Bjurberg et al. [43] followed by a rapid decrease. In general, timing of the monitoring seems to be important. In our analyses uptake of the PET tracers was measured after 3 days of drug incubation, thereby bypassing any eventual, initial flare phenomena. The observed cell number-independent increase in [¹⁸F]FDG signal, coupled to other known drawbacks of [¹⁸F]FDG PET in PC (general low

uptake, disturbing sensitivity to inflammatory processes, scar tissue and radiotherapy mediated effects) together with the proportional, observed treatment effects in [¹⁸F]FCH uptake, contribute to a preferential role rising up for [¹⁸F]FCH PET compared to [¹⁸F]FDG PET as a candidate drug response monitoring tool in PC patients.

CONCLUSIONS

Our *in vitro* data demonstrate that the cellular [¹⁸F]FCH uptake correlates well with viable tumor cell number after docetaxel and cabazitaxel for all prostate cancer cell lines, while [¹⁸F]FDG at times overestimated the cell number after drug exposure. This suggests that [¹⁸F]FCH is more accurate and therefore more suitable than [¹⁸F]FDG as a response monitoring PET tracer in chemotherapy of prostate cancer using docetaxel and cabazitaxel.

REFERENCES

1. Jemal A, Bray F, Center MM, Ferlay J, Ward E and Forman D. Global cancer statistics. *CA Cancer J Clin.* 2011;61:69–90
2. Fizazi K, Scher HI, Molina A, et al. Abiraterone acetate for treatment of metastatic castration-resistant prostate cancer: final overall survival analysis of the COU-AA-301 randomised, double-blind, placebo-controlled phase 3 study. *Lancet Oncol.* 2012;13:983–992
3. Ryan CJ, Smith MR, De Bono JS, et al. Abiraterone in metastatic prostate cancer without previous chemotherapy. *N Engl J Med.* 2013;368:138–148
4. Scher HI, Fizazi K, Saad F, et al. Increased survival with enzalutamide in prostate cancer after chemotherapy. *N Engl J Med.* 2012;367:1187–1197
5. Kantoff PW, Higano CS, Shore ND, et al. Sipuleucel-T immunotherapy for castration-resistant prostate cancer. *N Engl J Med.* 2010;363:411–422
6. Berthold DR, Pond GR, Soban F, de Wit R, Eisenberger M and Tannock IF. Docetaxel plus prednisone or mitoxantrone plus prednisone for advanced prostate cancer: updated survival in the TAX 327 study. *J Clin Oncol.* 2008;26:242–245
7. De Bono JS, Oudard S, Ozguroglu M, et al. Prednisone plus cabazitaxel or mitoxantrone for metastatic castration-resistant prostate cancer progressing after docetaxel treatment: a randomised open-label trial. *Lancet.* 2010;376:1147–1154
8. Parker C, Nilsson S, Heinrich D, et al. Alpha emitter radium-223 and survival in metastatic prostate cancer. *N Engl J Med.* 2013;369:213–223
9. Basch EM, Somerfield MR, Beer TM, et al. American Society of Clinical Oncology endorsement of the Cancer Care Ontario Practice Guideline on nonhormonal therapy for men with metastatic hormone-refractory (castration-resistant) prostate cancer. *J Clin Oncol.* 2007;25:5313–5318
10. Heidenreich A, Bastian PJ, Bellmunt J, et al. EAU guidelines on prostate cancer. Part II: Treatment of advanced, relapsing, and castration-resistant prostate cancer. *Eur Urol.* 2014;65:467–479
11. Scher HI, Morris MJ, Basch E and Heller G. End points and outcomes in castration-resistant prostate cancer: from clinical trials to clinical practice. *J Clin Oncol.* 2011;29:3695–3704
12. Lilja H, Ulmert D and Vickers AJ. Prostate-specific antigen and prostate cancer: prediction, detection and monitoring. *Nat Rev Cancer.* 2008;8:268–278
13. Wahl RL, Jacene H, Kasamon Y and Lodge MA. From RECIST to PERCIST: Evolving Considerations for PET response criteria in solid tumors. *J Nucl Med.* 2009;50 (Suppl 1):122S–150S
14. Costelloe CM, Chuang HH, Madewell JE and Ueno NT. Cancer Response Criteria and Bone Metastases: RECIST 1.1, MDA and PERCIST. *J Cancer.* 2010;1:80–92
15. Wallace TJ, Torre T, Grob M, et al. Current Approaches, Challenges and Future Directions for Monitoring Treatment Response in Prostate Cancer. *J Cancer.* 2014;5:3–24
16. Price DT, Coleman RE, Liao RP, Robertson CN, Polascik TJ and DeGrado TR. Comparison of [¹⁸F]fluorocholine and [¹⁸F]fluorodeoxyglucose for positron emission tomography of androgen dependent and androgen independent prostate cancer. *J Urol.* 2002;168:273–280
17. Morris MJ, Akhurst T, Larson SM, et al. Fluorodeoxyglucose positron emission tomography as an outcome measure for castrate metastatic prostate cancer treated with antimicrotubule chemotherapy. *Clin Cancer Res.* 2005;11:3210–3216
18. Oyama N, Hasegawa Y, Kiyono Y, et al. Early response assessment in prostate carcinoma by ¹⁸F-fluorothymidine following anticancer therapy with docetaxel using preclinical tumour models. *Eur J Nucl Med Mol Imaging.* 2011;38:81–89
19. Yu EY, Muzy M, Hackenbrach JA, et al (2011) C11-acetate and F-18 FDG PET for men with prostate cancer bone metastases: relative findings and response to therapy. *Clin Nucl Med.* 2011;36:192–198
20. Witney TH, Fortt RR and Aboagye EO. Preclinical Assessment of Carboplatin Treatment Efficacy in Lung Cancer by ¹⁸F-ICMT-11-Positron Emission Tomography. *PLoS One.* 2014;9:e91694
21. Afshar-Oromieh A, Zechmann CM, Malcher A, et al. Comparison of PET imaging with a (⁶⁸)Ga-labelled PSMA ligand and (¹⁸F)-choline-based PET/CT for the diagnosis of recurrent prostate cancer. *Eur J Nucl Med Mol Imaging.* 2014;41:11–20

22. DeGrado TR, Baldwin SW, Wang S, et al. Synthesis and evaluation of (¹⁸F)-labeled choline analogs as oncologic PET tracers. *J Nucl Med.* 2001;42:1805–1814
23. Evangelista L, Zattoni F, Guttilla A, et al. Choline PET or PET/CT and biochemical relapse of prostate cancer: a systematic review and meta-analysis. *Clin Nucl Med.* 2013;38:305–314
24. Cimitan M, Bortolus R, Morassut S, et al. [¹⁸F]fluorocholine PET/CT imaging for the detection of recurrent prostate cancer at PSA relapse: experience in 100 consecutive patients. *Eur J Nucl Med Mol Imaging.* 2006;33:1387–1398
25. Umbehr MH, Müntener M, Hany T, Sulser and Bachmann LM. The role of ¹¹C-choline and ¹⁸F-fluorocholine positron emission tomography (PET) and PET/CT in prostate cancer: a systematic review and meta-analysis. *Eur Urol.* 2013;64:106–117
26. Beheshti M, Vali R, Waldenberger P, et al. The use of F-18 choline PET in the assessment of bone metastases in prostate cancer: correlation with morphological changes on CT. *Mol Imaging Biol.* 2009;11:446–454
27. Beheshti M, Vali R, Waldenberger P, et al. Detection of bone metastases in patients with prostate cancer by ¹⁸F fluorocholine and ¹⁸F fluoride PET-CT: a comparative study. *Eur J Nucl Med Mol Imaging.* 2008;35:1766–1774
28. Müller SA, Holzapfel K, Seidl C, Treiber U, Krause BJ and Senekowitsch-Schmidtke R. Characterization of choline uptake in prostate cancer cells following bicalutamide and docetaxel treatment. *Eur J Nucl Med Mol Imaging.* 2009;36:1434–1442
29. Geldof AA, Rao BR and de Voogt HJ. Direct effects of chemotherapeutic agents on rat prostate tumor clonogenic cells. *Anticancer Res.* 1986;6:837–840
30. Oprea-Lager DE, Bijnsdorp I V, Van Moorselaar RJA, Van Den Eertwegh AJM, Hoekstra OS and Geldof AA. ABCC4 Decreases docetaxel and not cabazitaxel efficacy in prostate cancer cells in vitro. *Anticancer Res.* 2013;33:387–391
31. Bijnsdorp IV, Kruyt FA, Gokkoel S, Fukushima M and Peters GJ. Synergistic interaction between trifluorothymidine and docetaxel is sequence dependent. *Cancer Sci.* 2008;99:2302–2308
32. Mastbergen SC, Duijvenvoorden I, Versteegh RT and Geldof AA. Cell cycle arrest and clonogenic tumor cell kill by divergent chemotherapeutic drugs. *Anticancer Res.* 2000;20:1833–1838
33. Altman DG and Bland JM. Measurement in Medicine: the Analysis of Method Comparison Studies. *Stat.* 1983;2:307–317
34. Bland JM and Altman DG. Statistical methods for assessing agreement between two methods of clinical measurement. *Lancet.* 1986;1:307–310
35. Schwarzenböck S, Souvatzoglou M and Krause BJ. Choline PET and PET/CT in Primary Diagnosis and Staging of Prostate Cancer. *Theranostics.* 2012;2:318–330
36. Vrignaud P, Sérimond D, Lejeune P, et al. Preclinical antitumor activity of cabazitaxel, a semisynthetic taxane active in taxane-resistant tumors. *Clin Cancer Res.* 2013;19:2973–2983
37. Schwarzenböck S, Sachs D, Souvatzoglou M, et al. [¹⁴C]choline as a pharmacodynamic marker for docetaxel therapy. Response assessment in a LNCaP prostate cancer xenograft mouse model]. *Nuklearmedizin.* 2013;52:141–147
38. Krause BJ, Souvatzoglou M, Herrmann K, et al. [¹⁴C]Choline as pharmacodynamic marker for therapy response assessment in a prostate cancer xenograft model. *Eur J Nucl Med Mol Imaging.* 2010;37:1861–1868
39. Jensen LR, Huuse EM, Bathen TF, et al. Assessment of early docetaxel response in an experimental model of human breast cancer using DCE-MRI, ex vivo HR MAS, and in vivo ¹H MRS. *NMR Biomed.* 2010;23:56–65
40. Awwad HM, Geisel J and Obeid R. The role of choline in prostate cancer. *Clin Biochem.* 2012;45:1548–1553
41. Taguchi C, Inazu M, Saiki I, et al. Functional analysis of [methyl-(³H)choline uptake in glioblastoma cells: Influence of anti-cancer and central nervous system drugs. *Biochem Pharmacol.* 2014;88:303–312
42. Engles JM, Quarless SA, Mambo E, Ishimori T, Cho SY and Wahl RL. Stunning and its effect on ³H-FDG uptake and key gene expression in breast cancer cells undergoing chemotherapy. *J Nucl Med.* 2006;47:603–608
43. Bjurberg M, Henriksson E, Brun E, et al. Early changes in 2-deoxy-2-[¹⁸F]fluoro-D-glucose metabolism in squamous-cell carcinoma during chemotherapy in vivo and in vitro. *Cancer Biother Radiopharm.* 2009;24:327–332



CHAPTER 4

Quantification of [¹⁸F]fluoromethylcholine kinetics in patients with prostate cancer

Eline E. Verwer^{1*}

Daniela E. Oprea-Lager^{1*}

Alfons J.M. van den Eertwegh²

Reindert J.A. van Moorselaar³

Albert D. Windhorst¹

Lothar A. Schwarte⁴

N. Harry Hendrikse¹

Robert C. Schuit¹

Otto S. Hoekstra¹

Adriaan A. Lammertsma¹

Ronald Boellaard¹

¹Department of Radiology and Nuclear Medicine, VU University Medical Center, Amsterdam, the Netherlands

²Department of Medical Oncology, VU University Medical Center, Amsterdam, the Netherlands

³Department of Urology, VU University Medical Center, Amsterdam, the Netherlands; ⁴Department of Anesthesiology, VU University Medical Center, Amsterdam, the Netherlands

* Contributed equally to this work

ABSTRACT

Choline kinase is upregulated in prostate cancer (PC), resulting in increased [¹⁸F]fluoromethylcholine ([¹⁸F]FCH) uptake. This study used pharmacokinetic modeling to validate the use of simplified methods for quantification of [¹⁸F]FCH uptake in a routine clinical setting.

METHODS

Forty-minute dynamic PET/CT scans were acquired after injection of 204 ± 9 MBq [¹⁸F]FCH, from eight patients with histologically proven metastasized PC. Plasma input functions were derived using continuous arterial blood sampling (BSIF) as well as using image-derived (IDIF) methods. Manual arterial blood samples were used for calibration and correction for plasma-to-blood ratio and metabolites. Time activity curves (TAC) were derived from volumes of interest (VOI) in all visually detectable lymph node metastases (LNM). [¹⁸F]FCH kinetics were studied by non-linear regression fitting of several single- and two-tissue plasma input models to the TAC. Model selection was based on Akaike information criterion (AIC) and measures of robustness. In addition, the performance of several simplified methods, such as standardized uptake value (SUV), was assessed.

RESULTS

Best fits were obtained using an irreversible compartment model with blood volume parameter. Parent fractions were 0.12 ± 0.4 after 20 min, necessitating individual metabolite corrections. Correspondence between venous and arterial parent fractions was low as determined by the intraclass correlation coefficient (ICC = 0.61). Results for IDIF derived from VOI in blood pool structures distant from tissues of high [¹⁸F]FCH uptake, yielded good correlation to those for BSIF ($R^2 = 0.83$). SUV showed poor correlation to parameters derived from full quantitative kinetic analysis ($R^2 < 0.34$). In contrast, lesion activity concentration normalized to the integral of the blood activity concentration over time (SUV_{AUC}) showed good correlation ($R^2 = 0.92$ for metabolite corrected plasma and $R^2 = 0.65$ for whole-blood activity concentrations).

CONCLUSION

SUV cannot be used to quantify [¹⁸F]FCH uptake. A clinical compromise could be SUV_{AUC} derived from two consecutive static PET scans, one centered on a large blood pool structure during 0-30 min after injection to obtain the blood activity concentrations and the other a whole-body scan at 30 min after injection to obtain lymph node activity concentrations.

INTRODUCTION

Prostate cancer (PC) is one of the most commonly diagnosed neoplasms in men worldwide and incidence is increasing [1]. Accurate diagnostic procedures are essential, because therapeutic options vary greatly with extent of the disease [1, 2]. Conventional imaging techniques, including transrectal ultrasound, computed tomography (CT) and magnetic resonance imaging are used routinely in PC, but their diagnostic accuracy is suboptimal [3].

Positron emission tomography (PET) provides a sensitive and accurate non-invasive method to study metabolic activity of tumor tissue *in vivo*. The most commonly used oncological PET tracer, fluorodeoxyglucose (¹⁸F-FDG), shows limited sensitivity for the detection of androgen dependent PC [4]. In contrast, encouraging results have been published using both ¹¹C and ¹⁸F labeled choline derivatives as PET tracers for PC [5–9].

The amino acid choline is an important precursor for the biosynthesis of phosphatidylcholine, a key component of the cell membrane phospholipids. Following transport into the cell, choline is phosphorylated by choline kinase to phosphocholine and trapped within the cell [10]. Most types of cancer, including PC, are characterized by increased choline transport and over-expression of choline kinase, in response to enhanced demand of phosphatidylcholine in highly proliferating cells [6, 11].

Because of its longer half-life [12], ¹⁸F-labeled choline is more suitable for routine clinical use than ¹¹C-labeled choline. At present, ¹⁸F-fluoromethylcholine ([¹⁸F]FCH) is used mainly for restaging of PC in case of biochemical relapse. As uptake of [¹⁸F]FCH should reflect viable tumor tissue, changes over time may serve as a measure of response to therapy. For monitoring response to systemic treatment in metastasized PC, however, accurate quantification is required.

To date, [¹⁸F]FCH biodistribution has been assessed with encouraging results [13–16], but full kinetic analysis has not yet been reported. In the present study, pharmacokinetic modeling of dynamic PET data, in combination with arterial blood sampling, was used to determine the appropriate plasma input compartment model for [¹⁸F]FCH. In addition, the validity of using an image-derived input function in combination with manual venous blood samples instead of arterial blood sampling was investigated and the validity of using simplified methods for quantification of [¹⁸F]FCH was assessed.

MATERIALS AND METHODS

Patients

Eight patients with histologically proven PC with lymphatic and/or haematogeneous metastases were included. Inclusion criteria were presence of at least 2 metastases (diameter ≥ 1.5 cm) and ability to remain supine for 50 min. Exclusion criteria were claustrophobia, multiple malignancies and anticoagulant therapy. The study was approved by the Medical Ethics Review Committee of the VU University Medical Center. Prior to inclusion, each patient signed a written informed consent after receiving verbal and written explanation.

Synthesis of [^{18}F]fluoromethylcholine

[^{18}F]FCH was synthesized according to the methods proposed by DeGrado et al. [6] with minor modifications and by use of automated modules [17]. Details are given in supplemental data 1.

Data acquisition

Each patient received a low dose CT (50 mAs, 120 kVp), followed by a 40-min dynamic PET scan with the field of view (FOV) centered over the largest metastases (abdominal region: $n = 5$; lung area: $n = 3$), on a Gemini TF-64 PET/CT (Philips Medical Systems, Cleveland, Ohio, USA). At the start of the PET scan a bolus injection of approximately 204 ± 9 MBq [^{18}F]FCH (specific activity 94.9 ± 65.7 GBq· μmol^{-1}) was administered intravenously using an automated injector (Medrad, Pittsburgh, USA) and flushed with 40 mL of saline (5 mL at $0.8 \text{ mL}\cdot\text{s}^{-1}$ followed by 35 mL at $2 \text{ mL}\cdot\text{s}^{-1}$).

PET data were normalized and corrected for attenuation, dead time, randoms, scatter and decay, and reconstructed into 34 frames ($1 \times 10, 8 \times 5, 4 \times 10, 3 \times 20, 5 \times 30, 5 \times 60, 4 \times 150, 4 \times 300$ s) with a matrix size of $144 \times 144 \times 45$ voxels ($4 \times 4 \times 4 \text{ mm}^3$) using a 3-dimensional row action maximum likelihood reconstruction algorithm (3D-RAMLA) [18].

Arterial blood activity concentration over time was determined by continuous arterial blood sampling ($5 \text{ mL}\cdot\text{min}^{-1}$ for 5 min, $2.0 \text{ mL}\cdot\text{min}^{-1}$ thereafter) using an automated blood sampling device [19] connected to a cannula inserted into the radial artery. At 6 time points (5, 10, 15, 20, 30 and 40 min after injection) manual arterial blood samples were collected, while the blood sampler operation was briefly paused. In addition, manual venous blood samples were collected at 5, 15 and 30 min after injection. After each sample, the cannula was flushed with heparinized saline to prevent clotting.

Each manual sample was analyzed for whole-blood activity concentration, plasma-to-whole blood ratio and presence of radiolabeled metabolites in plasma. After plasma protein extraction, metabolite analysis was performed on the remaining plasma (extraction efficiency of 88%) using a method based on Sutinem et al. [11] involving high performance liquid chromatography.

Kinetic analysis

In pharmacokinetic modeling, tracer kinetics are assumed to be separable into compartments that are connected in series to the arterial blood compartment, represented by the plasma input function, by (transport) rate constants. For example, in the irreversible two-tissue compartment model (2T₃k) the first compartment often represents tracer free in tissue while the second represents irreversible specific uptake. From the rate constants connecting the compartments, the net influx rate for the second compartment can be calculated: $K_i = K_1 k_3 / (k_2 + k_3)$. The supplemental data 2 provides more details on each of the models and associated quantification parameters.

Metabolite-corrected blood sampler plasma input functions (BSIF) were derived from blood sampler data (corrected for intermittent reductions in counts associated with saline flushes), calibrated using whole-blood activity concentrations measured from manual arterial blood samples. In addition, data were multiplied by the plasma-to-blood ratio curves and parent fraction curves derived from manual arterial blood samples using a single exponential fit and Watabe fit [20], respectively, and corrected for delay [21]. Metabolite corrected image-derived plasma input functions (IDIF) were derived from volumes of interest (VOIs) (2.85 ± 1.65 mL; range: 0.64-5.89 mL) defined manually on an early PET frame most clearly displaying the blood pool (Figure 1A), within the largest arterial blood pool structures available (left ventricle or aortic, femoral or iliac arteries). These VOIs were then projected onto the dynamic PET scan to derive time activity curves (TAC), which were processed in the same fashion as BSIF.

TACs were derived from several tissue VOIs. Lesion VOIs were defined using a 50% threshold technique with background correction, in all metastatic lymph nodes that were clearly visible on the averaged PET image over 25-40min after injection (24 in total; 4.76 ± 3.54 mL; range: 0.7-12.8 mL). Healthy tissue VOI were manually defined using the lowdose CT (muscle, fat, liver).

Several standard compartment models were then fitted to the lesion TAC using standard non-linear regression analysis (NLR) routines [22], with both BSIF or IDIF as input functions. Models evaluated were the general irreversible and reversible single-tissue compartment models ($1T1k$ and $1T2k$, respectively) and the irreversible and reversible two-tissue compartment models ($2T3k$ and $2T4k$, respectively). To account for contribution of blood activity concentrations to the tissue TAC, performance of all models was evaluated with and without blood volume parameter (V_B). Boundary conditions for all estimated kinetic parameters were determined after multiple runs (K_1 : [0, 3], k_2 : [0, 2], k_3/k_4 : [0, 10] and V_B : [0, 1]). Fits with low precision (as indicated by $SE > 500\%$ in at least one of the estimated rate constants) were considered unsuccessful and excluded from further analysis. Robustness of the model was evaluated as the percentage of successfully fitted lesion time-activity curves.

Validation

Model selection. The model providing the best fits to the lesion time–activity curves was selected on the basis of the Akaike information criterion (AIC) for small sample sizes [23] and model robustness. In clinical practice, lengthy (dynamic) scanning procedures are less attractive. Therefore, the minimal scan duration required to derive accurate results was assessed by comparing relevant uptake parameters resulting from kinetic modeling of parts of the dynamic scan (0–5 min, 0–10 min, 0–15 min, 0–20 min, 0–25 min or 0–30 min after injection) with those of the full dynamic scan (0–40 min after injection).

Alternatives to arterial blood sampling. Deriving an accurate plasma input function requires insertion of an arterial cannula, automated blood sampling and specialist metabolite analysis. As these methods may not be feasible in a routine clinical setting, the validity of using IDIF instead of BSIF as well as the need for manual arterial or venous blood samples, were assessed.

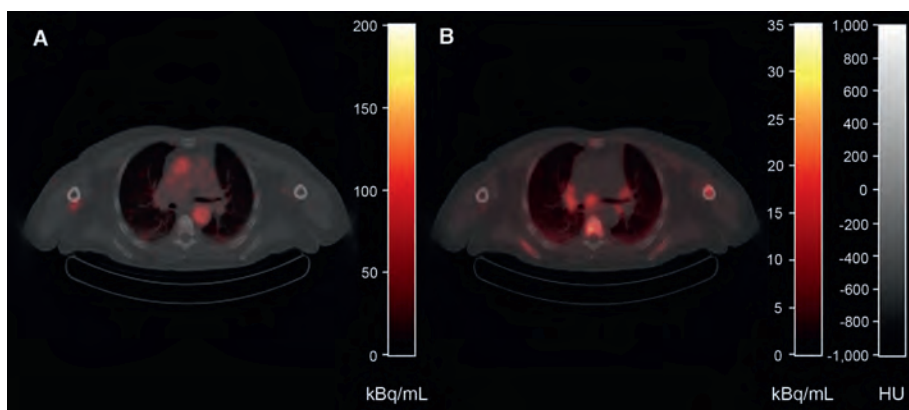
Simplified methods. Once validated, simplified methods can provide estimates of relevant uptake parameters using a far simpler imaging protocol than that required for full kinetic modeling. Therefore, performance of several simplified measures was evaluated, for example, lesion-to-muscle ratio (LMr), lesion-to-blood ratio (LBr) and standardized uptake value (SUV) for several normalization factors: body weight (BW), body surface area (BSA), lean body mass (LBM), body mass index (BMI) and ideal body weight (IBW).

RESULTS

Patients

Eight patients diagnosed with PC were included: age 66 ± 8 y, weight 89 ± 12 kg, height 185 ± 7 cm, T-stage ≥ 2 , Gleason score 7 ($n = 2$) or 9 ($n = 6$) and high PSA at the time of PET/CT imaging (113 ± 91 ng/ml). Patients were previously treated by prostatectomy ($n = 4$) or external beam radiotherapy on the prostate in combination with anti-hormonal therapy ($n = 4$). Three patients were receiving therapy at the time of PET/CT imaging: luteinizing hormone-releasing hormone (LHRH) antagonists, oral androgen receptor inhibitor Enzalutamide and dendritic cell therapy, respectively. Figure 1 shows typical [¹⁸F]FCH PET/CT images. Two typical examples of acquired blood activity concentrations are shown in Figure 2.

Figure 1. Typical example of PET/CT images acquired from patient diagnosed with PC. Shown are low-dose CT (gray scale) fused with early PET image acquired from 35 to 40 s after injection displaying blood pool (A) and averaged image over 25–40 min after [¹⁸F]fluoromethylcholine injection (B) (color).



Validation

Model selection. Typical tissue TACs are shown in Figure 3A. Figure 3B shows the same lesion TAC with associated nonlinear regression analysis fits. AIC results indicate irreversible kinetics, with $2T_3k+V_B$ producing the best fits (preferred model in 7/24 lesion TAC), followed by the simpler irreversible model $2T_3k$ (7/24) and $1T_1k+V_B$ (5/24).

Figure 2. Two typical examples of measured whole-blood time–activity curves for patient imaged over thorax region (A) and patient imaged over abdominal region (B). Lines represent calibrated blood sampler data; dashed lines (image-derived) aortic arch; dash-dot lines (image-derived) abdominal descending aorta; triangles manual arterial blood samples; squares manual venous blood samples.

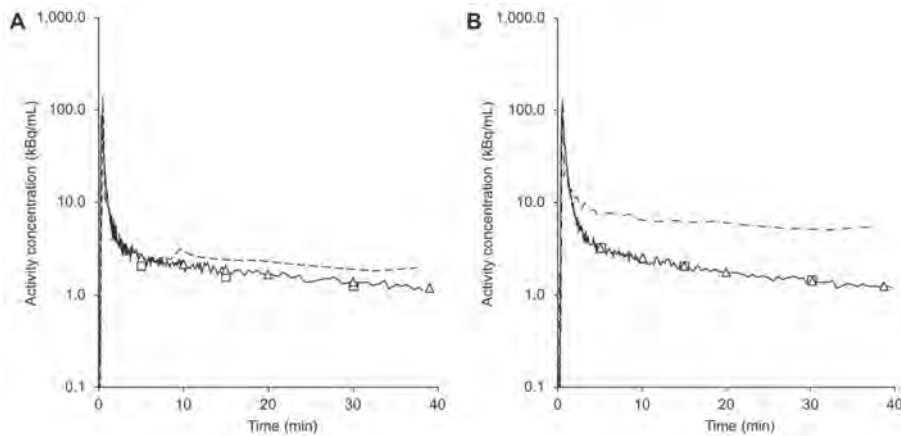
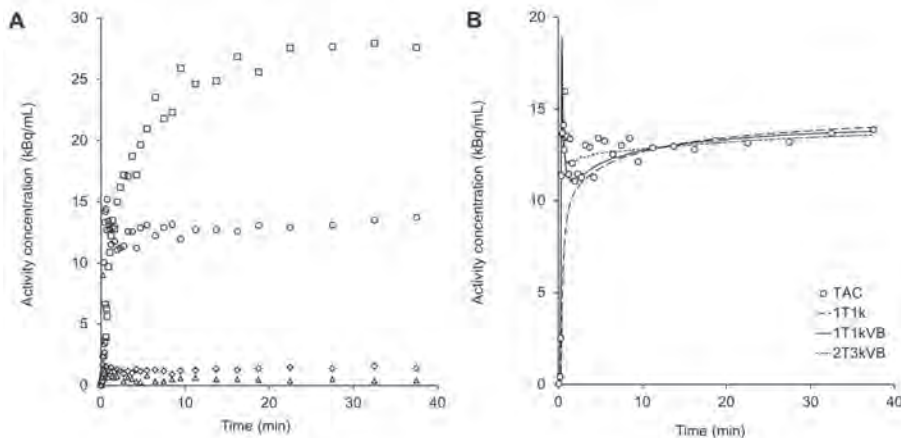


Figure 3. (A) Typical measured time–activity curves for the same patient shown in Figure 1. Square represents liver, circle lesion, diamond muscle and triangle fat tissue. (B) Nonlinear regression fits to lesion time–activity curve displayed in A, using various compartment models.



However, as displayed in Table 1, 2T3k+V_B was less robust than 1T1k+V_B whereas correspondence between respective quantification parameters was excellent ($R^2=0.96$; $ICC=0.94$; Table 2) and remained so even for K_1 derived from shorter scan durations ($R^2>0.92$; $ICC>0.89$; $SE[K_1<5\%]$; for scan durations $>20\text{min}$).

Table 1. Comparing scan durations.

Parameter (model)	Scan duration (min)	Robustness (%)	Slope	Linear regression analysis		
				Intercept	R ²	ICC*
K _i (1T1k+V _B)	5	100	0.98	0.05	0.82	0.84
	10	100	0.98	0.03	0.94	0.95
	15	100	0.99	0.02	0.97	0.98
	20	100	1.01	0.01	0.99	0.99
	30	100	1.00	0.00	1.00	1.00
K _i (2T3k+V _B)	5	60	0.82	0.09	0.59	0.75
	10	65	0.93	0.03	0.97	0.98
	15	75	1.07	-0.02	0.94	0.97
	20	75	1.05	-0.01	0.90	0.95
	30	80	1.03	-0.01	1.00	1.00

Results for comparison of quantification parameters from short scan durations derived from full 40/min dynamic scan

Table 2. Comparing 1T1k+V_B to 2T3k+V_B.

Scan duration (min)	Linear regression analysis			
	Slope	Intercept	R ²	ICC*
5	0.98	0.09	0.69	0.65
10	0.98	0.07	0.82	0.79
15	1.01	0.05	0.88	0.85
20	1.03	0.03	0.92	0.89
30	1.04	0.02	0.95	0.93
40	1.04	0.02	0.96	0.94

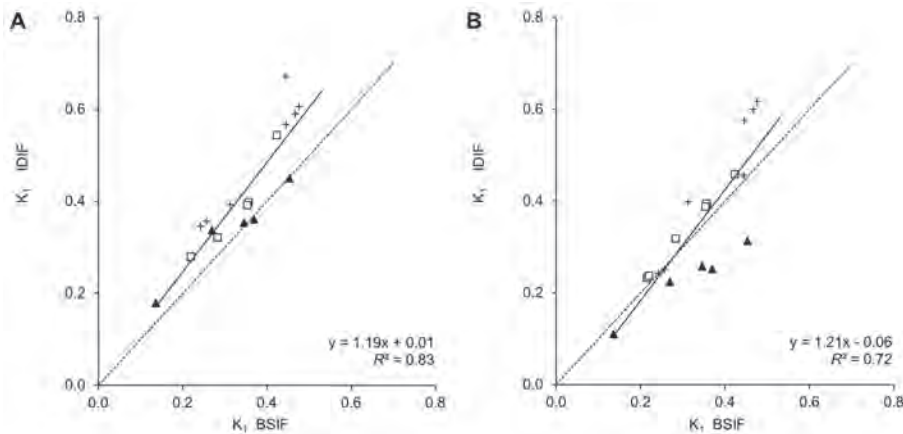
*Comparison of K_i derived with 1T1k+V_B for various scan durations to K_i derived with 2T3k+V_B from full 40-min dynamic scan.

It is therefore conceivable that K_i can be substituted by K_i produced by the 1T1k+V_B model without loss of accuracy. Therefore, in the validation analysis presented in this article, K_i produced by full kinetic modeling with 1T1k+V_B for the 40-min dynamic PET scan will be used as reference. One patient was excluded because this patient's estimated K_i values were outside the expected physiologic range (see the "Discussion" section). For the sake of completeness, the supplemental data 3 show the results for 2T3k+V_B.

Alternatives to arterial blood sampling. IDIFs overestimate whole-blood activity concentrations at later time points, compared to BSIF (as illustrated in Figure 2), most markedly when derived from VOI located near high [¹⁸F]FCH uptake structures, such as the liver (Figure 2B) or kidneys. Figure 4 shows nonlinear regression analysis results

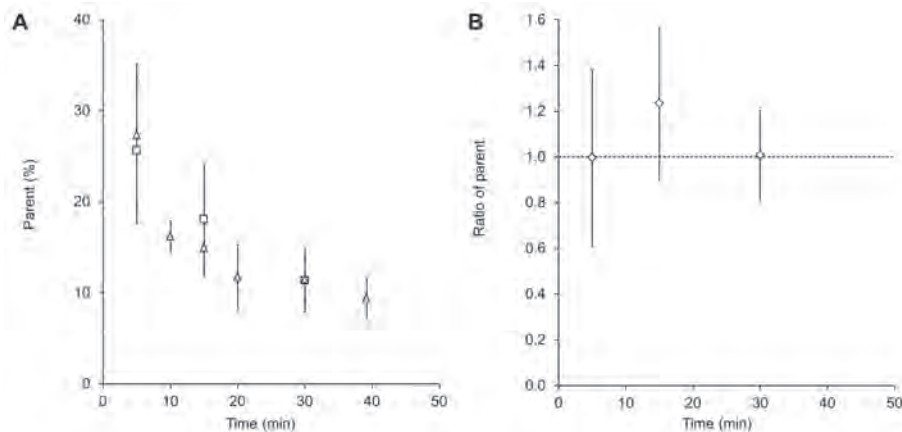
using IDIF derived from VOIs in blood structures located away from the liver or kidneys only, compared with those using BSIFs.

Figure 4. K_t obtained using $1T1k+V_B$ with (A) calibrated and (B) noncalibrated IDIF derived compared with BSIF method. Symbols indicate IDIF origin: triangle aortic arch, square descending aorta, plus femoral artery.



To minimize calibration errors due to possible overestimation at late time points, calibration of IDIF was performed at approximately 500–1,500 s after injection. For one patient, imaged over the abdominal region, no suitable IDIF could be found because marked overestimation of blood activity concentrations was observed all along the descending aorta. Good correlation was found for calibrated IDIFs (calibration factor 0.82 ± 0.13), although a bias was observed ($R^2 = 0.83$, slope = 1.19; ICC = 0.74). Figure 4B shows results for noncalibrated IDIFs ($R^2 = 0.72$; ICC = 0.80). Input function correction based on venous blood samples was not equivalent to correction based on arterial blood samples. Although good correspondence was found for whole-blood activity concentrations at late time points, and for plasma-to-blood ratios (ICC = 0.89; supplemental data 4), parent fraction measures were significantly different (ICC = 0.61; Figure 5).

Figure 5. Manual blood sample data as function of time: (A) mean parent fractions (triangle arterial, square venous) and (B) ratio of venous to arterial parent fractions. Error bars represent \pm SD.



Simplified methods. Correlation between SUV (35-40 min after injection) en K_1 was poor (Table 3; Figure 6A) with $R^2 < 0.34$, irrespective of the normalization factor used. LMr (35-40 min after injection; Figure 6B) and LBr (35-40 min p.i) performed somewhat better ($R^2 = 0.50$ and $R^2 = 0.44$, respectively).

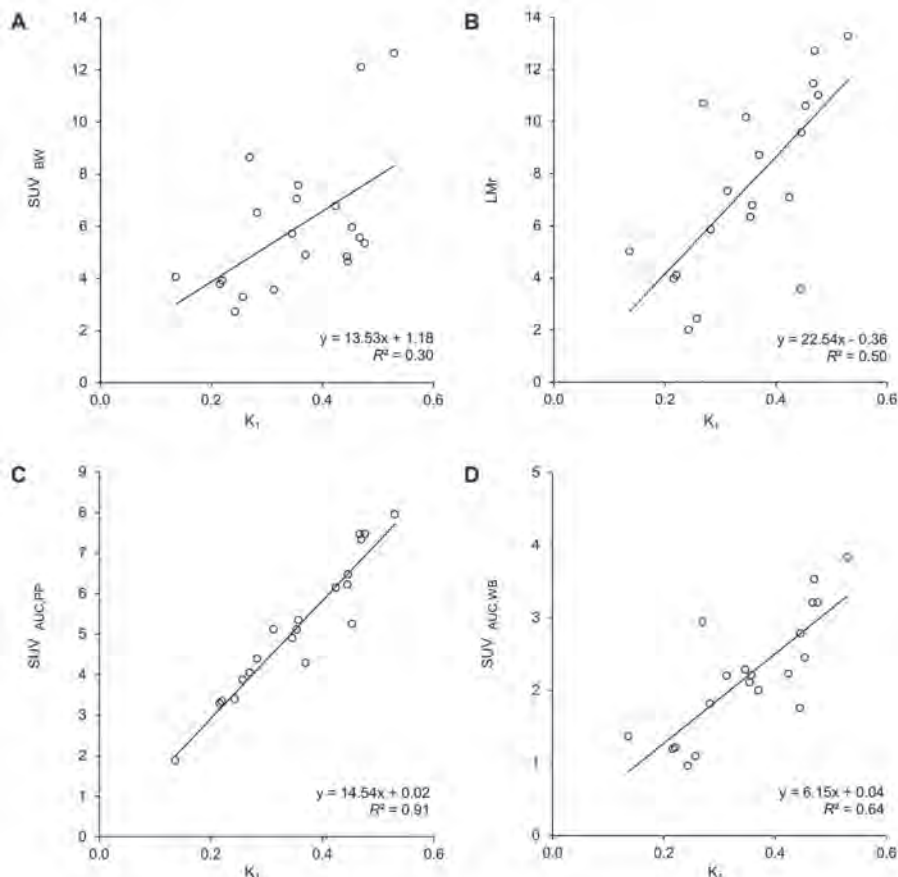
Table 3. Comparison of simplified parameters to K_1 resulting from full kinetic modeling with $1T1k+V_B$.

Simplified parameter	Linear regression analysis		
	Slope	Intercept	R^2
SUV_{BW}	13.53	1.18	0.30
SUV_{BSA}	315.39	27.53	0.33
SUV_{LBM}	9.02	0.86	0.32
SUV_{BMI}	4.65	0.20	0.34
SUV_{IBW}	10.96	1.28	0.31
LMr	22.54	-0.36	0.50
LBr	30.38	0.32	0.44
$SUV_{AUC,WB}$	5.88	-0.02	0.65
$SUV_{AUC,PP}$	14.73	-0.20	0.92

SUV_{BW} = SUV normalized to body weight; SUV_{BSA} = SUV normalized to body surface area; SUV_{LBM} = SUV normalized to lean body mass; SUV_{BMI} = SUV normalized to body mass index; SUV_{IBW} = SUV normalized to ideal body weight; LMr=lesion to muscle ratio; LBr=lesion to blood ratio; $SUV_{AUC,WB}$ =SUV whole-blood area under the curve; $SUV_{AUC,PP}$ =SUV parent plasma area under the curve.

In contrast, $SUV_{AUC,PP}$ calculated by dividing lesion activity concentrations (35-40 min after injection) by cumulative delivery, that is, the area under curve (AUC) of the parent plasma input function (0-40 min after injection), provided an excellent correlation to K_1 ($R^2 = 0.92$). This correlation reduced to R^2 of 0.65 when using whole-blood AUC rather than parent plasma AUC ($SUV_{AUC,WB}$). SUV_{AUC} calculated from lesion activity concentrations at 30-40 min after injection and AUC over 0-30 min after injection resulted in similar correlations: an R^2 of 0.91 for $SUV_{AUC,PP}$ (Figure 6C) and 0.64 for $SUV_{AUC,WB}$ (Figure 6D), respectively. Good correspondence was found between SUV_{AUC} derived from BSIF and SUV_{AUC} derived from IDIF (calibrated: $R^2 = 0.98$; ICC = 0.93; non-calibrated: $R^2 = 0.86$; ICC = 0.91).

Figure 6. Correlation between simplified uptake measures and K_1 ($1T1k1VB$). (A) SUV normalized to body weight (SUV_{BW}), (B) LMr and lesion activity concentration in kBq at 30-40 min after injection divided by AUC of parent plasma (C), and whole-blood activity concentration (D) in MBq over 0-30 min ($SUV_{AUC,PP}$ and $SUV_{AUC,WB}$, respectively).



DISCUSSION

This study focused on pharmacokinetic analysis of [¹⁸F]FCH in PC metastases and investigated the validity of strategies to simplify acquisition and analysis, to enable quantification of [¹⁸F]FCH uptake in a routine clinical setting.

On the basis of AIC alone, [¹⁸F]FCH kinetics in PC lymph node metastases could best be described using a $2T_3k + V_B$ model. However, the fitting procedure proved nonrobust, particularly for shorter scan durations (as shown in Table 1). We hypothesize that this is caused by the rapid uptake in combination with limited efflux to the blood pool (k_2). This renders the model unable to accurately distinguish K_1 and k_3 , which also explains why $1T_1k + V_B$ yielded similar results ($R^2 = 0.96$; $ICC = 0.94$). This also explains why $1T_1k + V_B$ yielded similar results ($R^2 = 0.96$; $ICC = 0.94$). This indicates that, even though AIC selected $2T_3k + V_B$, $1T_1k + V_B$ can be used without loss of quantification accuracy. Moreover, $1T_1k + V_B$ results were more robust and consistent for shorter scan durations, indicating this to be the most suitable model.

An additional issue arising from the fast kinetics observed for [¹⁸F]FCH is inability of either model to accurately distinguish between the first tissue compartment (influx K_1 and efflux k_2) and signal originating from blood volume in the VOI. High V_B areas were therefore excluded.

One patient was excluded as K_1 estimates were found to be unrealistically high ($K_1 > 1$) using either irreversible model. We hypothesize this may be the result of high lesion blood volume fraction; despite our efforts to exclude large blood volume structures, as described previously, V_B estimates were 0.49 ± 0.05 . As rapid lesion uptake occurs, delayed arrival of blood activity concentrations in blood pool structures may have rendered them visually indistinguishable from lesion tissue. Another explanation may be markedly different kinetics in this patient, leading to inaccurate estimates caused by using the wrong model. We were unable to verify or reject either hypothesis based on the available data. Interestingly, all lesions were located within the mediastinum. In the rest of the study population, 3 out of 4 mediastinal lesions also showed increased V_B estimates (0.23 ± 0.11 compared to 0.08 ± 0.05 for all other lesions studied). Also of interest is that this particular patient had received an experimental type of therapy (dendritic cell therapy; up to 1 month prior to the PET/CT scan). Because many patients eligible for [¹⁸F]FCH PET will receive some form of therapy, the possible influence of drugs on [¹⁸F]FCH kinetics should be investigated. For example, it has been suggested

that androgen deprivation therapy (ADT), a pharmaceutical used to maintain the biochemical castration level in recurrent PC, causes decreased choline uptake in hormone-sensitive PC in various studies [24]. In the present study, one patient was on ADT during the scan. Nevertheless, results were consistent with the rest of the study population, indicating negligible influence on $[^{18}\text{F}]$ FCH uptake for this patient.

Having determined the kinetic model and relevant quantification parameter, the possibilities for simplifying the acquisition protocol and analysis methods were investigated, i.e. alternatives for deriving plasma input functions as well as the validity of using simplified methods for quantification.

For several blood VOI locations, overestimation of blood activity concentrations was observed (for this reason 1 patient could not be analyzed with IDIF). We hypothesize that the apparent increase in image-derived blood activity concentrations near high $[^{18}\text{F}]$ FCH uptake structures is caused by incorrect scatter correction in these areas, possibly leading to large quantification errors with IDIFs derived from blood VOIs in these areas. For other blood VOI, however, good correspondence was found for results with IDIF and BSIF ($R^2 = 0.83$ and $ICC = 0.74$ for calibrated IDIF). The observed 19% bias was mainly caused by results for IDIF originating from small (femoral) arteries (Figure 4), indicating that these may not be suitable for deriving IDIF. In summary, IDIF derived from *large* blood pool structures located away from high-uptake structures, such as the aortic arch, can substitute continuous arterial blood sampling. Unfortunately, manual arterial blood samples and specialized lab analysis remain necessary as parent fractions are greatly reduced shortly after injection and variability between patients is high ($12 \pm 4\%$ at 20 min after injection; Figure 5). Parent fractions measured from venous blood showed low correspondence to those obtained from arterial blood samples.

High metabolite formation rates may also complicate quantification when radiolabeled metabolites enter tissue. Main metabolite is betaine, an organic osmolyte [10]. Because the presence of ^{18}F -betaine will not be specific to lesions and LMr as high as 7.84 ± 3.15 were observed (Figure 6B), it is unlikely that radiolabeled betaine significantly affected observed lesion activity concentrations.

A major simplification of the imaging protocol would be to use simplified methods instead of full kinetic modeling. Simplified methods, such as SUV, however, do not take into account possible influences on quantification by, for example, V_b and metabolite

formation. Therefore, results obtained using simplified methods were compared to those obtained with full kinetic modeling. Commonly used simplified methods showed poor correlation to results from full kinetic modeling (SUV, $R^2 < 0.34$; LMr, $R^2 = 0.50$; LBr, $R^2 = 0.44$). We hypothesize that as [¹⁸F]FCH kinetics is very rapid and irreversible, even late-time lesion activity concentrations will depend heavily on the AUC of the plasma input function, a characteristic not accounted for in commonly used simplified methods. SUV_{AUC} performs better because it incorporates information from the input function itself ($R^2 = 0.92$ for SUV_{AUC,PP} and $R^2 = 0.65$ for SUV_{AUC,WB}).

In a routine clinical setting, static imaging would be preferable. Whole-blood AUC can be image-derived directly from a static PET image acquired over 0-40 min after injection ($R^2 = 0.98$), from a VOI within the aortic arch defined using the lowdose CT. However, simultaneous imaging of both the lesions and the aortic arch will be impossible in the majority of patients, as the typical metastatic pattern of PC usually involves the pelvic or abdominal region. Therefore, SUV_{AUC} was also validated when obtained from two consecutive time intervals: AUC over 0-30 min after injection and lesion activity concentrations averaged over 30-40 min after injection ($R^2 = 0.91$ for metabolite-corrected plasma data, and 0.64 for whole-blood data). As lesion activity concentrations appear stable from 10 min onward, the latter can also be obtained with a whole-body PET scan. To obtain SUV_{AUC,PP} arterial blood sampling and analysis would be required. It should also be noted that with the proposed static imaging protocol, VOIs cannot be adjusted to exclude high-V_B areas because for this purpose an early PET image over the lesion is required. Apart from aforementioned modeling issues, high V_B causes underestimation in simplified parameters. We therefore recommend caution when evaluating lesions near arterial structures until the clinical impact of these potential errors has been fully investigated.

Characteristics such as metabolism, perfusion and blood volume fraction are likely to change over the course of therapy. Therefore, the performance of the parameters presented in this paper should be verified in test-retest and longitudinal trials, before they can be validated or disqualified for application in a clinical (response monitoring) setting. Should [¹⁸F]FCH metabolism remain constant throughout the response monitoring study, performance of SUV_{AUC,WB} and to a lesser extent SUV may be equivalent to SUV_{AUC,PP} as a relative measure of response. Challapalli et al. recently reported on a novel ¹⁸F-labeled choline tracer that metabolizes less rapidly than [¹⁸F]FCH, with parent fractions gradually decreasing to approximately 0.3 over the first hour

after injection [25–26]. With decreased inter-patient variability in parent fractions, performance of SUV and $\text{SUV}_{\text{AUC,WB}}$ may improve with respect to $\text{SUV}_{\text{AUC,PP}}$

CONCLUSION

^{18}F -fluoromethylcholine uptake should be quantified using full kinetic modeling with $1\text{T1k}+\text{V}_\text{B}$ and metabolite-corrected plasma input function based on arterial blood sampling. Results indicate that SUV cannot be used to estimate $[^{18}\text{F}]$ FCH uptake. A clinically feasible alternative could be $\text{SUV}_{\text{AUC,WB}}$ based on two consecutive static PET scans. Further studies are needed to substantiate these findings.

ACKNOWLEDGEMENTS

The authors would like to thank our colleagues at the Department of Radiology & Nuclear Medicine involved in tracer production and data acquisition for this study. We are also grateful to the urologists from VUmc (Dr. André N. Vis), Amstelland Hospital Amstelveen (Dr. Cobi Reisman, Dr. Joop W. Noordzij) and Medical Center Alkmaar (Dr. Ton A. Roeleveld) as well as the VUmc oncologists (Dr. Jens Voortman, Dr. Marije M. Vleugel, Dr. Liselot Wertenbroek, Dr. Maurice J.D.L. van der Vorst) for their contribution to patient selection and inclusion.

REFERENCES

- Bray F, Lortet-Tieulent J, Ferlay J, Forman D and Auvinen A. Prostate cancer incidence and mortality trends in 37 European countries: an overview. *Eur J Cancer*. 2010;46:3040–3052
- Heidenreich A, Bastian PJ, Bellmunt J, et al. EAU guidelines on prostate cancer. part 1: screening, diagnosis, and local treatment with curative intent-update 2013. *Eur Urol*. 2014;65:124–137
- Schwarzenböck S, Souvatzoglou M and Krause BJ. Choline PET and PET/CT in primary diagnosis and staging of prostate cancer. *Theranostics*. 2012;2:318–330
- Price DT, Coleman RE, Liao RP, Robertson CN, Polascik TJ and DeGrado TR. Comparison of [¹⁸F]fluorocholine and [¹⁸F]fluorodeoxyglucose for positron emission tomography of androgen dependent and androgen independent prostate cancer. *J Urol*. 2002;168:273–280
- Bauman G, Belhocine T, Kovacs M, Ward A, Beheshti M and Rachinsky I. ¹⁸F-fluorocholine for prostate cancer imaging: a systematic review of the literature. *Prostate Cancer Prostatic Dis*. 2012;15:45–55
- DeGrado TR, Baldwin SW, Wang S, et al. Synthesis and evaluation of (¹⁸F)-labeled choline analogs as oncologic PET tracers. *J Nucl Med*. 2001;42:1805–1814
- Fuccio C, Rubello D, Castellucci P et al. Choline PET/CT for prostate cancer: main clinical applications. *Eur J Radiol*. 2011;80:e50–e56
- Picchio M, Briganti A, Fanti S, et al. The role of choline positron emission tomography/computed tomography in the management of patients with prostate-specific antigen progression after radical treatment of prostate cancer. *Eur Urol*. 2011;59:51–60
- Reske SN, Blumstein NM, Neumaier B, et al. Imaging prostate cancer with ¹¹C-choline PET/CT. *J Nucl Med*. 2006;47:1249–1254
- Rovainen A, Forsback S, Gronroos T, et al. Blood metabolism of [methyl-¹¹C]choline; implications for in vivo imaging with positron emission tomography. *Eur J Nucl Med*. 2000;27:25–32
- Sutinen E, Nurmi M, Rovainen A, et al. Kinetics of (¹¹C)Choline uptake in prostate cancer: a PET study. *Eur J Nucl Med Mol Imaging*. 2004;31:317–324
- Jadvar H. Prostate cancer: PET with ¹⁸F-FDG, ¹⁸F- or ¹¹C-acetate, and ¹⁸F- or ¹¹C-choline. *J Nucl Med*. 2011;52:81–89
- DeGrado TR, Reiman RE, Price DT, Wang S and Coleman RE. Pharmacokinetics and radiation dosimetry of ¹⁸F-fluorocholine. *J Nucl Med*. 2002;43:92–96
- Oprea-Lager DE, Vincent AD, van Moorselaar RJ, et al. Dual-phase PET-CT to differentiate [¹⁸F]Fluoromethylcholine uptake in reactive and malignant lymph nodes in patients with prostate cancer. *PLoS One*. 2012;7:e48430
- Tavola F, Janzen T, Giussani A, et al. Nonlinear compartmental model of ¹⁸F-choline. *Nucl Med Biol*. 2012;39:261–268
- Uusijarvi H, Nilsson LE, Bjartell A and Mattsson S. Biokinetics of ¹⁸F-choline studied in four prostate cancer patients. *Radiat Prot Dosimetry*. 2010;139:240–244
- Windhorst AD, Linden TT, de Nooij A, et al. A complete, multipurpose, low cost, fully automated and GMP compliant radiosynthesis system. *J Labelled Comp Radiopharm*. 2001;44:S1052–S1054
- Boellaard R, O'Doherty MJ, Weber WA, et al. FDG PET and PET/CT: EANM procedure guidelines for tumour PET imaging: version 1.0. *Eur J Nucl Med Mol Imaging*. 2010;37:181–200
- Boellaard R, van LA, van Balen SC, Hoving BC and Lammertsma AA. Characteristics of a new fully programmable blood sampling device for monitoring blood radioactivity during PET. *Eur J Nucl Med*. 2001;28:81–89
- Watabe H, Channing MA, Der MG, et al. Kinetic analysis of the 5-HT_{2A} ligand [¹¹C]MDL 100,907. *J Cereb Blood Flow Metab*. 2000;20:899–909
- Lammertsma AA, Bench CJ, Hume SP, et al. Comparison of methods for analysis of clinical [¹¹C]raclopride studies. *J Cereb Blood Flow Metab*. 1996;16:42–52
- Yaqub M, Boellaard R, Kropholler MA and Lammertsma AA. Optimization algorithms and weighting factors for analysis of dynamic PET studies. *Phys Med Biol*. 2006;51:4217–4232
- Glatting G, Kletting P, Reske SN, Hohl K and Ring C. Choosing the optimal fit function: comparison of the Akaike information criterion and the F-test. *Med Phys*. 2007;34:4285–4292

24. Giovacchini G. Do we have to withdraw antiandrogenic therapy in prostate cancer patients before PET/CT with [¹¹C]choline? *Eur J Nucl Med Mol Imaging*. 2011; 38:1964–1966
25. Challapalli A, Sharma R, Hallett WA, et al. Biodistribution and radiation dosimetry of deuterium-substituted ¹⁸F-fluoromethyl-[1, 2-²H₂]choline in healthy volunteers. *J Nucl Med*. 2014;55:256–263
26. Witney TH, Alam IS, Turton DR, et al. Evaluation of deuterated ¹⁸F- and ¹¹C-labeled choline analogs for cancer detection by positron emission tomography. *Clin Cancer Res*. 2012;18:1063–1072

SUPPLEMENTAL DATA 1

[¹⁸F]fluoromethylcholine synthesis

Cyclotron produced ¹⁸F-fluoride (30-40 GBq) was reacted with dibromomethane and the obtained ¹⁸F-fluorobromomethane was purified over 4 in-line connected Waters Sep-Pak silica plus long cartridges (Waters, Etten-Leur, The Netherlands) [1] and passed over two Waters tC18 Sep-pak plus cartridges connected in-line (pretreated with 10 mL of 96% ethanol and subsequently 10 mL of water for injection), containing the precursor 2-(dimethylamino)ethanol. Alkylation of the precursor on the Sep-pak was done at room temperature. After completion of the reaction, the product was rinsed of the tC18 Sep-pak cartridges and passed over a Waters Accell plus CM Sep-pak cartridge (pretreated with 8 mL of 1M HCl) to trap the precursor. The ethanolic solution of [¹⁸F]fluorocholine was diluted with a solution of 0.9% NaCl (Fresenius Kabi) to a ethanol concentration of less than 2% and passed over sterile 0.22 µm Millex-GV filter (Millex, Barendrecht, the Netherlands) yielding 2-5 GBq ¹⁸F-fluorocholine (6-16% uncorrected yield) as a sterile, isotonic and pyrogen free solution. The radiochemical purity was > 99% and no chemical impurities were detected as assessed by analytical radio/ultraviolet-HPLC (UV-HPLC). Residual concentrations of dibromomethane and 2-(dimethylamino)ethanol were determined by flame ionization detector – gas chromatography and were below 25 and 400 ppm respectively.

Reference

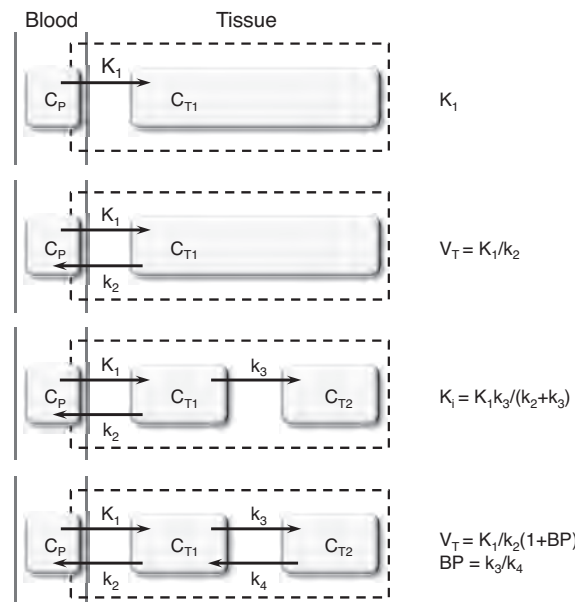
1. Iwata R, Pascali C, Bogni A, Furumoto S, Terasaki K, Yanai K. [¹⁸F]fluoromethyl triflate, a novel and reactive [¹⁸F]fluoromethylating agent: preparation and application to the on-column preparation of [¹⁸F]fluorocholine. *Appl Radiat Isot*. 2002;57(3):347-352.

SUPPLEMENTAL DATA 2

Compartment models and relevant associated quantification parameters

Supplemental Figure 1s

Schematic representation of standard single and two tissue compartment models and associated quantification parameters. From top to bottom: single tissue irreversible model, single tissue reversible model, two tissue irreversible model and two tissue reversible model. C_p = activity concentration in plasma; $C_{T_1} + C_{T_2}$ = activity concentration in tissue; V_T = volume of distribution; K_i = net influx rate; BP = binding potential; Dashed line indicates compartments (or parts of compartments) a PET VOI can contain. Please note that the distinction between tissue compartments denotes a difference in kinetics and is not per se associated with a spatial separation. The region where the dashed line intersects the blood compartment represents the blood volume fraction (V_B).



SUPPLEMENTAL DATA 3

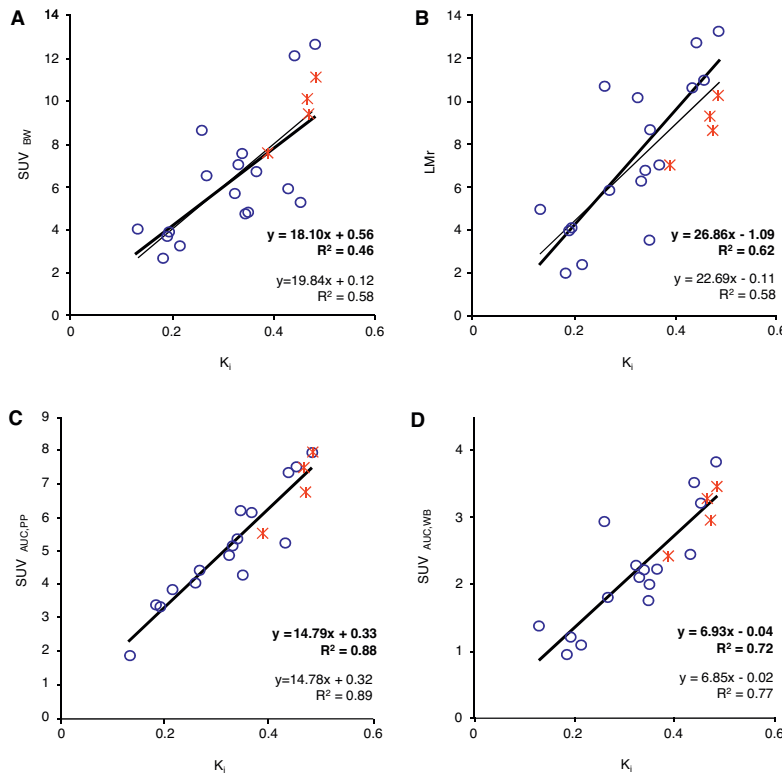
SUV validation results for 2T3k+VB

Data for the patient excluded from the validation analysis presented in the paper is indicated using stars. As the 2T3k+ V_B model has more parameters available than 1T1k+VB, it is better equipped to deal with the more complex TAC. Although resulting

estimates of individual parameters for this patient remain unrealistic, over- and underestimations in individual parameters could cancel out in calculating K_i . Although the magnitude correlation coefficients are naturally different, the conclusions about the relative performance of the simplified quantification parameters are conserved, i.e. $SUV_{AUC,PP}$ performs best, followed by $SUV_{AUC,WB}$, then LMr and SUV_{BW} .

Supplemental Figure 2s.

Correlation between simplified uptake measures and K_i derived from irreversible two tissue compartment model. (A) standard uptake value normalized to body weight (SUV_{BW}), (B) lesion-to- muscle ratio (LMr) (C) lesion activity concentration in kBq at 30-40 min p.i. divided by AUC of parent plasma activity concentration in MBq over 0-30 min ($SUV_{AUC,PP}$) and (D) lesion activity concentration in kBq at 30-40 min p.i. divided by AUC of whole blood activity concentration in MBq over 0-30 min ($SUV_{AUC,WB}$). 3 data points were excluded for unreliable fits ($SE > 500\%$ in one of the estimated rate constants). Fits for one patient (indicated by star) were suspected to be unreliable. Thick regression line (top equation) excludes this patient's data. Thin regression line includes this data.

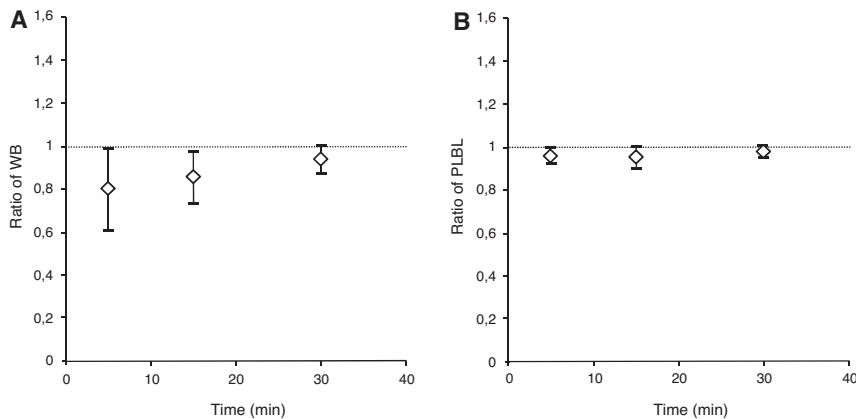


SUPPLEMENTAL DATA 4

Manual blood sample data

Supplemental Figure 3s.

Manual blood sample data as function of time: (A) ratio of venous to arterial whole-blood activity concentrations (WB) and (B) ratio of venous to arterial plasma-to-blood ratios (PLBL). Error bars represent \pm SD.





CHAPTER 5

Repeatability of quantitative [¹⁸F]fluoromethylcholine PET/CT studies in prostate cancer

Daniela E. Oprea-Lager¹

Gem Kramer¹

Peter M. van de Ven²

Alfons J.M. van den Eertwegh³

Reindert J.A. van Moorselaar⁴

Patrick Schober⁵

Otto S. Hoekstra¹

Adriaan A. Lammertsma¹

Ronald Boellaard¹

¹Department of Radiology and Nuclear Medicine, VU University Medical Center, Amsterdam, the Netherlands

²Department of Epidemiology and Biostatistics, VU University Medical Center, Amsterdam, the Netherlands

³Department of Medical Oncology, VU University Medical Center, Amsterdam, the Netherlands

⁴Department of Urology, VU University Medical Center, Amsterdam, the Netherlands

⁵Department of Anesthesiology, VU University Medical Center, Amsterdam, the Netherlands

ABSTRACT

PURPOSE

Repeatable quantification is essential when using [¹⁸F]fluoromethylcholine ([¹⁸F]FCH) PET/CT for monitoring treatment response in prostate cancer (PC). It has been shown that SUV normalized to the area under the curve of the blood activity concentration (SUV_{AUC}) provides better correlation with full kinetic analysis than standard SUV. However, precision of SUV_{AUC} is not known yet. The purpose of this study was to assess repeatability of various semi-quantitative [¹⁸F]FCH parameters in PC.

METHODS

Twelve patients (64±8 years) with metastasized PC underwent 2 sets of [¹⁸F]FCH PET/CT scans, on consecutive days. Each set consisted of a 30 minutes dynamic PET/CT scan of the chest, after intravenous administration of 200 MBq [¹⁸F]FCH, followed by a whole body (WB) PET/CT at 40 minutes. The dynamic scan was used to derive AUC of the blood activity concentration. Lesion uptake was derived from the WB scan using various types of volumes of interest (VOIs): maximum, peak and mean. Each of these parameters was normalized to injected activity/weight, blood AUC and blood concentration itself at 40 minutes, resulting in several SUV, SUV_{AUC} and SUV_{TBR} values. Test-retest repeatability of these metrics, metabolic tumor volume (MTV) and total lesion choline uptake (TLCU), respectively, were studied. The level of agreement between test-retest data and reliability was assessed using Bland-Altman plots, repeatability coefficients (RC) and intraclass correlation coefficients.

RESULTS

A total of 67 choline avid metastases were identified, 44 bone and 23 lymph node lesions. In case of SUVmax, RC for SUV, SUV_{AUC} and SUV_{TBR} were 26% (ICC=0.95), 31% (ICC=0.95) and 46% (ICC=0.89), respectively. Similar values were obtained for SUVpeak and SUVmean. Repeatability of SUV_{AUC} was comparable with that of SUV, for maximum, peak and mean values. Tissue type and tumor localization did not affect repeatability. MTV <4.2 cm³ had larger variability than larger volumes (RC 45% versus 29%, p=0.048). Repeatability did not differ between lesions with SUVpeak above or below the median value of 8.3 (RC 19% versus 28%, p=0.264).

CONCLUSION

The repeatability of SUV_{AUC} was comparable to that of standard SUV. RC of various semi-quantitative [¹⁸F]FCH parameters (SUV, MTV, TLCU) were ~35%. Larger differences are likely to represent treatment effects.

INTRODUCTION

Prostate cancer (PC) is the second most common cancer in men worldwide and was the third most diagnosed malignancy in Europe in 2012, with 92,000 death reported [1, 2]. This androgen-dependent neoplasm is characterized by a good initial response to (anti)hormonal therapy (HT) and an unpredictable latent castration-resistant (CR) status [3]. At the beginning of this decennium, molecular profiling studies have improved knowledge about the heterogeneous biological behavior of PC. It was found that even in the presence of a castrate range (<1.7 nmol/L) of testosterone in the blood of castration-resistant PC (CRPC) patients, a proportion of these tumors remains dependent on androgen-receptor signaling for growth [4]. Five potential mechanisms of development of CRPC were described, based on ligand and androgen-receptor dependence [5].

Nowadays, a multitude of therapeutic options against CRPC is available, including either cytotoxic (docetaxel, cabazitaxel), hormonal (abiraterone, enzalutamide), immunotherapeutic (sipuleucel-T) and bone-targeting (Ra-223 dichloride) agents [6–13]. However, despite this variety of new agents with demonstrated significant improvement in life expectancy, proper sequencing (e.g., modality, timing) in individual patients with metastatic PC is unclear [14]. Since therapeutic options vary greatly with stage and grade of the disease, specific patterns of metastatic spread (i.e., hematogeneous and/or lymphatic) and dominant phenotype, accurate diagnostic “instruments” for response evaluation are essential [15, 16].

Non-invasive, hybrid positron emission tomography/computed tomography (PET/CT) has proven to be a valuable diagnostic tool by acquiring and combining metabolic and anatomic information *in vivo* [17]. Encouraging results have been reported on the usefulness of radiolabeled-choline PET/CT in PC [18, 19]. Apart from its main recognized application in restaging disease in case of biochemical relapse [20, 21], [¹⁸F]fluoromethylcholine ([¹⁸F]FCH) might also qualify as a biomarker of response to therapy. Since conceptually, choline uptake represents viable tumor cells, tracer uptake changes over time might serve as an improved read-out of treatment efficacy.

In vitro experiments have shown promising results in the use of radiolabeled-choline to monitor anti-androgen treatment or chemotherapy [22, 23]. Recently, simplified quantitative methods for [¹⁸F]FCH have been developed and validated [24]. It has been

shown that standardized uptake value (SUV) normalized to the area under the curve (AUC) of the blood activity concentration (SUV_{AUC}) provides better correlation with full kinetic analysis than standard SUV [24]. However, precision of SUV_{AUC} , and also that of SUV itself, is as yet unknown. The purpose of this study was to prospectively assess repeatability of semi-quantitative [^{18}F]FCH PET/CT parameters in PC, also including metabolic tumor volume (MTV) and total lesion choline uptake (TLU). Such knowledge is essential for proper interpretation of signal changes of [^{18}F]FCH over time, thus improving personalized therapy strategies for PC patients.

MATERIALS AND METHODS

Patients

Twelve patients with histologically proven PC (n=4 CRPC), with lymphatic and/or hematogeneous metastases, were included prospectively. Inclusion criteria were presence of at least 2 metastases (diameter $\geq 1.5\text{cm}$) detected by recently (≤ 3 months prior to PET/CT) performed conventional imaging and ability to remain supine for 60 minutes. Exclusion criteria were claustrophobia and coexistence of multiple malignancies. The study was approved by the Medical Ethics Review Committee of the VU University Medical Center. Prior to inclusion, each patient signed a written informed consent, after receiving verbal and written explanation.

Personal and demographic data regarding patient's age, body weight, Gleason score and value of prostate-specific antigen (PSA; ng/ml) at the time of PET/CT, together with information on previous therapy were collected. Metastatic lesion characteristics such as location (intrathoracically/intra-abdominal or in the pelvic region), number and type (bone/ lymph nodes) were also registered. Values are presented as mean \pm SD.

Data aquisitions

All patients underwent repeated [^{18}F]FCH (synthesis details see [24]) PET/CT scans at the same time on two consecutive days. Patients were not on therapy at the time of scanning. The minimal interval of time between last treatment and first PET/CT scan was 19 days. Patient preparation was similar to that required for [^{18}F]-2-fluoro-2-deoxy-D-glucose ([^{18}F]FDG) [25]. Patients were scanned using a Gemini TF-64 PET/CT scanner (Philips Medical Systems, Cleveland, Ohio, USA).

Each patient received a low dose CT (30 mAs, 120 kV), followed by a 30 minutes dynamic PET scan of the thoracic region (for details see [24]), which was centered over a large blood pool structure (e.g., aorta ascendens), to obtain an image derived input function. At the start of the dynamic [¹⁸F]FCH scan a bolus injection of 205 \pm 9 and 206 \pm 7 MBq [¹⁸F]FCH (days 1 and 2, respectively) was administered intravenously using an automated injector (Medrad, Pittsburgh, USA) and which was flushed with 40mL of saline (5mL at 0.8mL·s⁻¹ followed by 35mL at 2mL·s⁻¹). The dynamic PET data were normalized and corrected for decay, scatter, random coincidences and photon attenuation, and reconstructed into 25 frames (1x10, 8x5, 5x20, 5x60, 3x150, 3x300 s) with a matrix size of 144x144x45 voxels (4x4x4 mm³) using a 3-dimensional row action maximum likelihood reconstruction algorithm (3D-RAMLA).

After a standard (5 min) micturition break to warrant a proper visual assessment of the pelvic region, a whole body (WB) [¹⁸F]FCH scan (mid-thigh to skull base) was performed 40 min post injection. Following this PET acquisition (10 bed positions; each of 2 min), a second low dose CT (50 mAs, 120 kV) was acquired for anatomical correlation and attenuation correction. WB data were corrected for dead time, decay, scatter and randoms, and reconstructed into 34 frames (1x10, 8x5, 4x10, 3x20, 5x30, 5x60, 4x150, 4x300 s) with a matrix size of 144x144 and voxels of 4x4x4 mm³, using a time of flight iterative reconstruction method (BLOB-OS-TF). The transaxial spatial resolution was \sim 5 mm full width at half maximum in the center of the field of view, similarly to that of the dynamic scan.

Data analysis

Reconstructed images were transferred to off-line workstations for further analysis. Data were analyzed on a volume of interest (VOI) basis [26]. The dynamic scan was used to derive the AUC of the blood activity concentration, by defining a cylindrical VOI with 1.5 cm diameter extending over 5 consecutive axial planes within the lumen of the ascending aorta. Next, lesion uptake (defined as [¹⁸F]FCH accumulation exceeding local background and incompatible with physiological [¹⁸F]FCH biodistribution) was derived from the WB scan.

The term MTV was used to indicate tumor volumes that were derived directly from the PET studies, quantified as the VOI size [26]. VOIs were defined by a semiautomatic delineation tool, applying a background adapted 50% of maximum isocontour (i.e., contour value equals 50% of maximum + background). For each of these VOIs,

maximum, peak and mean uptakes were calculated. In addition, each of these parameters was normalized to injected activity/body weight (SUV), AUC of blood activity concentration (SUV_{AUC}), as derived from the dynamic scan, and blood concentration at 40 minutes post injection (SUV_{TBR}), as derived from the WB scan. For SUV_{mean} associated parameters, also total lesion choline uptake (defined as $\text{SUV}_{\text{mean}} \times \text{MTV}$) was calculated, resulting in $\text{TLCU}_{\text{mean}}$, TLCU_{AUC} and TLCU_{TBR} , respectively. Test-retest repeatability of all metrics was calculated using both standard repeatability coefficients (RC) (defined as $1.96 \times \text{SD}$ of the difference between test-retest) and relative RC (test-retest difference in percentage).

Statistical analysis

Data were analyzed using SPSS version 15.0. Test-retest repeatability was quantified using intraclass correlation coefficients (ICC; based on absolute agreement), RC and displayed graphically using Bland-Altman and/or box plots. ICCs were calculated for each SUV measure as the ratio of between-lesion variability and total variability (both between-lesion and within-lesion). Variance components for patient, lesion within patient and (repeated) measurements within lesions were estimated using mixed models. Total variability was calculated as the sum of these three variance components. Between-lesion variability was calculated as the sum of the variance components for patient and lesion-within patient. Confidence intervals for ICCs were determined using the delta-method. Reliability coefficients were based on the relative difference:

$$100\% * (\text{SUV}_{\text{test}} - \text{SUV}_{\text{retest}}) / [0.5 * (\text{SUV}_{\text{test}} + \text{SUV}_{\text{retest}})]$$

The method in Bland [27] was used to take into account correlation of measurements between different lesions within the same patient (intra-patient), when calculating RC. Differences in repeatability of the different SUV measures (max, peak, mean) and methods of normalization (SUV, SUV_{AUC} and SUV_{TBR}) were assessed by comparing the variances of the relative test-retest differences, using the Pitman-Morgan test [28] for correlated variances. Differences in repeatability of SUV measures related to location, metastatic lesion type and size were assessed by comparing the variances of the relative test-retest differences between the subgroups of lesions, using Levene's test [29]. Overall type I error, within each set of comparisons, was controlled at 5%, using a Bonferroni correction.

RESULTS

Patients

Patient characteristics (Table 1) were: age 64±8 years, weight 88±9 kg, Gleason score 7 (n=3) or more (n=9) and a median PSA at the time of PET/CT of 46 ng/ml (range 2-226). Patients had been treated previously by prostatectomy and lymph node dissection (n=3), HT (n=7), external beam radiotherapy (EBRT) on the prostate (n=1), EBRT in combination with HT (n=5), chemotherapy (n=4) or immunotherapy (n=1).

67 metastases were identified at PET, with a median of 6 per patient (range 3-8), 44 of which were bone and 23 lymph node metastases. Twelve metastases were localized above the diaphragm, the others were intra-abdominal and/or in the pelvic region (n=55). The malignant nature of the metastases was confirmed radiologically, based on progression of pre-existent lesions and/or new metastatic sites. VOI size [median/interquartile range (IQR)] was 4.9/7.6 cm³ with a lesion SUVpeak (median/IQR) of 8.3/5.2.

Repeatability data was analyzed using a volume threshold of 4.2 cm³, based on a repeatability study of metabolic tumor volume with ¹⁸F-FDG and ¹⁸F-fluorothymidine (¹⁸F-FLT) in lung cancer [26]. In that study, changes of >37% for ¹⁸F-FDG in lesions larger than 4.2 cm³ were found to represent a biologic effect. This volume threshold corresponds by approximation to a diameter of 2 cm (for spherical metastatic lesions), which equals about 4 times the spatial resolution of PET below which quantification, VOI definition and detectability are hampered by partial-volume effects.

Repeatability of semi-quantitative [¹⁸F]FCH parameters

Repeatability of each semi-quantitative [¹⁸F]FCH parameters (i.e., SUV, MTV and TLCU) was studied as a function of uptake (median SUV_{peak} 8.3), MTV (larger or smaller than 4.2 cm³), metastatic tissue type (bone/ lymph node) and location (intrathoracically versus abdominal/pelvic), respectively. These test-retest aspects are discussed below.

Repeatability of SUV

In case of SUVmax, RC (for relative differences) were 26%, 31% and 46%, respectively. Similar values were observed for SUVpeak and SUVmean. ICCs for SUV and SUV_{AUC} were all approximately 0.95, whereas ICCs for SUV_{TBR} were 0.89 (Table 2).

Table 1. Patient characteristics.

Patient	Age (yr)	Weight (kg)	Gleason			PSAtt (ng/ml)	HT	Previous therapy				
			≤6	7	>7			CT	EBRT	RALP	LND	Immun
1	65	78			9	93	1	1				
2	55	89			8	18	1	1	1			
3	74	90		7		43	1			1	1	
4	68	79			10	8	1	1				
5	66	83			8	54	1		1	1		
6	60	85			9	137	1		1	1		
7	54	98		7		2	1		1			
8	72	84		7		54	1		1			
9	54	85			9	2	1					
10	54	108			9	226	1		1			1
11	71	81			8	39	1	1				
12	70	101			8	49	1					

PSAtt prostate-specific antigen at the time of performing the PET/CT scans; HT (anti)hormone therapy; CT chemotherapy; EBRT external beam radiotherapy; RALP robot assisted laparoscopic prostatectomy; LND lymph node dissection; Immun immunotherapy.

Table 2. Test-retest differences, intraclass correlation coefficients and repeatability coefficients, for different types of SUVs (max, mean and peak) and their normalizations (SUV, SUV_{AUC} and SUV_{TBR}).

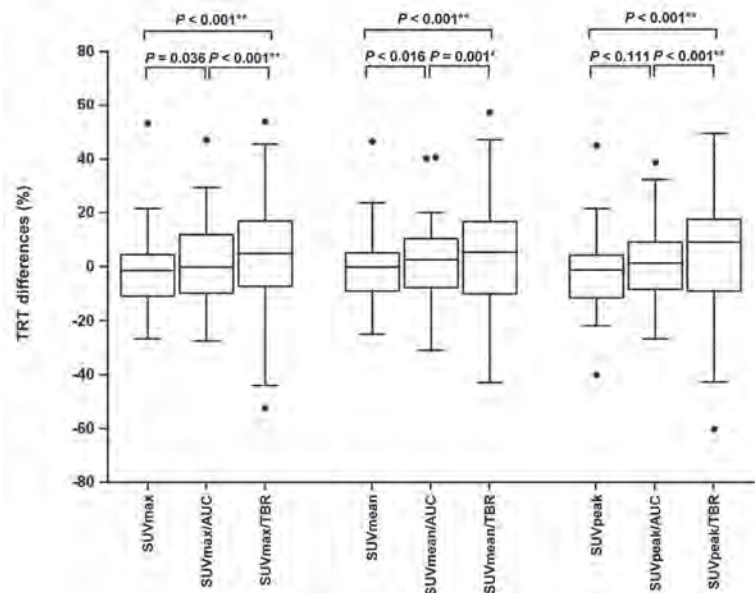
		TRT diff (mean±SD)	ICC (95%CI)	RC*
SUVmax	SUV	-0.38±1.45	0.95 (0.91-0.98)	26.1%
	SUV _{AUC}	0±0.88	0.95 (0.92-0.99)	30.9%
	SUV _{TBR}	1.0±3.9	0.89 (0.81-0.97)	46.2%
SUVpeak	SUV	-0.26±0.97	0.96 (0.94-0.98)	23.8%
	SUV _{AUC}	0.02±0.70	0.95 (0.93-0.98)	27.5%
	SUV _{TBR}	0.76±3.02	0.89 (0.83-0.95)	45.4%
SUVmean	SUV	-0.13±0.76	0.96 (0.94-0.99)	22.3%
	SUV _{AUC}	0.05±0.52	0.95 (0.92-0.98)	27.7%
	SUV _{TBR}	0.68±2.3	0.89 (0.81-0.96)	42.4%

TRT diff test-retest differences; ICC intra class coefficients; RC repeatability coefficients; *for relative differences according to Bland (2007) method.

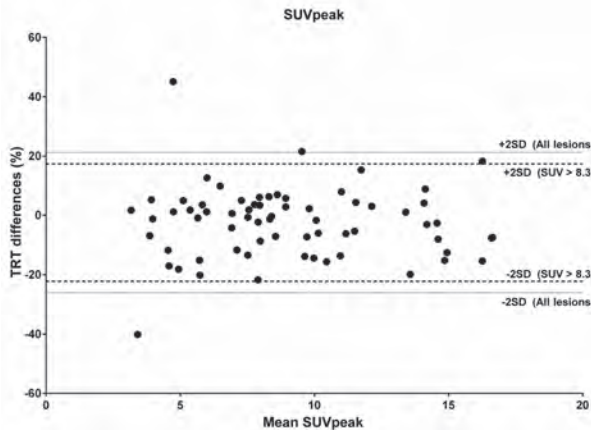
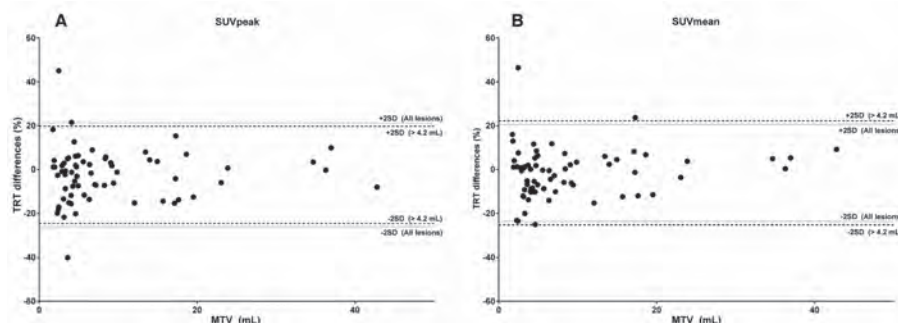
Nine pairwise comparisons for different methods of SUV normalization were performed to estimate variances of relative test-retest differences. After correcting for multiple comparisons (Bonferroni corrected significant difference at 5% level $p < 0.0056$ and at 1% level $p < 0.0011$, respectively), only SUV_{TBR} parameters were found to have consistently larger variances ($p < 0.001$) (Supplemental Table 1s). The relative differences (in percentage) between test-retest data and the mean values for the

different types of SUVs (max, mean and peak) and their normalizations (SUV, SUV_{AUC} and SUV_{TBR}) are presented in Figure 1. The repeatability of SUV_{AUC} for max, peak and mean values were comparable with those of the corresponding SUV measures (Supplemental Table 2s).

Figure 1. Relative differences between test-retest data and the mean values for the different types of SUVs (max, mean and peak) and their normalizations (SUV, SUV_{AUC} and SUV_{TBR}). Black dots represent outliers (more than 2 SD). Bonferroni-corrected significance level $p < 0.0056$ (for significance level of 5%, denoted by *) and $p < 0.0011$ (for significance level of 1%, denoted by **).

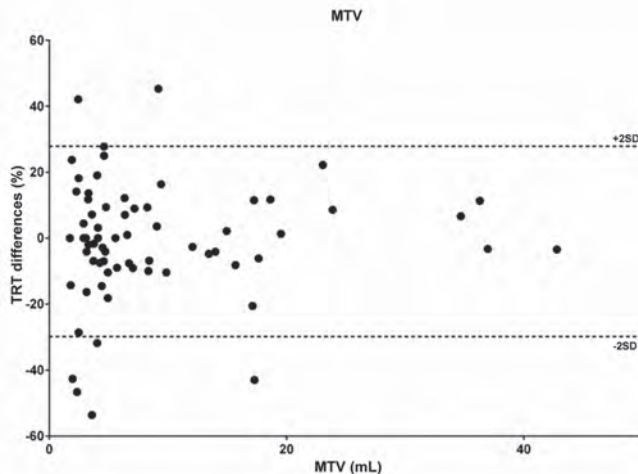


Repeatability did not differ between lesions with a SUV_{peak} above or below the median value of 8.3 (RC 19% versus 28%, $p=0.264$) (Fig. 2 and Supplemental Fig. 1s). These values were comparable with those of $\text{SUV}_{\text{peakAUC}}$ [RC 23% ($\text{SUV}_{\text{peak}} > 8.3$) versus 31% ($\text{SUV}_{\text{peak}} < 8.3$), $p=0.136$]. Moreover, repeatability of SUV_{peak} and SUV_{mean} was independent of MTV (Fig. 3) as well as of tissue type and tumor location (Supplemental Fig. 2s and Supplemental Table 3s).

Figure 2. Bland-Altman plots for relative differences between test-retest data and mean values for SUV_{peak} .**Figure 3.** Bland-Altman plots for the relative test-retest repeatability of SUV_{peak} (A) and SUV_{mean} (B), as a function of metabolic tumor volume (MTV).

Repeatability of MTV

For MTV, test-retest difference was 0.03 ± 1.63 and the relative test-retest difference 36% (Fig. 4). Repeatability of MTV was independent of SUV_{peak} [RC 34.25% ($\text{SUV}_{\text{peak}} > 8.3$) versus 36.43% ($\text{SUV}_{\text{peak}} < 8.3$), $p=0.933$]. MTV $< 4.2 \text{ cm}^3$ had larger variability than larger volumes (RC 45% versus 29%, $p=0.048$) (Supplemental Fig. 1s). Repeatability of MTV did not differ between bone/lymph nodes (RC 34% versus 36.4%, $p=0.684$) and location [RC 36.7% (intrathoracically) versus RC 34.4% (intra-abdominal/pelvic), $p=0.820$].

Figure 4. Relative differences between test-retest for metabolic tumor volume (MTV) as a function of MTV.

Repeatability of TLCU

Repeatability of the TLCU and TLCU_{AUC} were comparable (RC 33% versus 31%, $p=0.954$), while TLCU_{TRR} showed larger variance of 51% ($p < 0.001$) (Supplemental Fig. 3s). No significant difference was found between lesions with a total choline uptake below or above the median value of 30.9 [RC 40.9% (<30.9) versus 23.1% (>30.9), $p=0.093$].

Repeatability of TLCU was independent of uptake [RC 31% ($\text{SUV}_{\text{peak}} < 8.3$) versus 34% ($\text{SUV}_{\text{peak}} > 8.3$), $p=0.139$] and MTV [RC 42.1% ($<4.2 \text{ cm}^3$) versus 25.3% ($>4.2 \text{ cm}^3$), $p=0.037$], respectively. Repeatability of TLCU was also independent of tissue type [RC 30.8% (bone) versus 35.7% (lymph nodes), $p=0.241$] and location [RC 35.5% (intrathoracically) versus RC 32.4% (intra-abdominal/pelvic), $p=0.778$].

An overview of all RC of the semi-quantitative [¹⁸F]FCH parameters (SUV, MTV and TLCU), as a function of uptake, MTV and metastatic tissue type/location, is presented in Supplemental table 4s (relative test-retest difference in percentage) and Supplemental table 5s (test-retest difference), respectively. Additionally, individual patient RC for all semi-quantitative parameters are provided in the supplemental figures 4s, 5s and 6s. Comparable RC across the majority of subjects were observed. Patient 1 had the poorest RC regarding SUV (~35% on all 9 combinations of SUV types and normalizations). Patients 2, 4 and 7 had the poorest RC regarding MTV (all ~51%) and TLCU (55%, 51% and 67%, respectively).

DISCUSSION

In a previous study we investigated the [¹⁸F]FCH kinetics in metastatic PC [24], and demonstrated that SUV cannot be used to estimate [¹⁸F]FCH uptake. Whole-blood activity concentration SUV (SUV_{AUC}), based on two consecutive PET scans was proposed as a clinically feasible alternative. In the present study, repeatability of quantitative [¹⁸F]FCH PET/CT parameters in patients with PC was assessed prospectively. We found that repeatability of SUV_{AUC} is comparable to that of standard SUV and that [¹⁸F]FCH PET/CT uptake differences of 30% or more are likely to represent treatment effects.

Test-retest repeatability is essential for clinical implementation of any parameter of response assessment. Due to the heterogeneous biological behavior of PC [4] and in the light of rapidly evolving treatment modalities [14], there is a need for identification of biological markers that are able to monitor response to therapy in an adequate way. Standard treatment response evaluation criteria in solid tumors do not apply to metastatic PC, further complicating the issue of treatment response [30]. A newly proposed system for measuring functional response with [¹⁸F]FDG PET/CT, PET Response Criteria In Solid Tumours (PERCIST), might potentially be applicable to radiolabeled choline as well [31]. Nevertheless, before [¹⁸F]FCH PET/CT can be implemented as a biomarker for response evaluation in PC, the repeatability of the tracer should be known [32].

To the best of our knowledge, repeatability of [¹⁸F]FCH measurements in metastatic PC has not been assessed previously. A single study of Pegard et al. [33] addressed the reproducibility of inter- and intra-observer interpretation (i.e., visual evaluation and classification of foci with increased uptake as being malignant or benign) of [¹⁸F]FCH PET/CT examinations in patients suffering from biochemically recurrent PC. The authors describe a good concordance when evaluating bone metastases and abdominal/pelvic lymphatic recurrences in previously treated patients. A limited usefulness was found at the prostate level in untreated patients.

Observed repeatabilities were within the range seen with other commonly used radiotracers, such as [¹⁸F]FDG and [¹⁸F]fluorothymidine ([¹⁸F]FLT). When analyzing [¹⁸F]FDG uptake changes, the generally accepted PERCIST response classification system assumes the presence of a biological change when SUVpeak changes exceed 30%, in combination with 0.8 unit change of the absolute SUVpeak value [31]. In a meta-

analysis on the repeatability of [¹⁸F]FDG uptake measurements in tumors, de Langen et al. [34] identified 8 eligible studies. SUVmean was found to have better repeatability performance than SUVmax. A minimal relative change of 20% in combination with 1.2 unit change of SUVmean was presumed to represent a biological change. Comparable results were reported by Rockall et al. [35] in a study on repeatability of quantitative [¹⁸F]FDG PET/CT in recurrent ovarian carcinoma. RC suggested that a decrease in [¹⁸F]FDG uptake (SUV) up to 20% from baseline and a decrease in tumor size up to 15% could be used to determine (early) tumor response. In a study addressing repeatability and reproducibility of [¹⁸F]FDG and [¹⁸F]FLT PET tumor volume measurements, Hatt et al. [36] found comparable percentage differences for these two tracers datasets. Differences larger than 30% were considered indicative for treatment response evaluation.

Frings et al. [26] analyzed the repeatability of MTV with [¹⁸F]FDG and [¹⁸F]FLT in lung cancer. Repeatability was better for larger tumors. Changes of >37% for [¹⁸F]FDG in lesions larger than 4.2 cm³ represented a biologic effect. We obtained comparable results when using this MTV threshold for analyzing [¹⁸F]FCH test-retest data. A larger variability was found in small metabolic volumes (<4.2 cm³), suggesting that a similar lower threshold for MTV in treatment response evaluation studies should be used. In case of TLCU, RC were not significantly different for lesions smaller or larger than 4.2 cm³ (after correcting for multiple comparisons; Bonferroni corrected significance level $p<0.0056$). However, the uncorrected p equaled 0.037, suggesting a trend towards poorer repeatability for smaller lesions.

Two recently published papers explored the prognostic value of metabolic parameters when using [¹⁸F]FCH PET/CT in biochemical recurrent PC [37] or in CRPC [38]. In a multivariate analysis, Colombié et al. [37] identified age <70 years, SUVmean ≥ 3 and a standardized metabolic activity ≥ 23 , as being independent prognostic factors for disease-free survival. In a prospective study, Kwee et al. [38] found that WB tumor indices based on quantifying net metabolically active tumor volume and total lesion activity [¹⁸F]FCH PET/CT were predictive of overall survival. In our study we used comparable metrics, with an emphasis on repeatability of the use of [¹⁸F]FCH as a potential biomarker for response evaluation in PC.

RC for the individual patients were comparable across the majority of subjects. However, patient 1 had the poorest RC regarding SUV, due to a small (1.5 cm short axis diameter)

bone metastasis located right paramedian in the anterior aspect of the corpus of the 10th thoracic vertebra, in the vicinity of the liver. We hypothesize that the relative large test-retest difference (~35%) in this particular lesion was caused by incorrect scatter, due to an increase in image-derived blood activity concentrations near physiologically high avid [¹⁸F]FCH structures. This can possibly lead to large quantification errors with image derived input function obtained from blood VOI in these areas [24]. Three patients (2, 4 and 7) had larger RC for MTV and TLCU than the other subjects. This is likely explained by difficulty in lesion segmentation, such that errors in MTV are also propagated into poorer repeatability for TLCU. Besides, all these patients presented with small metastatic lesions (~1.5cm), with slightly increased [¹⁸F]FCH uptake on PET/CT.

A mention has to be made with regard to the chosen 30% cut-off value for the semi-quantitative SUV measures. As shown in Figure 2, the test-retest differences pooled over all lesions or those with SUV >8.3 are ~20%. However, for the lesions with a SUV <8.3, the calculated RC are ~30% (supplemental Table 4s). Since in clinical practice, the majority of patients will have a combination of metastatic lesions with SUV above or below 8.3, we have decided to adopt the more conservative value of 30%.

A possible limitation of the present study is the limited number of subjects. The minimum required was calculated as a total of 12 patients (with minimal two measurements per patient). This sample size yields 80% power for testing the hypothesis: $ICC \leq 0.6$ against the one-sided alternative ($ICC > 0.6$) at a significance level of 5% when the true ICC is equal to 0.9 [39]. Moreover, this sample size of 12 patients resulted in confidence intervals for the limits of agreement ranging to approximately 1.1 times the standard deviation of the difference scores, at either side of the estimated limit of agreement [27]. Thus, present study still provides a reasonable estimate of the expected RC.

CONCLUSION

In patients with metastatic prostate cancer, repeatability of SUV_{AUC} was comparable to that of standard SUV and indicated that [¹⁸F]FCH PET/CT uptake differences of 30% or more are likely to represent treatment effects. Repeatability of MTV and TLCU, respectively, was ~35%. Observed repeatabilities are of the same order of magnitude as those seen for other commonly used radiotracers, such as [¹⁸F]FDG and [¹⁸F]FLT.

ACKNOWLEDGMENTS

The authors would like to thank their colleagues at the Department of Radiology & Nuclear Medicine involved in tracer production and data acquisition. They are also grateful to the urologists from the VU University Medical Center (André N. Vis, MD, PhD) and Amstelland Hospital Amstelveen (Joop W. Noordzij MD; Sven Nadorp, MD) as well as the VU University Medical Center oncologists (Catharina Menke-van der Houven van Oordt MD, PhD; Joyce van Dodewaard-de Jong MD; Jens Voortman MD, PhD) for their contribution to patient selection and inclusion.

REFERENCES

1. Jemal A, Bray F, Center MM, et al. Global cancer statistics . *CA Cancer J Clin.* 2011;61:69–90
2. Ferlay J, Steliarova-Foucher E, Lortet-Tieulent J, et al. Cancer incidence and mortality patterns in Europe: estimates for 40 countries in 2012. *Eur J Cancer.* 2013;49:1374–1403
3. Pienta KJ, Bradley D. Mechanisms underlying the development of androgen-independent prostate cancer. *Clin Cancer Res.* 2006;12:1665–1671
4. Scher HI, Sawyers CL. Biology of progressive, castration-resistant prostate cancer: directed therapies targeting the androgen-receptor signaling axis. *J Clin Oncol.* 2005;23:8253–8261
5. Feldman BJ and Feldman D. The development of androgen-independent prostate cancer. *Nature Rev Cancer.* 2001;1:34–45
6. Tannock IF, De Wit R, Berry WR, et al. Docetaxel plus prednisone or mitoxantrone plus prednisone for advanced prostate cancer. *N Engl J Med.* 2004;351:1502–1512
7. de Bono JS, Oudard S, Ozguroglu M, et al. Prednisone plus cabazitaxel or mitoxantrone for metastatic castration-resistant prostate cancer progressing after docetaxel treatment: a randomised open-label trial. *Lancet.* 2010;376:1147–1154
8. Fizazi K, Scher HI, Molina A, et al. Abiraterone acetate for treatment of metastatic castration-resistant prostate cancer: final overall survival analysis of the COU-AA-301 randomised, double-blind, placebo-controlled phase 3 study. *Lancet Oncol.* 2012;13:983–992
9. Ryan CJ, Smith MR, de Bono JS, et al. Abiraterone in metastatic prostate cancer without previous chemotherapy. *N Engl J Med.* 2013;368:138–148
10. Scher HI, Fizazi K, Saad F, et al. Increased survival with enzalutamide in prostate cancer after chemotherapy. *N Engl J Med.* 2012;367:1187–1197
11. Beer TM, Armstrong AJ, Rathkoph DE, et al. Enzalutamide in metastatic prostate cancer before chemotherapy. *N Engl J Med.* 2014;371:424–433
12. Kantoff PW, Higano CS, Shore ND, et al. Sipuleucel-T immunotherapy for castration-resistant prostate cancer. *N Engl J Med.* 2010;363:411–422
13. Parker C, Nilsson S, Heinrich D, et al. Alpha emitter radium-223 and survival in metastatic prostate cancer. *N Engl J Med.* 2013;369:213–223
14. van Dodewaard-de Jong JM, Verheul HM, Bloemendaal HJ, de Klerk JM, Carducci MA, van den Eertwegh AJ. New Treatment Options for Patients With Metastatic Prostate Cancer: What Is The Optimal Sequence? *Clin Genitourin Cancer.* 2015;13:271–279
15. Bray F, Lortet-Tieulent J, Ferlay J, et al. Prostate cancer incidence and mortality trends in 37 European countries: an overview. *Eur J Cancer.* 2010;46:3040–305216.
16. Heidenreich A, Bastian PJ, Bellmunt J, et al. EAU guidelines on prostate cancer. Part 1: screening, diagnosis, and local treatment with curative intent–update 2013. *Eur Urol.* 2014;65:124–137
17. Schiepers C, Dahlbom M. Molecular imaging in oncology: the acceptance of PET/CT and the emergence of MR/PET imaging. *Eur Radiol.* 2011;21:548–554
18. Bauman G, Belhocine T, Kovacs M, et al. 18F-fluorocholine for prostate cancer imaging: a systematic review of the literature. *Prostate Cancer Prostatic Dis.* 2012;15:45–55
19. Fuccio C, Rubello D, Castellucci P, et al. Choline PET/CT for prostate cancer: main clinical applications. *Eur J Radiol.* 2011;80:e50–e56
20. Umbehr MH, Müntener M, Hany T, et al. The role of 11C-choline and 18F-fluorocholine positron emission tomography (PET) and PET/CT in prostate cancer: a systematic review and meta-analysis. *Eur Urol.* 2013;64:106–117
21. Evangelista L, Zattoni F, Guttilla A, et al. Choline PET or PET/CT and biochemical relapse of prostate cancer: a systematic review and meta-analysis. *Clin Nucl Med.* 2013;38:305–314
22. Müller SA, Holzapfel K, Seidl C, et al. Characterization of choline uptake in prostate cancer cells following bicalutamide and docetaxel treatment. *Eur J Nucl Med Mol Imaging.* 2009;36:1434–1442
23. Oprea-Lager DE, van Kanter MP, van Moorselaar RJ, et al. [¹⁸F]fluoromethylcholine as a chemotherapy response read-out in prostate cancer cells. *Mol Imaging Biol.* 2015;17:319–327

24. Verwer EE, Oprea-Lager DE, van den Eertwegh AJ, et al. Quantification of ¹⁸F-Fluorocholine Kinetics in Patients with Prostate Cancer. *J Nucl Med.* 2015;56:365–371

25. Boellaard R, Delgado-Bolton R, Oyen WJ, et al. FDG PET/CT: EANM procedure guidelines for tumour imaging: version 2.0. *Eur J Nucl Med Mol Imaging.* 2015;42:328–354

26. Frings V, de Langen AJ, Smit EF, et al. Repeatability of metabolically active volume measurements with ¹⁸F-FDG and ¹⁸F-FLT PET in non-small cell lung cancer. *J Nucl Med.* 2010;51:1870–1877

27. Bland JM, Altman DG. Agreement between methods of measurement with multiple observations per individual. *Journal of Biopharmaceutical Statistics.* 2007;17:571–582

28. Garcia-Perez MA. Statistical criteria for parallel tests: A comparison of accuracy and power. *Behav Res.* 2013;45:999–1010

29. Keselman HJ, Wilcox RR, Algina J, Othman AR, Fradette K. A comparative study of robust tests for spread: Asymmetric trimming strategies. *Br J Math Stat Psychol.* 2008;61:235–253

30. Wallace TJ, Torre T, Grob M, et al. Current approaches, challenges and future directions for monitoring treatment response in prostate cancer. *Journal of Cancer.* 2014;5:3–24

31. Wahl RL, Jacene H, Kasamon Y, Lodge MA. From RECIST to PERCIST: Evolving considerations for PET response criteria in solid tumors. *J Nucl Med.* 2009;50(S1):122S–150S

32. Morisson CJ, Jerai R, Liu G. Imaging of castration-resistant prostate cancer: development of imaging response biomarkers. *Curr Opin Urol.* 2013;23:230–236

33. Pegard C, Gallazzini-Crépin, Gaij, et al. Study of inter- and intra-observer reproducibility in the interpretation of [¹⁸F]choline PET/CT examinations in patients suffering from biochemically recurrent prostate cancer following curative treatment. *EJNMMI Research.* 2014;4:25

34. de Langen AJ, Vincent A, Velasquez LM, et al. Repeatability of ¹⁸F-FDG uptake measurements in tumors : a meta-analysis. *J Nucl Med.* 2012;53:701–708

35. Rockall AG, Avril N, Lam R, et al. Repeatability of quantitative FDG-PET/CT and contrast-enhanced CT in recurrent ovarian carcinoma: test-retest measurements for tumor FDG uptake, diameter, and volume. *Clin Cancer Res.* 2014;20:2751–2760

36. Hatt M, Cheze-Le Rest C, Aboagye Eo, et al. Reproducibility of ¹⁸F-FDG and 3'-deoxy-3'-¹⁸F-fluorothymidine PET tumor volume measurements. *J Nucl Med.* 2010; 51:1368–1376

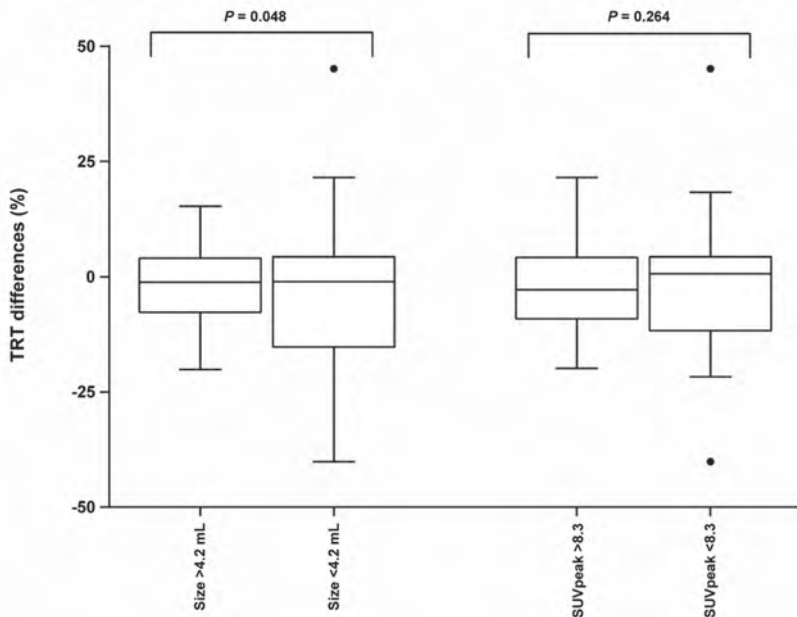
37. Colombié M, Campion L, Baily C, et al. Prognostic value of metabolic parameters and clinical impact of ¹⁸F-fluorocholine PET/CT in biochemical recurrent prostate cancer. *Eur J Nucl Med Mol Imaging.* 2015;42:1784–1793

38. Kwee SA, Lim J, Watanabe A, Kromer-Baker K, Coel MN. Prognosis related to metastatic burden measured by ¹⁸F-Fluorocholine PET/CT in castration-resistant prostate cancer. *J Nucl Med.* 2014;55:905–910

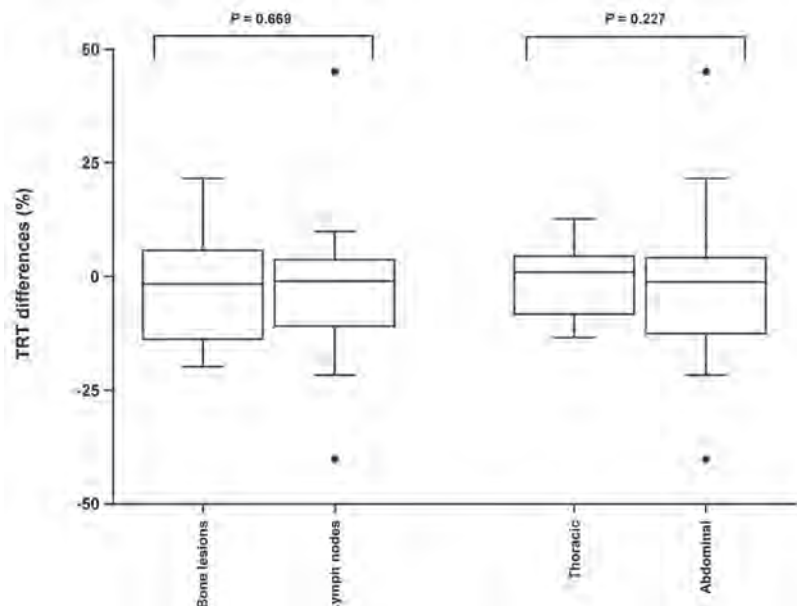
39. Shoukri MM, Asyali MH, Donner A. Sample size requirements for the design of reliability study: a review and new results. *Statistical Methods in Medical Research.* 2004; 13:251–271

SUPPLEMENTAL DATA

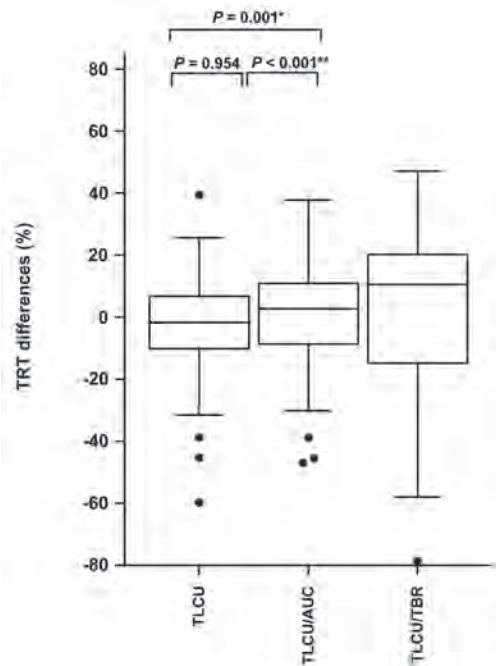
Supplemental Figure 1s. Relative test-retest repeatability for mean metabolic volume (left) and SUV_{peak} (right), respectively. Black dots represent outliers (more than 2 SD).



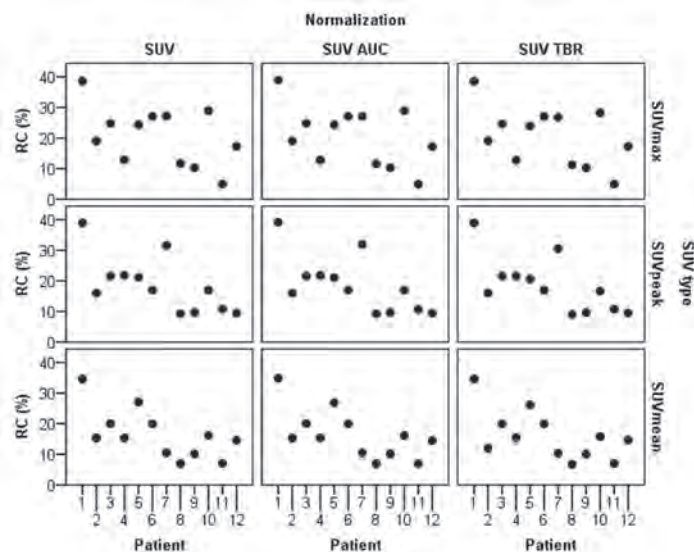
Supplemental Figure 2s. Relative differences between test-retest data (SUV_{peak}) and the type and anatomical localization of the metastatic lesions. Black dots represent outliers (more than 2 SD).



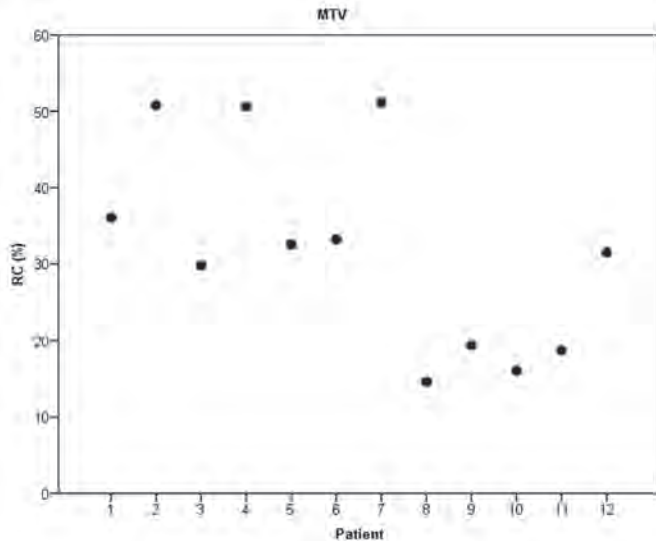
Supplemental Figure 3s. Relative differences between test-retest data (SUV_{mean}) and different types of normalized total lesion choline uptake (TLCU, $TLCU_{AUC}$ and $TLCU_{TBR}$). Black dots represent outliers (more than 2 SD). * p -value significant at 5% level ($p < 0.0056$) and ** p -value significant at 1% level ($p < 0.0011$).



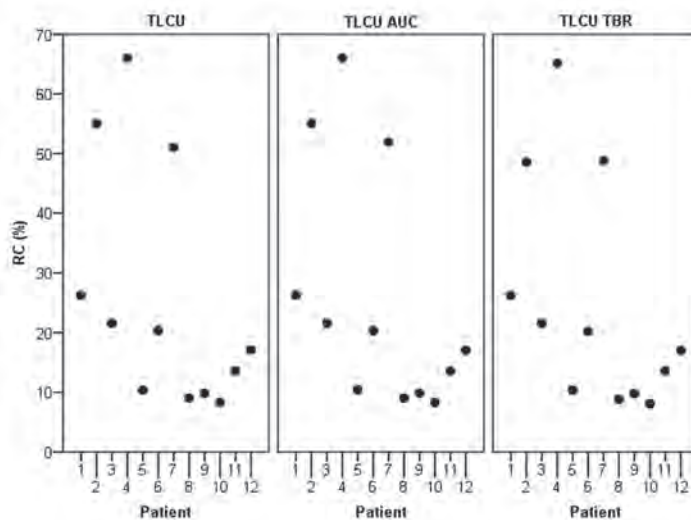
Supplemental Figure 4s. Repeatability coefficients (RC; in percentage) for the individual patients, regarding the different types of standardized uptake value (SUV_{max} , SUV_{peak} and SUV_{mean}) and their normalization (SUV, SUV_{AUC} and SUV_{TBR}).



Supplemental Figure 5s. Repeatability coefficients (RC; in percentage) for the individual patients, regarding the metabolic tumor volume (MTV). Comparable RC across the majority of subjects were observed. However, for 3 patients (2, 4 and 7) both MTV and total lesion choline uptake (TLCU) were larger than those of the other subjects. This is likely explained by difficulty in lesion segmentation, such that errors in MTV are also propagated into poorer repeatability for TLCU.



Supplemental Figure 6s. Repeatability coefficients (RC; in percentage) for the individual patients, regarding the total lesion choline uptake (TLCU) and corresponding normalizations (TLCU, TLCU_{AUC} and TLCU_{TBR}). Comparable RC across the majority of subjects were observed. However, for 3 patients (2, 4 and 7) both metabolic tumor volume (MTV) and TLCU were larger than those of the other subjects. This is likely explained by difficulty in lesion segmentation, such that errors in MTV are also propagated into poorer repeatability for TLCU.



Supplemental Table 1s. Comparison of repeatability (variance of relative test-retest difference) for different methods of normalization.

		Comparison		p-value Pitman-Morgan test
SUVmax	SUV	SUV _{AUC}	0.036	
	SUV	SUV _{TBR}	< 0.001 **	
	SUV _{AUC}	SUV _{TBR}	< 0.001 **	
SUVpeak	SUV	SUV _{AUC}	0.111	
	SUV	SUV _{TBR}	< 0.001 **	
	SUV _{AUC}	SUV _{TBR}	< 0.001 **	
SUVmean	SUV	SUV _{AUC}	0.016	
	SUV	SUV _{TBR}	< 0.001 **	
	SUV _{AUC}	SUV _{TBR}	0.001 *	

p-values for pairwise comparisons of variances of (selected combinations of) measures. * Significant at 5% level (Bonferroni-correction for 9 tests: p < 0.0056). ** Significant at 1% level (Bonferroni-correction for 9 tests: p < 0.0011).

Supplemental Table 2s. Comparison of repeatability (variance of relative test-retest differences) between SUVmax, SUVpeak and SUVmean using the Pitman-Morgan test.

		Comparison		p-value Pitman-Morgan test
SUV	SUVmax	SUVpeak	0.356	
	SUVmax	SUVmean	0.037	
	SUVpeak	SUVmean	0.455	
SUV _{AUC}	SUVmax	SUVpeak	0.184	
	SUVmax	SUVmean	0.081	
	SUVpeak	SUVmean	0.955	
SUV _{TBR}	SUVmax	SUVpeak	0.732	
	SUVmax	SUVmean	0.075	
	SUVpeak	SUVmean	0.219	

p-values for pairwise comparisons of variances of (selected combinations of) measures. Bonferroni correction for 9 tests performed by setting significance levels at 5% (0.05/9 = 0.0056) and at 1% (0.01/9 = 0.0011).

Supplemental Table 3s. Comparison of variance of relative test-retest differences between groups using the Levene's test (LevT).

		Type: (bone vs. lymph node)	Location: (intrathoracically vs. abdominal/pelvic)	Size: below median vs. median and above ¹
		p-value Lev test	p-value Lev test	p-value Lev test
SUVmax	SUV	0.754	0.944	0.092
	SUV _{AUC}	0.247	0.204	0.003*
	SUV _{TBR}	0.082	0.793	0.076
SUVpeak	SUV	0.655	0.808	0.264
	SUV _{AUC}	0.744	0.805	0.075
	SUV _{TBR}	0.226	0.354	0.459
SUVmean	SUV	0.718	0.725	0.556
	SUV _{AUC}	0.341	0.768	0.046
	SUV _{TBR}	0.257	0.541	0.537

¹median of the mean of the test and retest measurement; *Lev* Levene's test; * Significant at 5% level (Bonferroni-correction for 9 tests: p<0.0056)

Supplemental Table 4s. Relative test-retest difference (in percentage) of the semi-quantitative parameters as a function of uptake, metabolic tumor volume, metastatic tissue type and location.

RC (%)	SUVpeak	SUVpeak _{AUC}	SUVpeak _{TBR}	MTV	TLCU	TLCU _{AUC}	TLCU _{TBR}
All	24	28	45	36	33	31	51
SUVpeak >8.3	19	23	41	34	34	30	50
SUVpeak <8.3	28	31	47	36	31	32	51
MTV >4.2 cm ³	23	28	45	29	25	24	41
MTV <4.2 cm ³	25	24	44	45	42	40	62
Bone	24	27	47	34	31	30	52
Lymph node	23	28	36	36	36	32	48
Intrathoracically	17	23	39	37	36	40	48
Abdominal/pelvic	24	27	45	34	32	29	51

RC repeatability coefficients; SUV standardized uptake value; AUC area under the curve of blood activity concentration; TBR blood concentration 40 minutes after injection; MTV metabolic tumor volume; TLCU total lesion choline uptake.

Supplemental Table 5s. Test-retest difference of the semi-quantitative parameters as a function of uptake, metabolic tumor volume, metastatic tissue type and location.

RC (test-retest)	SUVpeak	SUVpeakAUC	SUVpeakTBR	MTV	TLCU	TLCUAUC	TLCUTBR
All	1.9	1.4	5.9	3.2	21	11	52
SUVpeak >8.3	2.3	1.7	7.5	3.9	28	13	61
SUVpeak <8.3	1.4	1.0	3.7	2.3	10	8.4	42
MTV >4.2 cm ³	2.0	1.6	6.9	3.9	27	14	62
MTV <4.2 cm ³	1.8	0.9	2.0	1.3	4.8	2.7	12
Bone	1.6	1.1	5.3	2.8	17	10	57
Lymph node	2.5	1.8	6.6	3.5	25	10	40
Intrathoracically	1.3	0.8	4.8	2.7	16	8.7	27
Abdominal/pelvic	2.0	1.5	6.1	3.3	23	11	51

RC repeatability coefficients; SUV standardized uptake value; AUC area under the curve of blood activity concentration; TBR blood concentration 40 minuten after injection; MTV metabolic tumor volume; TLCU total lesion choline uptake.



CHAPTER 6

A clinical and experimental comparison of time of flight PET/MRI and PET/CT systems

Daniela E. Oprea-Lager¹

Maqsood Yaqub¹

Indra C. Pieters¹

Rinze Reinhard¹

Reindert J.A. van Moorselaar²

Alfons J.M. van den Eertwegh³

Otto S. Hoekstra¹

Adriaan A. Lammertsma¹

Ronald Boellaard¹

¹Department of Radiology and Nuclear Medicine, VU University Medical Center, Amsterdam, the Netherlands

²Department of Urology, VU University Medical Center, Amsterdam, the Netherlands

³Department of Medical Oncology, VU University Medical Center, Amsterdam, the Netherlands

ABSTRACT

PURPOSE

The purpose of the study was to compare image quality and quantitative accuracy of positron emission tomography/ magnetic resonance imaging (PET/MRI) and PET/ computed tomography (PET/CT) systems with time of flight PET gantries, using phantom and clinical studies.

METHODS

Identical phantom experiments were performed on both systems. Calibration, uniformity, and standardized uptake value (SUV) recovery were measured. A clinical PET/CT versus PET/MRI comparison was performed using [¹⁸F]fluoromethylcholine ([¹⁸F]FCH).

RESULTS

Calibration accuracy and image uniformity were comparable between systems. SUV recovery met EANM/EARL requirements on both scanners.

Thirty-four lesions with comparable PET image quality were identified. Lesional SUVmax differences of $4\pm26\%$ between PET/MRI and PET/CT data were observed ($R^2=0.79$, slope=1.02). In healthy tissues, PET/MRI-derived SUVs were $16\pm11\%$ lower than on PET/CT ($R^2=0.98$, slope=0.86).

CONCLUSION

PET/MRI and PET/CT showed comparable performance with respect to calibration accuracy, image uniformity, and SUV recovery. [¹⁸F]FCH uptake values for both healthy tissues and lesions corresponded reasonably well between MR- and CT-based systems, but only in regions free of MR-based attenuation artifacts.

INTRODUCTION

Multimodality imaging has improved patient care over the past decade. Non-invasive, integrated positron emission tomography/ computed tomography (PET/CT) has proven to be a valuable diagnostic tool by combining *in vivo* metabolic and anatomic information [1]. Recently, several hybrid PET/ magnetic resonance imaging (PET/MRI) systems have become available clinically [2]. Strengths of MRI include its high soft tissue contrast, high spatial resolution, and lack of exposure to ionizing radiation. General Electric (GE) has built a tri-modality PET/CT and MRI system (tri-modality, Discovery PET/CT 690 & 3T Discovery MRI 750) [3]. Using silicon photomultiplier tubes (SiPMTs), GE also has developed a fully integrated PET/MRI system that has time of flight (TF) capabilities. However, this system still is a prototype and no (clinical) studies have been reported yet. Siemens has a fully integrated PET/MRI (Biograph mMR, Siemens Healthcare), which allows simultaneous PET and MRI acquisitions [4], enabling a reduction of total scan time. Philips has built a sequential PET and MRI system (Philips Ingenuity TF PET/MRI), with TF ability [5].

Although PET/CT was rapidly incorporated into routine clinical practice, PET/MRI faces a number of technical challenges. MRI requires well-controlled magnetic and radio frequency (RF) fields [5]. However, PET photomultiplier tubes (PMTs), which are needed to convert and amplify the signal from scintillation crystals into an electronic signal [6], do not function properly in a strong magnetic field. Solutions to this have included physically separating PET and MRI units [6] or using avalanche photodiodes (APDs), which in contrast to PMTs are not affected by the magnetic field [7]. APDs, however, have poorer timing resolution than PMTs and consequently they have no TF capability [8]. Recently, silicon PMTs (SiPMTs) have been described as a possible alternative to conventional PMTs, combining good energy and timing resolution with the ability to decode arrays of scintillator elements [9].

The second main challenge for PET/MRI is deriving accurate MR-based attenuation correction (MRAC) maps to correct corresponding PET data for tissue attenuation. Simultaneous Siemens PET/MRI systems use a four-tissue segmentation model, dividing a dedicated MR sequence in fat, air, lung, and soft tissue. Philips sequential PET/MRI systems employ a two- (air and soft tissue) or three-segmentation model (air, lung, and soft tissue). However, a limitation of all these approaches is that bone, the most attenuating tissue in the body, is not included in the segmentation process [10].

This yields underestimation of the standardized uptake values (SUVs) in bone lesions or lesions localized closed to bone structures. Furthermore, MRAC assumes uniform attenuation coefficients in lungs and suffers from MRI truncation due to the relatively small transaxial field of view (FOV; 45–50 cm) of the PET/MRI systems. All these shortcomings result in quantitative biases in the reconstructed PET images. Therefore, MRAC still requires major efforts to make PET/MRI studies accurate and robust [11].

PET/CT is used extensively in oncology for diagnosis, initial staging, restaging, therapy planning, and response monitoring of a variety of malignancies [12, 13]. Although PET/MRI is expected to be able to fulfill the same roles as PET/CT, this needs to be confirmed. There are promising initial results for several tumor types, including those seen in brain, head/neck, gynecological, and prostate [14–17]. However, just as for PET/CT, accurate SUV quantification [18] and, therefore, also accurate attenuation are required. With this in mind, it is important to know whether SUVs on PET/CT and PET/MRI are comparable.

The phantom and prospective clinical study presented here is distinct from other published work [19–20] with respect to two aspects. First of all, it represents a particular comparison of image quality and quantitative performance of PET studies using PET/CT and PET/MR systems from the same vendor with similar hardware and software for the PET TF gantries. Secondly, we performed PET/CT and PET/MRI studies in prostate cancer (PC) patients using [¹⁸F]fluoromethylcholine ([¹⁸F]FCH). Its known relatively stable biodistribution, with almost no radiotracer redistribution from about 10 to 90 min post injection (p.i.) [21], enables good scan statistics. This particular setup, the use of [¹⁸F]FCH and the two TF imaging systems, is suitable for evaluating the impact of MRAC on PET image quality and quantification.

MATERIALS AND METHODS

Scanners

The study was performed using a Gemini TF-64 PET/CT system (Philips Medical Systems, Best, the Netherlands) [8] and a 3.0 Tesla Ingenuity TF PET/MRI system (Philips Medical Systems, Cleveland, Ohio, USA). Both scanners are based on similar PET hardware, with some minor modifications necessary to make it compatible with the MRI scanner (Achieva 3T X-series MRI) [5]. The PET software version on the PET/

MRI is 9.7.1.0 and on the PET/CT is 9.5.1.4. Furthermore, on both scanners the same reconstruction algorithms are used, except that the attenuation correction maps (μ -maps) are different. For PET/CT, the μ -map is based on CT measurements of photon attenuation and uses a bilinear equation to convert to attenuation coefficients for 511-keV photon energies. For PET/MRI system, it is based on acquisition of a dedicated MR sequence (atMR), which subsequently is segmented into two (air and soft tissue) or three (air, lung, and soft tissue) classes of tissue, depending on the acquisition protocol (i.e., only pelvic region or body) and the ability of the software to detect lung contours [22]. The axial FOV (18 cm, with 9-cm overlap between bed positions) is the same for both systems and both have a 5.5-mm reconstructed isotropic spatial resolution.

Phantom measurements

Multiple phantom experiments were performed to determine specific performance characteristics of the PET/CT and PET/MRI systems, i.e. count rate linearity, calibration, uniformity, image quality, and contrast recovery. Both systems allow acquisitions in two modes: one specifically designed for the brain (brain mode, 2-mm voxels) and one for the body (body mode, 4-mm voxels). On both scanners, measurements were repeated up to five times, during a period of 1 year, using various acquisition protocols. In addition, phantom data were reconstructed using different algorithms and settings. All reconstructions included the usual corrections, such as detector normalization, decay, dead time, attenuation, as well as random and scatter corrections.

A cylindrical phantom (20-cm diameter, 9283 mL) filled with short-lived radionuclides (oxygen-15 and carbon-11) was used to assess count rate linearity over a wide range of radioactivity concentrations. The initial activity concentration was chosen to yield a single rate of 40 Mcps body dynamic acquisitions and 20 Mcps dynamic brain acquisitions. Data were reconstructed using a sinogram-based algorithm (3D-RAMLA) for the body mode and a non-sinogram-based algorithm (LOR-RAMLA) for the brain mode. Body mode images had a final voxel size of 4x4x4 mm³ and a spatial resolution of 5–7-mm full width at half maximum (FWHM) [5]. Brain mode images had a final voxel size of 2x2x2 mm³ and with similar spatial resolution. The dynamic image data was analyzed by defining one global region of interest in the phantom and calculating the average activity as a function of time. The calibration offset with regard to the true activity in the phantom was plotted versus true activity.

PET calibration and uniformity were assessed using the same cylindrical phantom as mentioned above. To assess image quality and SUV contrast recovery, the NEMA-NU2-2007 image quality (IQ) phantom (Data Spectrum Corporation, Durham, USA) was used. SUV contrast recovery was defined as the activity measured in the spheres relative to the true activity in the spheres (in %). Phantoms were filled with a 2-deoxy-2-[¹⁸F]-fluoro-D-glucose ([¹⁸F]FDG) solution using activity ranges of 1.3–3.9 (cylinder), 14.4–16.3 (spheres IQ), and 1.6–1.8 (background IQ) kBq·mL⁻¹ at the scan start time. Samples were taken and measured in a gamma well counter (Wallac 1480 Wizard 3" automatic gamma counter, Perkin Elmer Life Sciences, Zaventem, Belgium) in order to accurately define the activity in the phantoms and to be able to assess the calibration offset of the two scanners.

In the IQ phantom, the sphere to background radioactivity concentration ratio was set to ~10:1. Phantoms were scanned using the following acquisition protocols. First, using a single bed position, a 15-min acquisition was performed. Data were reconstructed using time of flight (blob-os-tf) [8] and sinogram-based (3D-RAMLA) algorithms, both resulting in a final voxel size of 4x4x4 mm³ and a spatial resolution of 5–7 mm FWHM. In clinical practice, blob-os-tf is used for static images and 3D-RAMLA for dynamic acquisitions. Second, a multi-bed position protocol, with 2 min per bed position, was performed.

In addition, the cylindrical phantom was scanned at a single bed position for 15 min in (dynamic) brain mode and reconstructed using a line of response-based reconstruction algorithm (LOR-RAMLA). This resulted in a final voxel size of 2x2x2 mm³ and the same spatial resolution as mentioned above. For the cylindrical phantom, image data acquired with and without the use of MR coils were assessed by measuring global and local (volumes of interest (VOIs) ~8 mL) calibration offsets and by visual inspection for artifacts. Data acquired with the IQ phantom were assessed for SUV performance compliance with European Association of Nuclear Medicine/Research Ltd (EANM/EARL) specifications [23].

Specific parameters and settings for phantom PET/MRI studies

The atMR sequence was used to generate μ -maps for the phantom studies. Specific attention to several points was required. Firstly, it is known that the signal from phantom walls is not detected by MRI. Therefore, attenuation by phantom walls is not corrected for, resulting in a constant underestimation of MRAC images (~5.5%

for 6-mm wall thickness). Secondly, for atMR acquisition on the MRI, phantoms were filled with a saline solution (~0.48%) in order to approximately match MR relaxation factors with those of patients. In addition, some MR processing parameters, such as inhomogeneity corrections, needed to be adjusted. Finally, dedicated MR sequences and image processing settings based on the two-class segmentation (water and air) were used in order to obtain appropriate μ -maps for the IQ phantom.

Patient studies

The clinical study was approved by the Medical Ethics Review Committee of the VU University Medical Center, Amsterdam, the Netherlands. All patients participating in the study provided written informed consent for undergoing additional PET/MRI examinations, following PET/CT scans acquired for clinical purposes. Inclusion criteria comprised the following: (1) ability to remain supine for an additional 60 min in the PET/MRI scanner after undergoing the PET/CT examination and (2) clinical indication for performing an [^{18}F]FCH PET/CT scan. Exclusion criteria were the standard absolute MRI contraindications (e.g. pacemaker, magnetic metal implants, neuro-stimulator, etc.). Relative (MRI) contraindications were claustrophobia and present or prior employment as a metalworker. For the latter patients, an X-ray of the orbit was performed prior to the PET/MRI in order to exclude possible metal splinters.

A total of 12 consecutive patients with histopathologically proven adenocarcinoma of the prostate were examined. Their mean age ($\pm\text{SD}$) was 66 ± 8 years. In all patients, the clinical indication for performing the PET/CT scans was restaging. This means suspected residual or recurrent disease after previous therapy, due to biochemical prostate-specific antigen (PSA) relapse. A PSA relapse was defined as a serum concentration level above $0.2\text{ ng}\cdot\text{mL}^{-1}$ after radical prostatectomy (RP) and more than $2\text{ ng}\cdot\text{mL}^{-1}$ above the nadir value in patients treated by means of external beam radiotherapy (EBRT) [24]. All examinations were performed at the VU University Medical Center between November 2012 and February 2014.

Patient characteristics, including age, year of PC diagnosis, type of primary treatment, PSA nadir, and PSA at the time of PET/CT and PET/MRI scans, as well as number, location, and visually assessed nature of all choline-avid lesions, are listed in Table 1.

Table 1. Patient and lesion characteristics.

Pat.	Age (years)	Diagnosis PC (year)	Previous therapy	PSAn (ng/ml)	PSAs (ng/ml)	Choline-avid lesions	Suspected benign			Suspected malignant	
							PET/CT	PET/MRI	PET/CT	PET/MRI	PET/CT
1	79	2002	EBRT	0.4	9.8	Prostate Th7					+
2	64	2011	EBRT	0.6	20.6	Prostate Sternum 10R	+	+			+
3	59	2010	RALP EBRT	0.2	17.4	Acetabull IliacL ParaAo Presacral Rib5R	+	+	+	+	+
4	73	2011	RALP	0.6	18	Th7 InguinalL InguinalR Presacral IliacR1 IliacR2	+	+	+	+	+
5	59	2010	RALP Anti-HT	7.7	8.7						+

Table1. Continued

Pat.	Age (years)	Diagnosis PC (year)	Previous therapy	PSAn (ng/ml)	PSAs (ng/ml)	Choline-avid lesions	Suspected benign		Suspected malignant	
							PET/CT	PET/MRI	PET/CT	PET/MRI
6	57	2010	RALP LND	6	14					
7	51	2007	RALP EBRT	0.2	5.4	iliacL			+	+
8	74	2007	Anti-HT Brachy	2.8	15.5	Prostate	+		+	
9	72	2007	Brachy	1.0	6.5	VesicleL	+	+	+	+
10	75	2009	Brachy Cryo	1.4	8.5	VesicleR Prostate iliac R	+	+	+	+
11	63	2011	RALP Anti-HT	0.8	4.5	Presacral1	+	+		
12	69	2010	RALP	0.2	2	Presacral2	+	+		
					10R		+	+		

Pat. Patient; PC prostate cancer; PSAn PSA nadir; PSAs PSA at the time of the PET scans; EBRT external beam radiation therapy; RALP robot-assisted laparoscopic prostatectomy; Anti-HT anti-hormonal therapy; LND lymph node dissection; Brachy, brachytherapy; Cryo cryotherapy; Para Ao para-aortic; Right, R; Left, L; Vesicle seminal vesicle.

PET/CT acquisition protocol

Patient preparation was similar to that required for [¹⁸F]FDG PET [22]. The standard activity of [¹⁸F]FCH was 4 MBq per kg body weight [21], resulting in an average (\pm SD) administered activity of 340 ± 57 MBq [¹⁸F]FCH. All patients underwent the same [¹⁸F]FCH PET/CT image acquisition protocol, including a low-dose CT (LD-CT) for anatomical localization and attenuation correction (AC), using a beam current of 30–50 mA at 100 keV. Thirty minutes p.i., a whole-body (WB) PET sequence was performed from mid-thigh to the base of the skull with arms up. The acquisition time was 2 min per bed position with a standard number of nine bed positions. The total acquisition time for the WB PET/CT was, on average, 30 min.

PET/MRI acquisition protocol

Subsequently to the PET/CT scans, PET/MRI acquisitions were obtained at 90 ± 3 min p.i., without administering an additional activity of [¹⁸F]FCH. The protocol included a survey MRI for defining the scan trajectory, followed by an atMR sequence used for AC of the subsequent PET scan. Next, a WB PET scan was performed, on average consisting of eight bed positions, each with 3-min acquisition time. The acquisition time was increased with 50% compared with the PET/CT scan to compensate for radioactive decay. The WB PET sequence also extended from mid-thigh to the base of the skull. Due to the small MRI gantry of the scanner, for the patient's convenience, all scans were acquired with arms down. Different diagnostic MRI protocols were applied as the MRI was done for initial MR optimization and to evaluate MR image quality and MR system performance and robustness. The following sequences were acquired: total body: coronal T1-weighted fast spin-echo (FSE), coronal short-tau inversion recovery (STIR), and axial Dixon sequences; prostatic region: T2-weighted turbo spin-echo (TSE) in axial, sagittal, or coronal planes and axial diffusion-weighted sequences. The total acquisition time for the WB PET/MRI protocol was, on average, 67 min.

Reconstruction of PET/CT and PET/MRI images

PET/CT and PET/MRI data were both reconstructed using the (same) vendor provided time of flight reconstruction algorithm (blob-os-tf), resulting in a final voxel size of $4 \times 4 \times 4$ mm³.

Image analysis

PET/CT and PET/MR images were interpreted in consensus by four experienced readers (two radiologists and two nuclear medicine physicians) who were aware of the clinical

history of the patients. Visual analysis of the images was performed on a dedicated Philips workstation (Philips Fusion Viewer on Extended Brilliance™ Workspace), following the approach used in clinical practice: (1) the lesions were evaluated on a single modality (e.g. PET), (2) they were evaluated on PET/CT and PET/MRI independently, and (3) PET/CT and PET/MRI findings were compared.

Lesions were defined as choline-avid structures (diffuse or focal [^{18}F]FCH uptake, exceeding background), incompatible with physiological uptake and with an anatomical substrate on MRI or CT. They were deemed benign or malignant based on the metastatic pattern of PC [25, 26]. Choline-avid lymph nodes in the mediastinal, hilar, or inguinal region were considered reactive/benign in the absence of a pathological lesion [27, 28]. [^{18}F]FCH uptake in all lesions (e.g., prostate, lymph nodes, bone) and certain normal tissues (e.g. lung, liver, and spleen) was assessed semi-quantitatively, by means of SUVs. This semi-quantitative approach was chosen to evaluate differences in [^{18}F]FCH uptake between the PET/CT and PET/MR scans and to eliminate observer variability. The method consisted of collecting different types of SUVs in target lesions or tissues, as a clinically preferred alternative to the gold standard full kinetic modeling [29]. Therefore, VOIs were drawn semi-automatically on PET images, as described previously [29, 30]. Maximum and 3D peak SUV, normalized to body weight (SUVmax and SUVpeak), were obtained for all lesions. In addition, mean SUV using a 2–3-cm diameter VOI was derived for healthy tissues, with one exception. In this patient, a VOI in normal lung could not be drawn due to an incomplete scan trajectory of the thorax. In all other 11 patients, VOIs were drawn in the left lung in order to avoid the effects of scatter effect from the physiologically intense choline uptake in the liver.

Statistical analysis

Pearson product moment correlation coefficients (R^2) were used to test agreement between visual ratings, and mean and maximum SUVs derived from PET/MRI and PET/CT. Correlations were assessed for bias using linear regression. In addition, percentage differences between PET/CT- and PET/MRI-derived SUVmax were plotted as function of the PET/CT derived SUVmax to illustrate relative differences in quantitative findings.

RESULTS

Phantom studies

Count rate linearity in brain mode was comparable between the two scanners. Calibration offsets, ranging from 2 to 10 kBq·mL⁻¹, were less than 10%. However, the performance in body mode showed slight differences between the systems with a stable performance (calibration offsets less than 5%) for PET/CT, whereas for PET/MRI, the calibration offsets were less than 10% with activity concentration ranging from 2 to 20 kBq·mL⁻¹ (supplemental Figure 1s). The images of the cylindrical phantom scanned on both systems showed uniform uptake and no visual artifacts.

Global calibration accuracy and image uniformity were comparable (within $\pm 10\%$) between PET/MRI and PET/CT systems (Table 2).

Table 2. Calibration offsets ranges (%) for PET/MRI and PET/CT systems for different reconstruction algorithms based on five measurements within 1 year. Calibration offset is defined as global activity of a cylindrical phantom in reconstructed PET images relative to the true activity measured using the dose calibrator.

Reconstruction	PET/MRI	PET/CT
Blob-os-tf	-5.8 to -1.5	-4.3 to 2.0
3D-RAMLA	-0.6 to 4.8	-6.9 to -0.4
LOR-RAMLA	-2.1 to 3.7	-6.5 to -0.3

PET/MRI studies with additional MRI coils required the use of additional template-based AC for the coils (Figure 1). However, template-based AC did not fully compensate for true attenuation of the coils, resulting in image artifacts in the PET images near the denser part of the coils. For example, image non-uniformities measured in a uniform source were up to 15% when using the neurovascular coils.

The NEMA NU-2 2007 image quality phantom was measured several times on both systems. The PET/CT met EANM/EARL requirements in all cases. Slightly higher contrast recoveries were found for the PET/MRI in comparison with the PET/CT (Figure 2) for smaller spheres (< 6 mL). Note that the AC by the phantom walls was not corrected because the signal from these walls (6 mm thick) is not detected by MRI. This resulted in a constant underestimation of the true recovery coefficients (5.5% lower activity concentration).

Figure 1. Example of coil attenuation effects: (a) image of the MR head-sense 8 coil, (b) PET acquisition including the MR head-sense 8 coil, but without a template for its attenuation correction, and (c) PET acquisition including the MR head-sense 8 coil and with a template for attenuation correction.

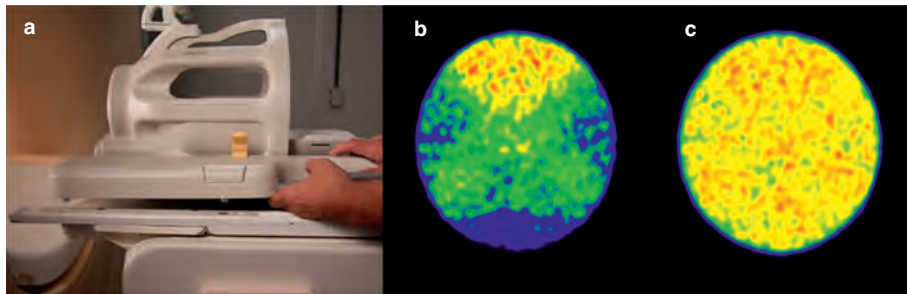
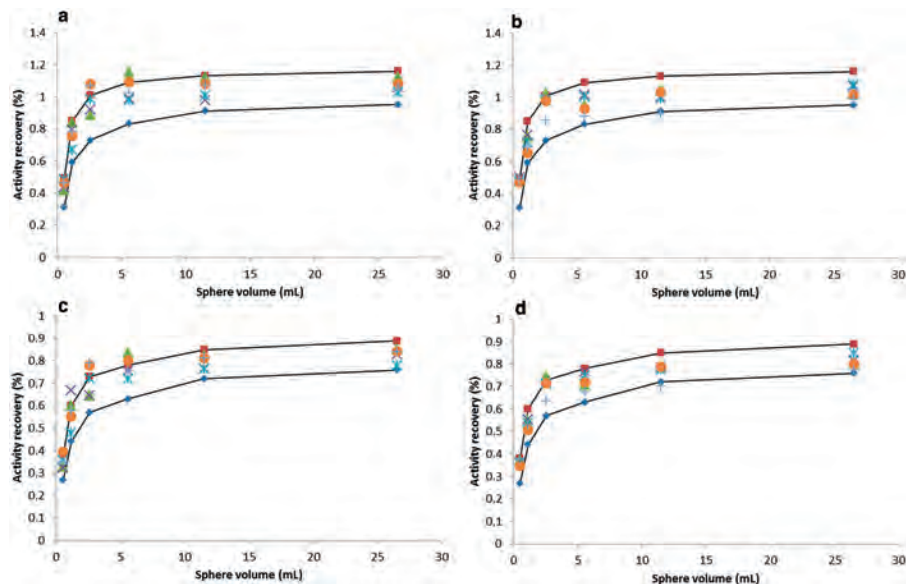


Figure 2. Measured activity recoveries (%) derived from the IQ phantom for both PET/MRI and PET/CT together with EARL boundaries (solid lines). Volumes of interest (VOIs) were defined based on a single voxel with maximum intensity (VOI_{max}) or as an isocontour at 50% of the maximum voxel intensity (VOI_{A50}): (a) PET/MRI VOI_{max}, (b) PET/CT VOI_{max}, (c) PET/MRI VOI_{A50}, (d) PET/CT VOI_{A50}. Five experiments were performed during a period of 1 year, each experiment indicated by a different symbol.

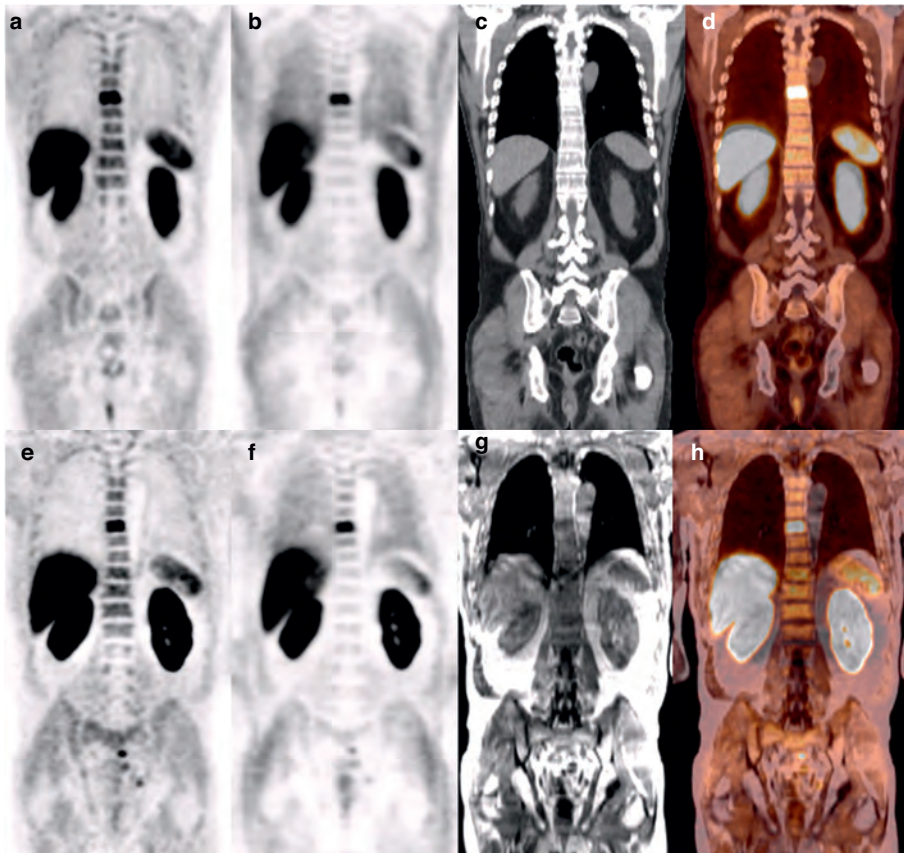


Patient results

A total of 12 benign and 22 suspected malignant lesions were identified on both PET/MRI and PET/CT systems. Coexistence of benign and malignant lesions was observed in five patients. In three patients no cause for an elevated PSA could be identified.

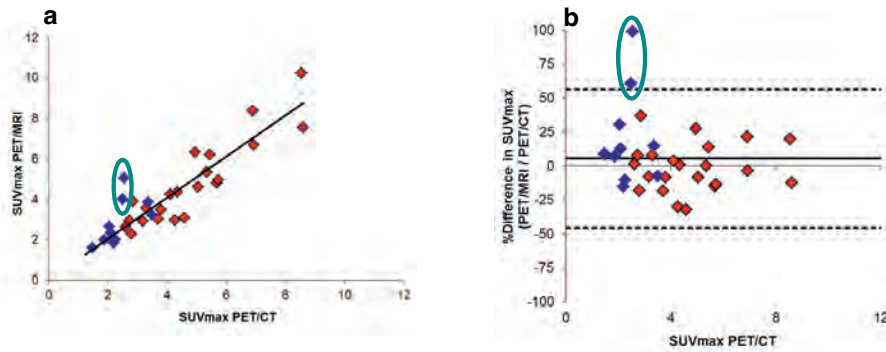
Benign/reactive lymph nodes were found in seven patients and were localized in the mediastinum ($n=2$), the lung hilar region ($n=3$) and the inguinal zone ($n=5$). In one patient, two pre-sacral lymph nodes with slightly increased choline uptake were seen. The intensity of uptake was less than on a PET/CT scan performed previously, consistent with a response to radiotherapy. Suspected malignant lesions were identified in nine patients and were represented by lymph nodes (seven iliac, two para-aortic, two pre-sacral), bone lesions (two thoracic vertebrae, one solitary acetabulum lesion, one rib, one sternal lesion) and residual/recurrent PC (four in the peripheral zone of the prostate and two in the seminal vesicles). Visual inspection showed comparable PET image quality for all lesions between both modalities (Figure 3).

Figure 3. $[^{18}\text{F}]$ FCH PET/CT and PET/MRI scans of patient 3 with recurrent prostate cancer and a PSA of $17.4 \text{ ng}\cdot\text{mL}^{-1}$. Both scans show comparable PET image quality in a suspected bone metastasis in the seventh thoracic vertebra: (a) attenuation corrected PET image of the PET/CT, (b) non-attenuation corrected PET image of the PET/CT, (c) low-dose CT image, (d) fusion image of $[^{18}\text{F}]$ FCH PET/CT, (e) attenuation corrected PET image of the PET/MRI, (f) non-attenuation corrected PET image of the PET/MRI, (g) MR-derived attenuation image, (h) fusion image of $[^{18}\text{F}]$ FCH PET/MRI.



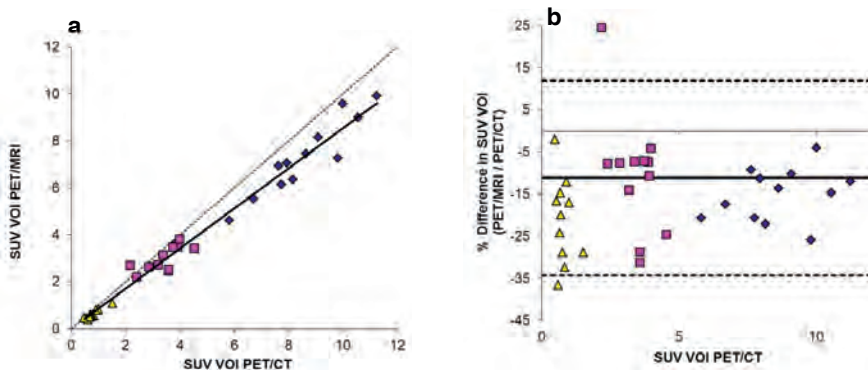
The semi-quantitative lesion analysis revealed a difference of $4\pm26\%$ in SUV values between PET/MRI and PET/CT data ($R^2=0.79$, slope=1.02) (Figure 4).

Figure 4. Results of the semi-quantitative analysis for benign (blue) and malignant (red) choline-avid lesions: (a) correlation between PET/MRI- and PET/CT-derived SUVmax ($R^2=0.79$, slope=1.02), and (b) corresponding Bland-Altman plot showing large differences for two intra-thoracic lesions (green ovals: one para tracheal and one hilar lymph node), which were due to incorrect lung segmentation of the PET/MRI scan.



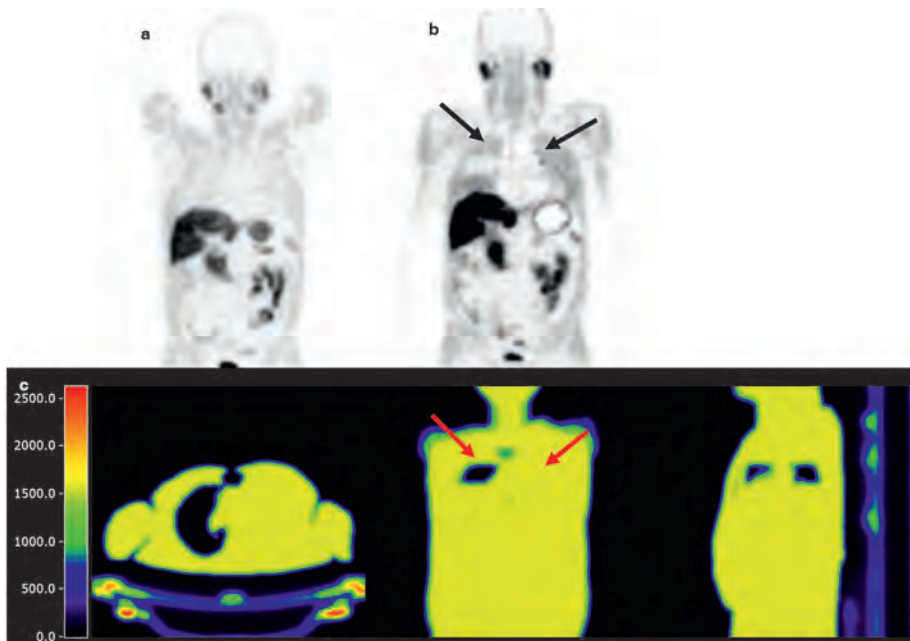
In normal tissues, PET/MRI SUV values were $16\pm11\%$ lower than corresponding values derived from PET/CT ($R^2=0.98$ slope=0.86) (Figure 5). The largest quantitative differences (up to -37%) were found in the lungs.

Figure 5. Results of the semi-quantitative analysis for healthy tissues: (a) correlation between PET/MRI- and PET/CT-derived SUVmax of liver (blue diamonds), spleen (pink squares) and lungs (yellow triangles) ($R^2=0.98$, slope=0.86) together with the line of identity, and (b) corresponding Bland-Altman plot showing the largest differences in the lungs (up to -37%).



Two out of 12 patients showed severe artifacts in the thorax region (patient no. 1: one lymph node in the right lung hilus; patient no. 2: one mediastinal left lower para tracheal lymph node) on PET/MRI images, resulting in discrepancies of more than 50%. These were due to incorrect lung segmentation in the MR μ -map (Figure 6). Incorrect AC in the lungs does affect the SUV of the lesions nearby located, such as the lung hilus or mediastinal space. This is because the measured lines of response going through both the lungs and adjacently regions are not correctly adjusted for attenuation. This means that the overall attenuation along each line of response determines the amplitude of the AC. Therefore, also activity adjacent to the lungs will suffer from errors in lung segmentation.

Figure 6. Impact of incorrect lung segmentation: (a) PET image using CT-based attenuation correction; (b) PET image using MRI-based attenuation correction, showing artificially increased uptake in the most of the lung tissue (black arrows); and (c) corresponding MRI- based attenuation map with incorrect lung segmentation (red left arrow: segmentation of only the apex of the right lung; red right arrow: no segmentation of the left lung).



DISCUSSION

The aim of this study was to directly compare image quality and quantitative performance of Philips Ingenuity TF PET/MRI with Gemini TF PET/CT systems, using phantoms and clinical data from a homogenous patient group. Because the PET gantries of both scanners are similar, it can be assumed that the performance of both PET units would be similar. To the best of our knowledge, this comparison has not previously been reported. In addition, by performing PET/CT and PET/MR studies in PC patients with [^{18}F]FCH, the relatively stable biodistribution with almost no pharmacokinetic changes between about 10 and 90 minutes p.i., minimizes radiotracer redistribution, and robust scan statistics are expected.

Phantom experiments

The phantom experiments showed comparable performances with respect to calibration accuracy, image uniformity, and contrast recovery. Due to differences between CT and MRI, some differences related to AC could be anticipated (e.g., phantom walls cannot be measured using MRI). This shortcoming, however, seemed to have a relatively low impact (not exceeding 5.5%) on final accuracy in the phantom studies. The calibration offset of PET/MRI, together with the expected underestimation, resulted in comparable calibration accuracy for PET/MRI and PET/CT. Furthermore, a cylindrical phantom reconstructed using various available methods showed, on both scanners, uniform uptake without visual artifacts.

Some differences were seen with respect to count rate linearity, which was more accurate on PET/CT than on PET/MRI. These might be due to differences in scanner calibration software between the systems—the PET/CT is equipped with a more recent software version incorporating improved calibration and dead time correction tables. Furthermore, slightly higher recoveries in the smaller spheres (<6 mL) were observed in case of the PET/MRI. These might be due to a combination of calibration offsets and shortcomings in the AC of the phantom. Apart from these minor differences, these initial phantom evaluations show that basic PET performance characteristics of PET/CT and PET/MRI systems are comparable.

MRAC remains challenging, especially when using WB PET/MRI for clinical purposes. Firstly, WB PET/MRI scan is a time-consuming procedure, requiring a stepwise optimization of the scan sequences [31]. Because of the small diameter of the MR

gantry, patients are scanned with arms down. A smaller transaxial MRI field of view than the patients' circumference may result in truncation artifacts in the MR images. Lung segmentation is another challenge, due to the diminished signal intensity of these air-containing organs in conventional MRI images. Furthermore, the current PET/MRI systems have no ability to characterize bone tissue [32], resulting in underestimation of the SUVs in bone lesions or in visceral lesions predominantly surrounded by bone structures (e.g., pelvic region).

Clinical evaluations

For the clinical comparison, [¹⁸F]FCH was used as radiotracer because of its known stable pharmacokinetic profile [24] with limited biological redistribution during the protocol period. At present, [¹⁸F]FCH is seen as one of the preferred tracers for restaging PC. A systematic review and meta-analysis [33] showed a pooled sensitivity and specificity to identify all recurrent/metastatic localizations (prostatic region, bone, or lymph node) of 85.6% (95% CI 82.9–88.1%) and 92.6% (95% CI 90.1–94.6%), respectively.

In the present study, visual assessment of choline-avid lesions showed comparable PET image quality on both PET/CT and PET/MRI systems. Although PET/MRI showed the same detection rate of lesions compared with PET/CT, severe artifacts due to incorrect lung segmentation were identified in a small number of patients. This underlines the necessity to always inspect μ -maps, as well as attenuation- (MRAC) and non-attenuation-corrected (NAC) images to avoid incorrect conclusions from severe AC artifacts.

Similar observations with respect to lesion detection and quantitative measurements were described by Tian et al. [34] in an [¹⁸F]FDG PET/CT and PET/MRI comparative study of 285 patients with different malignancies. A strong diagnostic concordance between [¹⁸F]FDG PET/CT and PET/MRI was also found by Kohan et al. [35] in the context of lymph node staging of lung cancer patients. The authors addressed both tissue AC and anatomical nodal localization issues by using a single morphological MRI sequence (3D T1-weighted spoiled gradient echo sequence; T1w 3D GRE). Nevertheless, the applied sequence yielded a number of artifacts on the PET/MRI, limiting the confident anatomic localization in some mediastinal lesions. Drzezga and colleagues [36] described comparable reliability of data derived from [¹⁸F]FDG PET/MRI and PET/CT studies in patients with suspected malignant lesions. Pace et al. [37] showed an equivalent performance of the two hybrid modalities in 36 patients with breast cancer undergoing initial staging or follow-up scans.

In PC, comparable results regarding lesion detection were described by Souvatzoglou et al. [19] in a study performed for (re)staging patients using [¹¹C]choline PET/CT, followed by an integrated PET/MRI. Evaluating 36 patients with histologically proven PC and suspected recurrent disease, Wetter et al. [20] found no difference in visual quality of PET images between [¹⁸F]FCH PET/MRI and PET/CT systems and concluded that the new [¹⁸F]FCH PET/MRI technique could be used with confidence in daily practice.

In the absence of PET/MRI artifacts (in two cases), the semi-quantitative analysis of the present data showed good correspondence in [¹⁸F]FCH uptake values between PET/CT and PET/MRI for both healthy tissues ($R^2=0.98$) and lesional data ($R^2=0.79$). Analysis of various lesions revealed slightly higher SUVs for PET/MRI ($4\pm26\%$) than for PET/CT, while values in normal tissues were systematically lower ($16\pm11\%$). The lowest SUVs were found in lungs, followed by spleen and liver. A possible reason for these differences might be a small ongoing redistribution of [¹⁸F]FCH with a slightly decreasing trend over time in normal or benign lesions and a stable or slightly increasing pattern in malignant lesions [28, 38–39]. As there was a mixture of benign and malignant lesions, this could have resulted in some over- and underestimations of PET/MR versus PET/CT data. However, the observed variability is likely also related to differences in AC performance between both systems.

Deriving accurate MRAC correction maps to correct corresponding PET data for tissue attenuation in PET/MRI remains a challenging task. Inadequate AC results in under- or overestimation of SUVs in different tissues (e.g., underestimation of the SUVs in bone lesions or lesions localized closed to bone structures, due to excluding the bone tissue in the segmentation process). In the particular case of the lungs, the theoretically assumed uniform attenuation coefficients are responsible for the lower SUVs in these organs [11]. In clinical practice, due to physiological, variable lung tissues densities, these attenuation coefficients lead to attenuation undercorrection and consequently to underestimation of the SUVs in the lungs.

Higher lesional SUVs on PET/MRI were also observed by Souvatzoglou et al. [19] with good correlation between [¹¹C]choline PET/MRI and PET/CT ($p=0.86$). In the same study, SUVs of various normal organs, except liver, were generally lower for PET/MRI and all these differences were attributed to the uptake mechanism of [¹¹C]choline. In contrast, statistically significant ($p<0.05$) lower lesional SUV values were reported by Wetter et al. [20] for bone and prostate, with slightly higher SUVs for lymph nodes. The

authors used [¹⁸F]choline as radiotracer for performing the scans on a simultaneous PET/MRI system. Possible explanations of the discrepancy between their findings and those from the group of Souvatzoglou were different techniques for AC and different biodistribution and biokinetics of [¹⁸F]FCH between early and delayed time points. The slight differences between the present findings and those of Wetter et al., while using the same radiotracer, underline the role of multiple factors contributing to underestimation in SUVs. In this respect, we agree with the German group's hypothesis suggesting that differences in SUVs on PET/MRI are possibly related to different examination time points and MRAC.

Although in our study we focused on PET image quality and quantitative accuracy, the opportunities of assessing patients with the combined and concurrent use of PET/CT and PET/MRI will be shortly discussed. Integrated PET/CT is nowadays recognized as a preferred hybrid oncological imaging technique. It combines the anatomical information derived from CT with the functional data of tumor metabolism from PET, in an efficient whole-body setting. Nevertheless, combining PET with MRI, simultaneously or sequentially, offers new perspectives in clinical molecular imaging [40]. Three evident advantages of the new hybrid technique are the superior soft tissue contrast of MRI above CT, less radiation exposure, and the additional functional information. Nevertheless, performing PET/MRI in a whole-body setting is a time-consuming procedure, in which adequate selection of the MR sequences, clinical indications, and workflow-related aspects have to be considered.

PET/MRI is expected to be more accurate than PET/CT for tumor staging in all indications in which MRI has proven to be more valuable than CT (e.g. head and neck tumors, breast and liver malignancies, musculoskeletal neoplasms, etc.). Comparable performance is expected for lymph node staging as N-disease assessment is mainly diagnosed on functional (PET) imaging. For metastatic disease, potential advantages of PET/MRI over PET/CT depend on the site of metastatic spread [15]. In case of prostate cancer, potential PET/MRI indications are staging in patients with a positive biopsy, assessment of tumor recurrence after treatment in patients with increasing PSA, and tumor detection in case of increased PSA but negative biopsies [31].

With regard to the quantification differences between PET/CT and PET/MRI systems in our study, several shortcomings of MR-based AC have to be mentioned. On the one hand, there are general aspects, all vendors having difficulties with MRI truncation

artifacts, not including bone structures in the segmentation process and assigning uniform lung attenuation coefficients. Specific for Philips TF PET/MRI is that it uses a three-tissue segmentation model, dividing a dedicated MR sequence in air, lung, and soft tissue. Other PET/MRI systems perform a four-segmentation model, including fat as an additional class for generating the attenuation maps. Ignoring fat may result in a small overall overestimation of the AC. Nevertheless, several approaches have been developed and evaluated to mitigate these shortcomings [41]. Furthermore, Philips designed a sequential PET/MRI system with TF ability, requiring longer acquisition time when compared with the simultaneous (e.g. Siemens) systems. However, MRAC is still work-in-progress, future clinical studies being needed to evaluate the usefulness of the different PET/MRI designs.

A limitation of the present study is represented by the sequential character of the study design, resulting in a possible redistribution of the tracer between the imaging time points of the PET/CT and PET/MRI. Nevertheless, we have specifically chosen [¹⁸F]FCH as radiotracer for this evaluation in order to minimize these effects. The good correspondence in SUVs across most lesions also points into this direction. Furthermore, a measurable difference in scan statistics can be expected by performing the PET/CT and the PET/MRI with a gap of 60 min. To compensate for this effect, the acquisition time on PET/MRI was increased with 50% compared with that applied during the PET/CT scan. Another possible limitation is the variability of the used MRI protocol, as MR images were acquired in a process of optimizing imaging procedures. Yet, the same amount of lesions was identified on both PET/CT as well as PET/MRI. In a more optimal MRI setting, it is anticipated that the PET/MRI will outperform PET/CT in, e.g., differentiation of benign versus malignant lesions and identification of tumor ingrowth in surrounding soft tissue structures, including the seminal vesicles or rectal wall. However, this was not the primary aim of the present study and this remains to be studied in further studies.

CONCLUSION

This study demonstrates that PET/MRI and PET/CT systems provide comparable performance with respect to calibration accuracy, image uniformity, and contrast recovery. In the absence of PET/MRI attenuation correction artifacts, there was reasonably good correspondence between [¹⁸F]FCH uptake in both healthy tissues and

suspect lesions, yet systematically lower SUVs in normal tissues were seen for PET/MRI. Therefore, further improvement of MR-based attenuation correction is warranted. Furthermore, it is recommended to inspect attenuation corrections maps in order to avoid (quantitative) misinterpretations due to attenuation correction artifacts.

ACKNOWLEDGMENTS

We thank all the patients participating in this study. We would also like to acknowledge the fine technical support of Femke Jongsma, Nasserah Sais, and Paul Horstman.

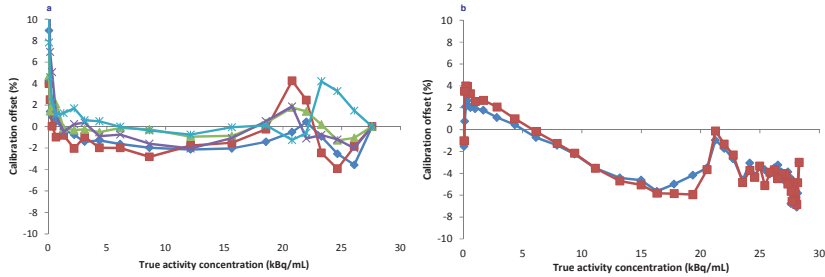
REFERENCES

1. Schiepers C and Dahlbom M. Molecular imaging in oncology: the acceptance of PET/CT and the emergence of MR/PET imaging. *Eur Radiol.* 2011;21:548–554
2. Pichler B, Kolb A, Nägele and Schlemmer HP. PET/MRI: paving the way for the next generation of clinical multimodality imaging applications. *J Nucl Med.* 2010;51:333–336
3. Bettinardi V, Presotto L, Rapisarda E, Picchio M, Gianolli L and Gilardi MC. Physical performance of the new hybrid PET/CT Discovery-690. *Med Phys.* 2011;38:5394–5411
4. Delso G, Furst S, Jakoby B, et al. Performance measurements of the Siemens mMR integrated whole-body PET/MR scanner. *J Nucl Med.* 2011;52:1914–1922
5. Zaidi H, Ojha N, Morich M, et al. Design and performance evaluation of a whole-body Ingenuity TF PET–MRI system. *Phys Med Biol.* 2011;56:3091–3106
6. Ter Pogossian MM, Phelps ME, Hoffman EJ and Mullani NA. A positron-emission transaxial tomograph for nuclear imaging (PETT). *Radiology.* 1975;114:89–98
7. Pichler BJ, Judenhofer MS, Catana C, et al. Performance test of an LSO-APD detector in a 7-T MRI scanner for simultaneous PET/MRI. *J Nucl Med.* 2006;47:639–647
8. Surti S, Kuhn A, Werner ME, Perkins AE, Kolthammer J and Karp JS. Performance of Philips Gemini TF PET/CT scanner with special consideration for its time-of-flight imaging capabilities. *J Nucl Med.* 2007;48:471–480
9. Roncali E and Cherry SR. Application of Silicon Photomultipliers to Positron Emission Tomography. *Annals of Biomedical Engineering.* 2011;39:1358–1377
10. Marshall HR, Patrick J, Laidley D, et al. Description and assessment of a registration-based approach to include bones for attenuation correction of whole-body PET/MRI. *Med Phys.* 2013;40:082509.doi: 10.1118/1.4816301
11. Hofmann M, Pichler B, Schölkopf B and Beyer T. Towards quantitative PET/MRI: a review of MR based attenuation correction techniques. *Eur J Nucl Med Mol Imaging.* 2009;36:93–104
12. Fletcher JW, Djulbegovic B, Soares HP, et al. Recommendations on the use of 18F-FDG PET in oncology. *J Nucl Med.* 2008;49:480–508
13. Juweid ME, Stroobants S, Hoekstra OS, et al. Use of positron emission tomography for response assessment of lymphoma: consensus of the Imaging Subcommittee of International Harmonization Project in Lymphoma. *J Clin Oncol.* 2007;25:571–578
14. Kjær A, Loft A, Law J, et al. PET/MRI in cancer patients: first experiences and vision from Copenhagen. *MAGMA.* 2013;26:37–47
15. Antoch G and Bockisch A. Combined PET/MRI: a new dimension in whole-body oncology imaging? *Eur J Nucl Med Mol Imaging.* 2009;36:S113–S120
16. Balyasnikova S, Löfgren J, de Nijs R, Zamogilnaya Y, Højgaard L and Fischer BM. PET/MR in oncology: an introduction with focus on MR and future perspectives for hybrid imaging. *Am J Nucl Med Mol Imaging.* 2012;2:458–474
17. Hirsch FG, Sattler B, Sorge I, et al. Initial clinical experience in paediatric oncology using an integrated PET/MR scanner. *Pediatr Radiol.* 2013;43:860–875
18. Boellaard R. Standards for PET Image Acquisition and Quantitative Data Analysis. *J Nucl Med.* 2009;50:11S–20S
19. Souvatzoglou M, Eiber M, Takei T, et al. Comparison of integrated whole-body [¹¹C]choline PET/MR with PET/CT in patients with prostate cancer. *Eur J Nucl Med Mol Imaging.* 2013;doi 10.1007/s00259-013-2467-y2013
20. Wetter A, Lipponer C, Nensa F, et al. Evaluation of the PET component of simultaneous [¹⁸F]choline PET/MRI in prostate cancer: comparison with [¹⁸F]choline PET/CT. *Eur J Nucl Med Mol Imaging.* 2014;41:79–88
21. DeGrado TR, Reiman RE, Price DT, Wang S and Coleman RE. Pharmacokinetics and radation dosimetry of 18F-fluorocholine. *J Nucl Med.* 2002;43:92–96
22. Hu Z, Ojha N, Renisch S, et al. MR-based Attenuation Correction for a Whole-body Sequential PET/MR System. *IEEE Nuclear Science Symposium Conference Record.* 2009;3508–3512
23. Boellaard R, O'Doherty MJ, Weber WA, et al. FDG PET and PET/CT: EANM procedure guidelines for tumour PET imaging: version 1.0. *Eur J Nucl Med Mol Imaging.* 2010;37:181–200
24. Heidenreich A, Bellmunt J, Bolla M, et al. EAU guidelines on prostate cancer. Part 1: screening, diagnosis, and treatment of clinically localised disease. *Eur Urol.* 2011;59:61–71

25. Bubendorf L, Schöpfer A, Wagner U, et al. Metastatic patterns of prostate cancer: an autopsy study of 1,589 patients. *Hum Pathol.* 2000;31:578–583
26. Tokuda Y, Carlino LJ, Gopalan A, et al. Prostate cancer topography and patterns of lymph node metastasis. *Am J Surg Pathol.* 2010;34:1862–1867
27. Rietbergen DDD, van der Hiel B, Vogel W and Stokkel M.P.M. Mediastinal lymph node uptake in patients with prostate carcinoma on ^{18}F -choline PET/CT. *Nucl Med Commun.* 2011;32:1143–1147
28. Oprea-Lager DE, Vincent AD, van Moorselaar RJ, et al. Dual-phase PET-CT to differentiate ^{18}F -fluoromethylcholine uptake in reactive and malignant lymph nodes in patients with prostate cancer. *PLoS One.* 2012;7:e48430
29. Frings V, de Langen AJ, Smit EF, et al. Repeatability of metabolically active volume measurements with ^{18}F -FDG and ^{18}F -FLT PET in non-small cell lung cancer. *J Nucl Med.* 2010;51:1870–1877
30. Cheebsumon P, van Velden FH, Yaqub M, et al. Effects of image characteristics on performance of tumor delineation methods: a test-retest assessment. *J Nucl Med.* 2011;52:1550–1558
31. Vargas MI, Becker M, Garibotto V, et al. Approaches for the optimization of MR protocols in clinical hybrid PET/MRI studies. *MAGMA.* 2013;26:57–69
32. Bezrukov I, Mantlik F, Schmidt H, Schölkopf B and Pichler BJ. MR-based PET attenuation correction for PET/MR imaging. *Semin Nucl Med.* 2013;43:45–59
33. Evangelista L, Zattoni F, Guttilla A, et al. Choline PET or PET/CT and biochemical relapse of prostate cancer—a systematic review and meta-analysis. *Clin Nucl Med.* 2013;38:305–314
34. Tian J, Fu L, Yin D, Zhang J, et al. Does the novel integrated PET/MRI offer the same diagnostic performance as PET/CT for oncological indications? *PLoS One.* 2014;9:e90844
35. Kohan AA, Kolthammer JA, Vercher-Conejero JL, et al. N staging of lung cancer patients with PET/MRI using a three-segment model attenuation correction algorithm: Initial experience. *Eur Radiol.* 2013;doi:10.1007/s00330-013-2914-y
36. Drzezga A, Souvatzoglou M, Eiber M, et al. First clinical experience with integrated wholebody PET/MR: comparison to PET/CT in patients with oncologic diagnoses. *J Nucl Med.* 2012;53:845–855
37. Pace L, Nicolai E, Luongo A, et al. Comparison of whole-body PET/CT and PET/MRI in breast cancer patients: lesion detection and quantitation of ^{18}F -deoxyglucose uptake in lesions and in normal organ tissues. *Eur J Radiol.* 2014;83:289–296
38. Beheshti M, Imamovic L, Broinger C, et al. ^{18}F choline PET/CT in the preoperative staging of prostate cancer in patients with intermediate or high risk of extracapsular disease: a prospective study of 130 patients. *Radiology.* 2010;254:25–33
39. Kwee SA, Wei H, Sesterhenn I, Yun D and Coel MN. Localization of primary prostate cancer with dual-phase ^{18}F -fluorocholine PET. *J Nucl Med.* 2006;47:262–269
40. Appenzeller P, Mader C, Huellner MW, et al. PET/CT versus body coil PET/MRI: how low can you go? *Insights Imaging.* 2013;4:481–490
41. Boellaard R, Hofman MB, Hoekstra OS and Lammertsma AA. Accurate PET/MR quantification using time of flight MLAA image reconstruction. *Mol Imaging Biol.* 2014;16:469–477

SUPPLEMENTAL DATA

Supplemental Figure 1s. The count rate linearity of the systems, as function of activity: PET/CT (a) and PET/MRI (b).



CHAPTER 7

GENERAL DISCUSSION, SYNTHESIS AND PERSPECTIVES

Prostate cancer (PC) represents a challenging oncological entity, with an increasing incidence with age and a very diverse clinical behavior. After treatment with curative intent, recurrence is common during the first decade. Despite initial response to anti-hormonal therapy, the majority of PC patients will ultimately progress and reach a castration-resistant (CR) state. Recently, several therapeutic options against castration-resistant prostate cancer (CRPC) have emerged, flowing from improved molecular profiling knowledge about the heterogeneous biological behavior of PC. Nevertheless, despite the variety of therapeutic options, proper sequencing (e.g., modality, timing) in individual patients with PC is unclear. To this end, it is essential to develop “instruments” able to identify which phenotype is predominant within PC patients and timely evaluate the response to therapy, thus avoiding futile costly and toxic treatments.

Hybrid imaging techniques (e.g., PET/CT, PET/MRI) play a pivotal role in clinical management of PC, offering both functional and anatomical information. However, the most commonly used oncological PET tracer, [¹⁸F]fluorodeoxyglucose ([¹⁸F]FDG), shows limited sensitivity for the detection of androgen dependent PC. Alternatively, encouraging results have been reported on the use of radiolabeled choline derivates as PET tracers for PC [1–5]. Because of its longer half-life (110 versus 20 minutes) and better spatial resolution, [¹⁸F]fluoromethylcholine ([¹⁸F]FCH) is more convenient for routine clinical use than ¹¹C-labeled choline, by providing more flexibility concerning imaging protocols and broader availability. Therefore, the aim of this thesis was to technically validate [¹⁸F]FCH as initial steps on the road towards imaging guided personalized therapy for metastatic PC.

Chapter 1 comprises the introduction and outline of this thesis. Some epidemiological aspects and biological characteristics of PC are discussed, followed by an overview of current therapeutic options in metastatic PC. The role of hybrid imaging in PC is outlined, together with the available qualitative and various quantitative approaches. Finally, [¹⁸F]FCH is introduced as a promising radioactive tracer, by describing its metabolic pathway and current clinical indications, as well as the potential use for response evaluation and prediction in PC.

Since [¹⁸F]FCH is rapidly cleared from the blood pool and, unlike ¹¹C-choline, is excreted via the kidneys, acquisition protocols have been designed with pelvic imaging prior to bladder filling (i.e., within minutes after injection), followed by a whole body scan after e.g., 30 min – the “dual-phase protocol”. Patterns of tracer uptake as a function

of time help to characterize intraprostatic tracer uptake, as well as sites of suspected haematogeneous metastases. It was suggested that increasing or stable [¹⁸F]FCH uptake over time is compatible with malignancy. However, for lymph node assessment this concept has not been validated. Therefore, in **chapter two** we investigated the diagnostic role of dual-phase [¹⁸F]FCH PET/CT in a clinical setting. We studied whether time-trends of enhanced radiolabeled choline in lymph nodes (LN) of PC patients can help to discriminate reactive from malignant ones, and whether single time point standardized uptake value (SUV) measurements may also suffice.

25 PC patients with inguinal (presumed benign) and enlarged pelvic LN (presumed malignant) showing enhanced [¹⁸F]FCH uptake at dual-phase PET/CT were analyzed. Associations between LN status (benign versus malignant) and SUV_{max} and $SUV_{meanA50}$, determined at 2 min (early) and 30 min (late) post injection (p.i.), were assessed. We considered two time-trends of [¹⁸F]FCH uptake: type A ($SUV_{early} > SUV_{late}$) and type B ($SUV_{late} \geq SUV_{early}$). Histopathology and/or follow-up were used to confirm the assumption that LN with type A pattern are benign, and LN with type B pattern malignant.

We identified 54 LN with enhanced [¹⁸F]FCH uptake, both at early (2 min p.i.) as well as late (30 min p.i.) time points. Highly significant associations were found between the LN status (inguinal/benign vs. enlarged pelvic/malignant) and the SUV_{max} and $SUV_{meanA50}$ 30 min p.i., and their absolute and relative differences ($p < 0.0001$). ROC analyses of uptake trends over time and of SUVs at either time-point showed that the SUV_{max} relative difference was the best predictor of the LN status.

In our referral-based spectrum of patients with enhanced [¹⁸F]FCH uptake in pelvic and inguinal lymph nodes, decreasing [¹⁸F]FCH uptake over time seems to be a reliable tool to differentiate benign and malignant nodes. Together with similar findings by others to classify radioactive choline positive lesions suspected to represent hematogeneous metastases, our results are relevant for clinical decision making and simplification of diagnostic procedures (e.g., in patients with elevated PSA and positive [¹⁸F]FCH PET findings). Moreover, the results underline the relevance of a sequential PET imaging protocol after a single injection of [¹⁸F]FCH to account for the time-trend of tracer uptake. Single time-point SUV measurements, 30 min p.i., may be a reasonable alternative for predicting the nodal status, but this remains to be validated in non-enlarged pelvic lymph nodes.

The results presented in our study pertain to the ability of tracer uptake time-trends to classify LN with enhanced [¹⁸F]FCH uptake. Reported 'sensitivity' and 'specificity' should not be confused with 'the accuracy' of [¹⁸F]FCH PET/CT to diagnose metastatic lymph nodes in prostate cancer. To date, discordant results have been presented in the literature on the usefulness of choline PET/CT in LN staging of newly diagnosed patients with PC. Sensitivity of this technique is influenced by the diameter of metastases and limited by the low PET spatial resolution [6–10]. However, in this setting, other imaging modalities [e.g., transrectal ultrasound, computed tomography (CT), magnetic resonance imaging (MRI)] are less accurate. In case of restaging patients with biochemical relapse, choline PET/CT seems to be a valuable tool, especially in presence of higher prostate-specific antigen (PSA) values and faster PSA kinetics [11, 12]. In this context, the major limitation of the present studies is the histopathological confirmation).

Upon establishing that radioactive choline can play a diagnostic role in clinical practice, in **chapter three** we studied an alternative potential application of [¹⁸F]FCH in metastatic PC. Since the actual response to (chemo)therapeutic regimens in individual PC patients is variable, and potentially effective alternative regimens are available, it is important to monitor therapeutic (in)efficacy in time. Presently, this is based on a response metrics construct of PSA measurements, CT scans and bone scintigraphy. The limitations of the current approach are related to the heterogeneity of metastasized PC (i.e., coexistence of androgen sensitive and insensitive components with different impact on e.g., PSA) and to its skeletal predominance (with bone- and CT-scans having difficulties in timely and accurately detecting response). Therefore, there is a clear need for more accurate response monitoring methods.

In-vitro data have shown promising results on the use of PET tracers to monitor anti-androgen treatment (e.g., bicalutamide) or chemotherapy (e.g., docetaxel) in androgen-independent cell lines [13]. There is some recent evidence that [¹⁸F]FCH might be also useful as a biomarker of response to anti-androgen therapy in patients with metastatic CRPC [14]. Whether [¹⁸F]FCH could also be employed in monitoring treatment response in patients receiving docetaxel and cabazitaxel therapy is unclear. Therefore, we investigated whether accumulation of [¹⁸F]FCH, in comparison with [¹⁸F]FDG, accurately reflects chemotherapy efficacy at the tumor cell level in PC, both in androgen-dependent and independent cell lines. We analyzed the effects of docetaxel and cabazitaxel on viable tumor cell numbers and tracer uptake in four PC cell lines.

Cellular uptake of [¹⁸F]FDG and [¹⁸F]FCH was measured using the sulforhodamine B (SRB) assay, cell counting and a colony formation assay (CFA), as metrics for viable tumor cell numbers.

Comparing the reduction in cellular uptake of radioactive [¹⁸F]FCH in prostate tumor cells *in vitro* as a function of different dosages of docetaxel and cabazitaxel, with parameters of cell viability, we found that the radiotracer uptake was proportional to the number of residual cells after therapy. These cell numbers correlated well to clonogenic capacity as an additional sign of (reproductive) viability of the cells surviving the treatment. Our *in vitro* data demonstrate that the cellular [¹⁸F]FCH uptake fits well with viable tumor cell number after docetaxel and cabazitaxel for all PC cell lines, while [¹⁸F]FDG at times overestimated the cell number after drug exposure. This suggests that [¹⁸F]FCH is more accurate and therefore more suitable than [¹⁸F]FDG to measure the response to docetaxel and cabazitaxel. Therefore, we propose to design clinical studies to validate these findings *in vivo*.

Since experiments *in vitro* suggested radiolabeled choline to be a suitable tracer for response monitoring in PC, in **chapter four** we investigated how [¹⁸F]FCH can be applied and reliably measured in a routine clinical setting. As uptake of [¹⁸F]FCH should reflect viable tumor tissue, changes over time may serve as a measure of response to therapy. For monitoring response to systemic treatment in metastasized PC, however, accurate quantification is required, preferably with clinically applicable, simple quantitative methods. Such simplifications need to be validated versus the standard kinetic modelling PET methods. Omitting this validation step may seriously confound the clinical biomarker validation process, as has been demonstrated with [¹⁸F]FDG and [¹⁸F]FLT. Therefore, pharmacokinetic modeling of dynamic PET data in combination with arterial blood sampling was used to determine the appropriate plasma input compartment model for [¹⁸F]FCH. In addition, the validity of using an image-derived input function in combination with manual venous blood samples, instead of arterial blood sampling, was investigated, and the validity of using simplified methods for quantification of [¹⁸F]FCH was assessed.

Forty-minute dynamic PET/CT scans were acquired after injection of 204 ± 9 MBq [¹⁸F]FCH, from eight patients with histologically proven metastasized PC. Plasma input functions were derived using continuous arterial blood sampling (BSIF) as well as using image-derived (IDIF) methods. Manual arterial blood samples were used for

calibration and correction for plasma-to-blood ratio and metabolites. Time activity curves (TAC) were derived from volumes of interest (VOI) in all visually detectable LN metastases. [¹⁸F]FCH kinetics were studied by non-linear regression fitting of several single- and two-tissue plasma input models to the TAC. Model selection was based on Akaike information criterion (AIC) and measures of robustness. In addition, the performance of several simplified methods, such as SUV, was assessed.

Best fits were obtained using an irreversible compartment model with blood volume parameter. Correspondence between venous and arterial parent fractions was low, as determined by the intraclass correlation coefficient (ICC = 0.61). Results for IDIF derived from VOI in blood pool structures distant from tissues of high [¹⁸F]FCH uptake, yielded good correlation to those for BSIF ($R^2 = 0.83$). SUV showed poor correlation to parameters derived from full quantitative kinetic analysis ($R^2 < 0.34$). In contrast, lesion activity concentration normalized to the integral of the blood activity concentration over time (SUV_{AUC}) showed good correlation ($R^2 = 0.92$ for metabolite corrected plasma and $R^2 = 0.65$ for whole-blood activity concentrations).

We concluded that [¹⁸F]FCH uptake should be quantified using full kinetic modeling with $1T1k + V_B$ and metabolite-corrected plasma input function based on arterial blood sampling. Results indicate that SUV cannot be used to estimate [¹⁸F]FCH uptake. A clinically feasible alternative could be $SUV_{AUC, WB}$ based on two consecutive PET scans.

Before clinical validation of [¹⁸F]FCH PET as a predictive biomarker of response can be initiated, it is essential to know the physiological range of day-to-day variability of the tracer uptake measures. This should help to assess whether observed changes during therapy represent true signal change instead of noise. This “repeatability” of a test is defined as the measurement precision with conditions that remain unchanged between replicate measurements (repeatability conditions) [15]. Knowledge of these operational characteristics of tests is an essential component of the technical biomarker validation process. Traditionally, changes of tracer uptake have dominated as PET-based response prediction biomarkers. More recently, evidence has emerged that measures of metabolically active tumor volume may also provide relevant information. To this end, in **chapter five**, we assessed the repeatability of various quantitative [¹⁸F]FCH parameters, including metabolic tumor volume (MTV) and total lesion choline uptake (TL CU), in PC.

Twelve patients (64±8 years) with metastasized PC underwent 2 sets of [¹⁸F]FCH PET/CT scans, on two successive days. Each set consisted of a 30 minutes dynamic PET/CT scan of the chest, after intravenous administration of 200 MBq [¹⁸F]FCH, followed by a whole body (WB) PET/CT at 40 minutes. The dynamic scan was used to derive the area under the curve (AUC) of the blood activity concentration. Lesion uptake was derived from the WB scan using various volumes of interest (VOI): maximum, peak and mean. Each of these parameters was normalized to injected activity/weight, blood AUC and blood concentration itself at 40 minutes, resulting in several SUV, SUV_{AUC} and SUV_{TBR} values. Repeatability of these semi-quantitative parameters, MTV and TLCU, respectively were studied. The level of agreement between test-retest data and reliability was assessed using repeatability coefficients (RC), intraclass correlation coefficients and Bland-Altman plots.

We identified 67 choline avid metastases, 44 bone and 23 lymph node lesions. 12 metastases were located in the chest. In case of SUV_{max}, repeatability coefficients for SUV, SUV_{AUC} and SUV_{TBR} were 26, 31 and 46%, respectively. Similar values were obtained for SUV_{peak} and SUV_{mean}. Repeatability of SUV_{AUC} was comparable with that of standard SUV, for maximum, peak and mean values. Tissue type (e.g., bone versus lymph node) and tumour location did not affect repeatability. Repeatability did not differ between lesions with SUV_{peak} above or below the median value of 8.3 ($p=0.264$). The relative test-retest difference for MTV was 36%. Repeatability of MTV was independent of uptake, tissue type and location. MTV smaller than 4.2 cm³ had larger variability than larger volumes (RC 45 versus 28%, $p=0.048$). Repeatability of TLCU and TLCU_{AUC} were comparable (RC 33 versus 31%, $p=0.954$), while TLCU_{TBR} showed larger variance of 51% ($p<0.001$). Repeatability of TLCU was independent of uptake, MTV, tissue type or location.

We concluded that repeatability of SUV_{AUC} was comparable to that of standard SUV, indicating that [¹⁸F]FCH PET/CT uptake differences of 30% or more are likely to represent treatment effects. Repeatability of MTV and TLCU, respectively was ~35%. Observed repeatabilities are of the same order of magnitude as those seen for other commonly used radiotracers, such as [¹⁸F]FDG and [¹⁸F]Fluorotymidine ([¹⁸F]FLT).

Since MRI is an important and potentially powerful diagnostic method in PC, perhaps challenging or complementing PET, we questioned if the knowledge acquired about the use of [¹⁸F]FCH PET/CT is also applicable to PET/MRI. Therefore, in **chapter six** we

performed a clinical and technical validation of [¹⁸F]FCH in PC, by comparing image quality and quantitative accuracy of PET/MRI and PET/CT systems with identical time-of-flight PET gantries, using phantom and clinical studies. The same phantom experiments were performed using both systems, by measuring calibration, uniformity, and SUV recovery. The clinical PET/CT versus PET/MRI comparison was performed using [¹⁸F]FCH.

Calibration accuracy and image uniformity were comparable between systems. SUV recovery met EANM/EARL requirements on both scanners. Thirty-four lesions with comparable PET image quality were identified. Lesional SUV_{max} differences of $4\pm26\%$ between PET/MRI and PET/CT data were observed ($R^2=0.79$, slope=1.02). In healthy tissues, PET/MRI-derived SUVs were $16\pm11\%$ lower than on PET/CT ($R^2=0.98$, slope=0.86). Our main conclusion was that PET/MRI and PET/CT showed comparable performance with respect to calibration accuracy, image uniformity, and SUV recovery. [¹⁸F]FCH uptake values for both healthy tissues and lesions corresponded reasonably well between magnetic resonance (MR)- and computed tomography (CT)-based systems, but only in regions free of MR-based attenuation artifacts. Nevertheless, the usefulness of PET/MRI remains to be elucidated in clinical, prospective studies with large cohorts of patients.

SYNTHESIS AND PERSPECTIVES

Taken together, $[^{18}\text{F}]$ FCH PET/CT may qualify as a biomarker of response in PC, based on its appropriate lesion to background contrast, its promising in vitro performance in detection of changing viable load during therapy, and the apparent accuracy of generally applicable, simplified quantitative whole body measures. The semi-quantitative methods have repeatability characteristics comparable with those observed with other broadly used tracers (e.g., $[^{18}\text{F}]$ FDG, $[^{18}\text{F}]$ FLT). As imaging plays an increasing role in the clinical management of PC, we also performed a technical and clinical validation of PET/CT and PET/MRI systems with identical time-of-flight gantries, using $[^{18}\text{F}]$ FCH. We found comparable performance between the systems with regard to the technical characteristics and an acceptable clinical correspondence, with limitations mainly due to inherent MR-based attenuation artifacts.

In case of PC, PET/MRI is presumed to be more accurate than PET/CT for primary staging, e.g., by combining high-resolution prostate images (e.g., diffusion weighted imaging (DWI)) and metabolic/molecular imaging ($[^{18}\text{F}]$ FCH PET). Comparable PET/CT and PET/MRI performance is expected for LN staging, as nodal disease (especially small < 8 mm metastatic LN) assessment is mainly diagnosed on functional (PET) imaging. For distant metastases, possible advantages of PET/MRI over PET/CT depend on the site of metastatic spread. Potential PET/MRI indications are staging in patients with a positive biopsy, assessment of tumor recurrence after treatment in patients with increasing PSA, and tumor detection in case of increased PSA but negative biopsies. However, MR attenuation correction remains a limiting factor, demanding research for technical improvement [16]. With regard to the whole body PET/MRI systems currently available, there is a clear preference for fully integrated PET/MRI scanners in daily practice. Truly simultaneous PET and MRI acquisitions carry less risk of patient movement since scan time is shorter than with sequential PET/MRI, improving patient throughput at the same time. [16].

Significant progress has recently been made in improving acquisition and interpretation of multiparametric MRI (mpMRI), with an extended role of mpMRI from local staging toward lesion detection and biopsy guidance [17]. Combining both anatomical and functional pulse sequences (i.e., T1-weighted MRI, T2-weighted MRI, DWI or MR spectroscopy), mpMRI shows promising results for biopsy planning and targeting. MpMRI is also useful in the evaluation of extracapsular extension, neurovascular bundle

involvement, seminal vesicle invasion and/or invasion of adjacent structures, such as rectum and urinary bladder, thus preventing futile curative surgery [18]. Developments in the acquisition of mpMRI are ongoing. The DW technique is improved by the use of high b-value DW-MRI. Progress in this field has resulted in implementation of high b-value DW-MRI as a component of the prostate imaging reporting and data system (PIRADS) evaluation criteria [19]. However, an important drawback of mpMRI is the difficulty in detecting small malignant foci in the prostate ($<0.5\text{ cm}^3$) and low-risk Gleason score lesions [20]. Future well-structured studies investigating the best manner to calculate high b-value DW-MRI are needed since functional information hereby provided may guide the optimal therapeutic choice.

Apart from radiolabeled choline, new tracers such as ^{18}F -16 β -18F-fluoro-5 α -dihydrotestosterone ($[^{18}\text{F}]$ FDHT), and ^{68}Ga -PSMA are demonstrating promising results in recurrent and metastatic PC. $[^{18}\text{F}]$ FDHT is a biomarker for androgen receptor (AR) expression in human PC, mainly useful in the CRPC state. It has good imaging characteristics, with rapid uptake in malignant cells at metastatic sites expressing AR [21]. Research is ongoing to investigate its role in stratification of patients for systemic therapy and in monitoring treatment effects in patients undergoing novel anti-androgen therapies.

Serial experiments have recently demonstrated the importance of targeting the prostate-specific membrane antigen (PSMA) with either ^{68}Ga - or ^{123}I -labelled PSMA inhibitors [22, 23]. PSMA is a membrane-type zinc protease which is negatively regulated by androgen and significantly overexpressed in androgen-independent PC. Increased PSMA expression in PC is associated with higher tumor grade and a high risk of disease progression, as defined by biochemical recurrence after initial curative therapy [24]. Since PSMA elevation is inversely correlated to time to prostate-specific antigen (PSA) progression and disease-free survival, this tracer has the potential to serve as a biomarker for estimating the aggressiveness of PC [24]. Furthermore, PSMA represents an ideal biological target for accurate functional imaging of PC, due to an improved sensitivity to detect small LN-, bone- and liver- metastases [22]. Advantages of ^{68}Ga - labelled PSMA ligands above choline tracers are twofold: a better signal to background ratio and no cyclotron requirement, since ^{68}Ga can be extracted from a commercially available $^{68}\text{Ge}/^{68}\text{Ga}$ radionuclide generator [18]. The role of labeled PSMA in PC is currently under investigation.

Another tracer, a radiolabeled leucine analogue, 1- amino-3-fluorocyclobutane-1-carboxylic acid in the 'anti' configuration ($[^{18}\text{F}]\text{FACBC}$), can be also used to depict amino acid transportation in PC. Since only a small fraction is excreted through the urinary tract after intravenous administration, its imaging characteristics seem to be favorable in the evaluation of prostate cancer [25]. Research data indicate that $[^{18}\text{F}]\text{FACBC}$ can be successfully used in the assessment of primary and metastatic PC. Preliminary results indicate also that $[^{18}\text{F}]\text{FACBC}$ may be superior to radiolabeled choline for the identification of disease recurrence in case of biochemical failure [26, 27]. Nevertheless, these findings have to be confirmed in larger, prospective studies.

An important aim of any "diagnosis-treatment" combination is to improve the quality of life of patients with metastatic PC. To validate that $[^{18}\text{F}]\text{FCH}$ may contribute to this purpose, we suggest the following research, beyond the technical validation described in this thesis. Firstly, $[^{18}\text{F}]\text{FCH}$ reproducibility studies (measuring test-retest variability in a multicenter setting) are needed to complete the technical validation. Secondly, clinical 'biological validation' studies to define the accuracy and optimal methodology of $[^{18}\text{F}]\text{FCH}$ to predict clinical response to systemic therapy are needed. Thirdly, comparative $[^{18}\text{F}]\text{FCH}$ PET/CT and DWI studies may be considered: if DWI and $[^{18}\text{F}]\text{FCH}$ PET have similar value in overall response prediction, a combination of $[^{18}\text{F}]\text{FDHT}$ and DWI might help to separate and quantify the androgen-receptor phenotype from the overall tumor load, before and during therapy. Moreover, by opting for active surveillance in case of a coexistent phenotype, these studies will provide the opportunity to timely start effective treatment in case of PC progression. Finally, cost-effectiveness of any diagnosis-therapy combination should be evaluated to support appropriate decision-making by clinicians, patients and health care providers during the management of metastatic prostate cancer.

REFERENCES

1. Bauman G, Belhocine T, Kovacs M, et al. ^{18}F -fluorocholine for prostate cancer imaging: a systematic review of the literature. *Prostate Cancer Prostatic Dis.* 2012;15:45–55
2. DeGrado TR, Baldwin SW, Wang S, et al. Synthesis and evaluation of (^{18}F) -labeled choline analogs as oncologic PET tracers. *J Nucl Med.* 2001;42:1805–1814
3. Fuccio C, Rubello D, Castellucci P, et al. Choline PET/CT for prostate cancer: main clinical applications. *Eur J Radiol.* 2011;80:e50–e56
4. Picchio M, Briganti A, Fanti S, et al. The role of choline positron emission tomography/computed tomography in the management of patients with prostate-specific antigen progression after radical treatment of prostate cancer. *Eur Urol.* 2011;59:51–60
5. Reske SN, Blumstein NM, Neumaier B, et al. Imaging prostate cancer with ^{11}C -choline PET/CT. *J Nucl Med.* 2006;47:1249–1254
6. Beheshti M, Imamovic L, Broinger G, et al. ^{18}F choline PET/CT in the preoperative staging of prostate cancer in patients with intermediate or high risk of extracapsular disease: a prospective study of 130 patients. *Radiology.* 2010; 254: 925–933
7. Poulsen MH, Bouchelouche K, Gerke O, et al. $[^{18}\text{F}]$ -fluorocholine positron-emissioncomputed tomography for lymph node staging of patients with prostate cancer: preliminary results of a prospective study. *BJU International.* 2010;106:639–643
8. De Jong IJ, Pruijm J, Elsinga PH, Vaalburg W, and Mensink HJ. Preoperative staging of pelvic lymph nodes in prostate cancer by ^{11}C -choline PET. *J Nucl Med.* 2003;44:331–335
9. Steuber T, Schlomm T, Heinzer H, et al. $[^{18}\text{F}]$ -fluoroethylcholine combined in-line PET-CT scan for detection of lymph-node metastasis in high risk prostate cancer patients prior to radical prostatectomy: preliminary results from a prospective histology-based study. *EJC.* 2010;2:449–455
10. Hacker A, Jeschke S, Leeb K, et al. Detection of pelvic lymph node metastases in patients with clinically localized prostate cancer: comparison of $[^{18}\text{F}]$ fluorocholine positron emission tomography-computerized tomography and laparoscopic radioisotope guided sentinel lymph node dissection. *J Urol.* 2006;176:2014–2019
11. Breeuwsma AJ, Pruijm J, van den Bergh ACM, et al. Detection of local, regional, and distant recurrence in patients with PSA relapse after external-beam radiotherapy using ^{11}C -choline positron emission tomography. *IJROBPS.* 2010;77:160–164
12. Cimitan M, Bortolus R, Morassut S, et al. $[^{18}\text{F}]$ fluorocholine PET/CT imaging for the detection of recurrent prostate cancer at PSA relapse: experience in 100 consecutive patients. *Eur J Nucl Med Mol Imaging.* 2006;33:1387–1398
13. Müller SA, Holzapfel K, Seidl C, Treiber U, Krause BJ and Senekowitsch-Schmidtke R. Characterization of choline uptake in prostate cancer cells following bicalutamide and docetaxel treatment. *Eur J Nucl Med Mol Imaging.* 2009;36:1434–1442
14. Caroli P, de Giorgi U, Moretti A, et al. Use of ^{18}F -Methylcholine PET/CT in early assessment of response to therapy with enzalutamide, in patients with metastatic castration-resistant prostate cancer: results of a pilot study. *J Nucl Med.* 2015;56(Suppl 3):52P
15. Sullivan DC, Obuchowski NA, Kessler LG, et al. Metrology Standards for Quantitative Imaging Biomarkers. *Radiology* 2016;000:1–13
16. Yaqub M, Oprea-Lager DE, Hofman M and Boellaard R. Methodological aspects of PET/MR imaging. *Tijdschr v Nucl Geneesk.* 2013;35:1153–1159
17. Bouchelouche K, Turkbey B and Choyke PL. Advances in imaging modalities in prostate cancer. Global cancer statistics. *Curr opin Oncol.* 2015;27:224–231
18. Picchio M, Mapelli P, Panebianco V, et al. Imaging biomarkers in prostate cancer: role of PET/Ct and MRI. *Eur J Nucl Med Mol Imaging* 2015;42:644–655
19. Barentsz JO, Richenberg J, Clements R, et al. ESUR prostate MR guidelines 2012. *Eur Radiol.* 2012;22:746–757
20. Turkbey B, Mani H, Aras O, et al. Prostate cancer: can multiparametric MR imaging help identify patients who are candidates for active surveillance? *Radiology* 2013;268:144–152
21. Larson SM and Schoder H. New PET tracers for evaluation of solid tumor response to therapy. *Q J Nucl Med Mol imaging.* 2009;53:158–166

22. Afshar-Oromieh A, Zechmann CM, Malcher A, et al. Comparison of PET imaging with a ⁶⁸Ga-labelled PSMA ligand and ¹⁸F-choline-based PET/CT for the diagnosis of recurrent prostate cancer. *Eur J Nucl Med Mol Imaging* 2014;41:11–20
23. Barrett JA, Coleman RE, Goldsmith SJ, et al. First-in-man evaluation of 2 high-affinity psma avid small molecules for imaging prostate cancer. *J Nucl Med*. 2013;54:380–387
24. Perner S, Hofer MD, Kim R, et al. Prostate-specific membrane antigen expression as a predictor of prostate cancer progression. *Human Pathology*. 2007;38:696–701
25. Oka S, Hattori R, Kurosaki F, et al. A preliminary study of anti-1-amino-3-18F-fluorocyclobutyl-1-carboxylic acid for the detection of prostate cancer. *J Nucl Med*. 2007;48:46–55
26. Schuster DM, Taleghani PA, Nieh PT, et al. Characterization of primary prostate carcinoma by anti-1-amino-2-[¹⁸F]-fluorocyclobutane-1-carboxylic acid (anti-3- [¹⁸F]FACBC) uptake. *Am J Nucl Med Mol Imaging*. 2013;3:85–96
27. Nanni C, Schiavina R, Boschi S, et al. Comparison of F-FACBC and ¹¹C-choline PET/ CT in patients with radically treated prostate cancer and biochemical relapse: preliminary results. *Eur J Nucl Med Mol Imaging*. 2013;40(Suppl 1):S11–17.

Addendum

LIST OF ABREVIATIONS

AC	Attenuation correction
ADT	Anti-androgen therapy
AIC	Akaike information criterion
APD	Avalanche photodiodes
AR	Androgen receptor
AUC	Area under the curve
BMI	Body mass index
BSA	Body surface area
BSIF	Blood sampling input function
BT	Brachytherapy
BW	Body weight
CFA	Colony formation assay
CK	Choline kinase
CR	Castration resistant
CRPC	Castration resistant prostate cancer
CSS	Cancer specific survival
CT	Computed tomography
DNA	Deoxyribonucleic acid
EANM/EARL	European Association of Nuclear Medicine/ Research Ltd
EBRT	External beam radiation therapy
FDHT	16β -18F-fluoro-5 α -dihydrotestosterone
FID-GC	Flame ionization detector-gas chromatography
FOV	Field of view
FWHM	Full width at half maximum
[¹⁸ F]FCH	[¹⁸ F]fluoromethylcholine
[¹⁸ F]FDG	[¹⁸ F]fluorodeoxyglucose
[¹⁸ F]FLT	[¹⁸ F]fluorothymidine
HPLC	High performance liquid chromatography
HT	Hormonal Therapy
IBW	Ideal body weight
ICC	Intraclass correlation coefficient
IDIF	Image derived input function
IQ	Image quality
IQR	Interquartile range
LBM	Lean body mass
LBr	Lesion to blood ratio

LD-CT	Low dose- computed tomography
LMr	Lesion to muscle ratio
LN	Lymph node
LNM	Lymph node metastasis
MLL	R 3327-MATLyLu
mpMRI	Multiparametric magnetic resonance imaging
MRAC	Magnetic resonance based attenuation correction
MRI	Magnetic resonance imaging
MTV	Metabolic tumor volume
NAC	Non attenuation correction
NLR	Non linear regression
p.i.	Post injection
PC	Prostate cancer
PET	Positron emission tomography
PLND	Pelvic lymph node dissection
PMT	Photomultiplier tubes
PSA	Prostate-specific antigen
PTS	Portable test system
PVDF	Polivinylidenedifluoride
ROC	Receiver operating characteristics
ROI	Region of interest
RP	Radical prostatectomy
RT	Radiation therapy
SiPMT	Silicon photomultiplier tubes
SRB	Sulforhodamine B
STIR	Short tau inversion recovery
SUV	Standardized uptake value
TAC	Time activity curve
TF	Time of flight
TLCU	Total choline lesion uptake
TSE	T2-weighted turbo spin echo
VOI	Volume of interest
WB	Whole body

DUTCH SUMMARY – NEDERLANDSE SAMENVATTING

Op weg naar geïndividualiseerde therapie voor gemetastaseerd prostaatcarcinoom: een technische validatie van [¹⁸F]fluoromethylcholine

PROSTAATKANKER

Prostaatkanker is de op een na meest voorkomende vorm van kanker bij mannen. Het komt vooral voor bij mannen van boven de 50 jaar, en de incidentie stijgt met de leeftijd. De uiting van prostaatkanker is heel divers. Sommige tumoren zijn indolent, goed gedifferentieerd, en geven geen klinische symptomen. Echter, bij een aanzienlijk percentage patiënten is er sprake van een agressievere vorm van prostaatkanker, waarbij uitzaaiingen (metastasen) ontstaan, die uiteindelijk tot de dood kunnen leiden.

De eerste vorm van systemische therapie, die wordt gegeven aan patiënten met een uitgezaaid prostaatcarcinoom, is hormonale behandeling. Hoewel bij de meeste patiënten de hormoontherapie aanvankelijk goed aanslaat, ontstaat er vaak progressie van ziekte onder therapie. Op dat moment is de prostaatkanker castratie refractair. Dit gebeurt meestal in een tijdsbestek van 18 tot 36 maanden.

Tot enkele jaren geleden was docetaxel chemotherapie elke 3 weken in combinatie met prednison de standaardbehandeling voor patiënten met een castratie refractair prostaatcarcinoom (CRPC). Deze behandeling geeft een overlevingswinst van enkele maanden. De laatste jaren zijn nieuwe behandel mogelijkheden ontwikkeld voor patiënten met CRPC, allen met een bewezen overlevingsvoordeel van enkele maanden. Cabazitaxel, een ander taxaan, is een vorm van tweedelijns chemotherapie. Daarnaast, zijn er op basis van moleculaire studies nieuwe middelen ontwikkeld die interfereren met de androgene stimulatie van tumorgroei. Zowel enzalutamide als abiraterone in combinatie met prednison hebben de mediane overleving van patiënten met CRPC verbeterd. Dit effect is aangetoond zowel pre- als postdocetaxel. Sipuleucel-T is een vorm van immuuntherapie, waarbij eigen mononucleaire cellen zodanig worden bewerkt dat zij de prostaatkankercellen gaan herkennen en 'aanvallen'. Hoewel Sipuleucel-T geen verbetering geeft van de progressie-vrije overleving, is er wel een bewezen positief effect op de mediane overleving. Sipuleucel-T is in Nederland niet beschikbaar. Tot slot is het botzoekende radionuclide Radium-223-chloride geregistreerd voor de behandeling van patiënten met vooral botmetastasen.

Doordat deze nieuwe behandel mogelijkheden in een korte tijd bestek zijn onderzocht en geïntroduceerd, is er onduidelijkheid ontstaan over de beste volgorde waarin deze middelen aan de patiënten kunnen worden voorgeschreven. Daarnaast moet rekening gehouden worden met de economische gevolgen van deze therapieën vanwege de relatief hoge kosten. Zowel uit ethisch als uit economisch oogpunt, is dus behoefte ontstaan om methoden te ontwikkelen die kunnen zorgen voor 'therapie-op-maat'. Hiervoor zijn instrumenten nodig waarmee het phenotype van de prostaatkanker in de individuele patiënt kan worden gekarakteriseerd. Als dit wordt gecombineerd met klinische parameters, zoals evaluatie van de respons op de behandeling, kan in de toekomst hopelijk beter voorspeld worden welke patiënt baat zal hebben van een bepaalde behandeling. Hiermee kunnen zinloze, dure en toxische behandelingen worden vermeden.

DE ROL VAN BEELDVORMING BIJ PROSTAATKANKER

Nauwkeurige diagnostiek bij prostaatkanker is essentieel, omdat de therapeutische mogelijkheden afhankelijk zijn van, onder andere, het stadium en de graad van de ziekte, en de manier van metastasering (dat wil zeggen: via de bloed- of de lymfebanen). Conventionele beeldvormingstechnieken, zoals transrectale echo, computertomografie (CT) en magnetische resonantie imaging (MRI) worden routinematiig gebruikt bij prostaatkanker, maar hun diagnostische nauwkeurigheid is niet optimaal. Multimodale beeldvorming heeft de patiëntenzorg verbeterd in de afgelopen tien jaar. De niet-invasieve functionele positronemissietomografie / computertomografie (PET/CT) blijkt een waardevol diagnostisch instrument. Het combineert "in vivo" metabolische en anatomische informatie.

PET is een beeldvormende techniek gebaseerd op de waarneming van gelijktijdig uitgezonden fotonen, afkomstig van de annihilatie van positronen met elektronen in de omliggende weefsels. PET maakt gebruik van radiofarmaca. Deze bestaan uit een radionuclide, in het geval van PET een positron emitter, gekoppeld aan een andere stof (ligand). De radiofarmaca worden via de aders toegediend aan patiënten en verzamelen zich op bepaalde plaatsen in het lichaam (bijvoorbeeld een tumor). Het radionuclide vervalt onder uitzending van een positron. Dit positron annihileert na het afleggen van een korte weg (1-2 mm) met een elektron, waarbij twee annihilatiefotonen met een energie van 511 keV onder een hoek van 180 graden ontstaan. De PET detectoren registreren deze fotonen "in coïncidentie". Voor elke annihilatie kan zo vastgelegd

worden, waar hij heeft plaatsgevonden en op die manier wordt een beeld gevormd van de verdeling van het radionuclide in het lichaam.

PET is een uiterst gevoelige beeldvormende modaliteit, waarvoor zeer kleine hoeveelheden radioactief gemerkte moleculen (tracers, ~ nM) worden geïnjecteerd. De meting van de tracerdistributie maakt kwantitatieve beoordeling van de weefselse functie mogelijk, zonder dat de onderliggende fysiologie wordt veranderd. Tegenwoordig is het met de huidige generatie PET/CT systemen met time-of-flight (TOF) mogelijk de exacte locatie van het annihileren van de fotonen te bepalen. Dit geeft beelden met een hoge resolutie en een betere signaal-ruisverhouding.

Een visuele, kwalitatieve beoordeling van de verzwakte en niet-verzwakte PET beelden vormt de basis van elke PET-interpretatie. Een tumor wordt op PET gedefinieerd als een gebied met hogere opname van radioactiviteit (bijv. radioactief gelabeld choline) dan de omringende achtergrond, die tevens incompatibel is met de fysiologische accumulatie van de tracer.

De belangrijkste valkuil met betrekking tot de beoordeling van PET-scans vormen significante verschillen in de PET-interpretatie tussen verschillende beoordelaars. Om dit te voorkomen is de juiste kwantificering van een nieuw radiofarmacaon nodig. Dit vereist kinetische modellering met behulp van een dynamische PET-scan vanaf injectie van de tracer, in combinatie met arteriële bloedafname (om informatie over de verdeling van het radiofarmacaon in een interesse gebied te verkrijgen en potentiële tracermetabolieten te meten). Voor een vereenvoudigde kinetische modellering is slechts een statische scan met enkele veneuze bloedmonsters tijdens de scan nodig.

Slechts een decennium na de succesvolle implementatie van PET met CT als geheel wordt de integratie van PET met magnetische resonantie beeldvorming (PET/MRI) geïntroduceerd als de volgende hybride beeldvorming. Sterke punten van MRI zijn onder meer het betere wekedelen contrast, hoge ruimtelijke resolutie, en het ontbreken van blootstelling aan ioniserende straling. Verschillende hybride PET/MRI-systemen zijn beschikbaar: een geïntegreerd systeem met beide componenten in één frame, of een gescheiden PET en MRI component aan weerszijden van een draaibare tafel. De eerste heeft het voordeel van echt simultane beeldacquisitie, maar de laatste doet geen concessie aan de beeldkwaliteit van een van beide componenten (PET of MRI) en is uitgerust met TOF. Huidige klinische toepassingen met PET/MRI staan nog in de kinderschoenen.

RADIOACTIEF GELABELD CHOLINE

De implementatie van efficiënte PET hard- en software in combinatie met de vooruitgang in de moleculaire biologie van het prostaatkarkoom, biedt mogelijkheden voor de ontwikkeling van nieuwe beeldvormende biomarkers en veelbelovende radiotracers. Voor multimodale beeldvorming (zoals PET/CT, PET/MRI) zijn meerdere radiofarmaca beschikbaar om fysiologische en metabole routes waar te nemen en te kwantificeren. De meest gebruikte oncologische PET tracer, [¹⁸F]fluorodeoxyglucose ([¹⁸F]FDG), heeft een beperkte sensitiviteit voor de detectie van het androgeen afhankelijke prostaatkarkoom.

In tegenstelling tot [¹⁸F]FDG, worden bemoedigende resultaten gemeld bij het gebruik van ¹¹C en ¹⁸F gelabeld choline als PET-tracers voor het prostaatkarkoom.

Het aminozuur choline is een belangrijke voorloper voor de biosynthese van fosfatidylcholine, een essentieel bestanddeel van de celmembraanfosfolipiden. Na transport in de cel, wordt choline gefosforyleerd door cholinekinase tot fosfocholine en opgesloten binnen de cel. De meeste soorten kanker, waaronder ook prostaatkanker, worden gekenmerkt door een verhoogd cholinetransport en over-expressie van cholinekinase, als reactie op een verhoogde vraag naar fosfatidylcholine in sterk prolifererende cellen.

Omdat de opname van [¹⁸F]fluoromethylcholine ([¹⁸F]FCH) in normaal, hyperplastisch (nog wel goedaardig) dan wel kwaadaardig prostaatweefsel overlapt, zijn er gemengde resultaten met betrekking tot de potentiële bruikbaarheid van deze tracer in de diagnose en stadiëring van een primair prostaatkarkoom. Momenteel wordt [¹⁸F]FCH vooral gebruikt voor restadiëring van het prostaatkarkoom bij een (biochemische) terugval, met een diagnostische waarde die lijkt te verbeteren bij een toenemende prostaat-specifiek antigen (PSA) waarde. Het gebruik van [¹⁸F]FCH PET/CT in de praktijk wordt niet aanbevolen bij een PSA niveau lager dan 1 ng/mL.

Als de opname van radioactief gelabeld choline vitaal tumorweefsel weergeeft, kan uit de veranderingen van het cholinesignaal in de tijd, de mate van respons op de therapie bepaald worden. Voor het meten van respons op systemische behandeling bij uitgezaaide prostaatkanker is kwantificatie nodig. Tot op heden is de [¹⁸F]FCH biodistributie en stralingsdosimetrie bestudeerd, maar een volledige kinetische analyse is nog niet gerapporteerd.

RESPONS EVALUATIE EN VOORSPELLING IN PROSTAATKANKER

De respons op (chemo)therapeutische regimes is bij elke prostaatkankerpatiënt anders. Het is daarom belangrijk om de (in)efficiëntie van de therapie te monitoren. Zo wordt voorkomen dat patiënten een nutteloze en dure behandeling te lang ondergaan. Alternatieve en mogelijk effectieve geneesmiddelen zijn beschikbaar. Momenteel wordt de monitoring van de voortgang gedaan met een combinatie van onderzoeken, waaronder een PSA-meting, een CT en een botscan. De beperkingen van de huidige aanpak zijn gerelateerd aan de heterogeniteit van het uitgezaaide prostaatcarcinoom (bijv. co-existentie van androgeen gevoelige en ongevoelige delen, met elk verschillende effecten op bijvoorbeeld het PSA) en het feit dat de ziekte meestal vooral ossaal gemitastaseerd is (waarbij het lastig is op bot- en CT-scans de respons op therapie tijdig en nauwkeurig waar te nemen). Daarom is er behoefte aan alternatieve en nauwkeurigere methoden om de respons op therapie te evalueren.

Met elk nieuw radiofarmacon is het de uitdaging om betrouwbare vereenvoudigde kwantitatieve methoden in te voeren, die in de dagelijkse klinische praktijk en op het hele lichaam toegepast kunnen worden. Of $[^{18}\text{F}]\text{FCH}$ ook kan worden gebruikt bij het monitoren van de respons op de behandeling van prostaatkankerpatiënten die behandeld worden met docetaxel of cabazitaxel, is onduidelijk. Definitieve gegevens uit klinische studies zijn nog niet beschikbaar. Desalniettemin tonen in-vitro experimenten veelbelovende resultaten voor het gebruik van PET-tracers bij patiënten die een hormonale (anti-androgeen) of chemotherapeutische behandeling krijgen.

Samengevat is PET-beeldvorming een veelbelovende aanpak, zowel in klinische als in wetenschappelijke toepassingen. PET maakt kwantitatieve metingen met een hoge sensitiviteit mogelijk. Het verschaft non-invasieve informatie over biologische processen in het lichaam. Standaard methoden van PET-kwantificering zijn moeilijk te implementeren in de dagelijkse klinische praktijk. Vereenvoudigde methoden voor kwantificering zijn beschikbaar, maar moeten worden gevalideerd ten opzichte van de standaardmethoden. Om biologische verandering van ruis te onderscheiden, moet informatie over de herhaalbaarheid van een scan met een tracer bekend zijn.

Door de toename van gebruik van $[^{18}\text{F}]\text{FCH}$ PET bij het prostaatcarcinoom zijn klinisch haalbare protocollen, op basis van betrouwbare en herhaalbare indices voor

tumoractiviteit, essentieel voor het monitoren van respons op de therapie. Complexe kwantitatieve analysemethoden worden waarschijnlijk overal in klinische setting beschikbaar. Dit vergroot het potentieel van de radioactief gemerkte choline PET bij de “op maat” behandeling, door een tijdige evaluatie van de effectiviteit van de therapie. Hierdoor worden ineffektieve, dure of risicovolle behandelingen vermeden.

INHOUD VAN DEZE THESIS

Het doel van dit proefschrift was het technisch valideren van $[^{18}\text{F}]$ FCH als eerste stap op weg naar een door beeldvorming geleide, geïndividualiseerde therapie voor het gemitastaseerd prostaatkanker.

In **hoofdstuk twee** bestuderen we de diagnostische rol van twee-fase $[^{18}\text{F}]$ FCH PET/CT in een klinische setting. Hiervoor hebben we onderzocht of de tijd-trends van de intensiteit van choline opname in de lymfklieren van prostaatkankerpatiënten kunnen helpen om onderscheid te maken tussen goede (reactieve) en kwaadaardige klieren, en of een enkel tijdstip meting met behulp van standardized uptake value (de zo genoemde SUV), ook kan volstaan.

In **hoofdstuk drie** bestuderen we een alternatieve toepassing van $[^{18}\text{F}]$ FCH in uitgezaaid prostaatkanker. In deze context is onderzocht of opname van $[^{18}\text{F}]$ FCH, vergeleken met $[^{18}\text{F}]$ FDG, de chemotherapiewerking op tumorcel niveau in prostaatkanker accuraat weergeeft.

In **hoofdstuk vier** onderzoeken we hoe de opname van $[^{18}\text{F}]$ FCH betrouwbaar kan worden gemeten in een klinische setting. Hiervoor worden farmacokinetische modellen van dynamische PET-data in combinatie met arterieel bloed sampling gebruikt om het correcte compartiment model voor $[^{18}\text{F}]$ FCH te bepalen. Aanvullend, is de geldigheid van het gebruik van vereenvoudigde werkwijzen voor het kwantificeren van $[^{18}\text{F}]$ FCH bepaald.

In **hoofdstuk vijf** onderzoeken we of de vereenvoudigde methoden voor het meten van $[^{18}\text{F}]$ FCH opname, zoals voorgesteld in hoofdstuk vier, herhaalbaar zijn in de dagelijkse praktijk. Hiervoor onderzoeken we de herhaalbaarheid van verschillende kwantitatieve $[^{18}\text{F}]$ FCH parameters, waaronder het metabole tumorvolume en de totale laesie cholineopname.

In **hoofdstuk zes** voeren we een klinische en technische validatie uit van $[^{18}\text{F}]$ FCH in prostaatkanker. Daarvoor vergelijken we beeldkwaliteit en kwantitatieve nauwkeurigheid van PET/MRI en PET/CT-systemen met identieke TF PET frames, met

behulp van fantomen en klinische studies. De fantoom experimenten zijn gebaseerd op onderzoek naar de kalibratie nauwkeurigheid, beeld uniformiteit, en SUV herstel van de hybride systemen. Bij de klinische studies is de mate van [¹⁸F]FCH opname geanalyseerd, in zowel gezonde weefsels als pathologische tumoren.

In **hoofdstuk zeven** worden de resultaten in het algemeen beschreven en samengevat, en de perspectieven gegeven.

ACKNOWLEDGEMENTS

Promoveren is veel meer dan het schrijven van een proefschrift. Het is een lange, soms hobbelige weg, vol met leuke en leerzame ervaringen, maar vooral één met kleine geluksmomenten. Het fijne is dat ik op deze weg nooit alleen ben geweest. Steeds kwam ik mensen tegen die mij wilden helpen, begeleiden, nieuwe dingen lieten ontdekken, steunden en wilden bijstaan in moeilijke tijden of me leerden te genieten van het leven. Al deze bijzondere mensen ben ik vandaag mijn dank verschuldigd.

Allereerst wil ik de patiënten en hun naasten bedanken voor de motivatie en de wil om deel te nemen aan de nucleaire studies. Een laatste eer aan de patiënten die, helaas, niet meer tussen ons op deze aarde zijn. Van u heb ik geleerd wat altruïsme en liefde voor de medemens betekent.

Verder wil ik mijn promotoren bedanken. Prof. dr. O.S.H. Hoekstra, beste Otto, dank voor de gegeven kans om mijn carrière als nucleair geneeskundige in het VUmc te mogen starten en later promotieonderzoek onder je begeleiding te mogen doen. Jouw kennis, expertise, passie voor de wetenschap en vlotte gedachtegangen zijn een enorme bron van inspiratie voor mij. Als geen ander kan jij uit het hoofd refereren naar een artikel met naam van de auteur, blad, jaar en volume nummer. Ik hoop nog veel artikelen samen te mogen schrijven, al ben ik ook tevreden met een impact factor onder de 14.

Prof. dr. R.J.A. van Moorselaar, beste Jeroen, bedankt voor je begeleiding en de klinische blik op het geheel. Jouw enthousiasme, hart voor kliniek, kennis over de laatste ontwikkelingen op urologisch gebied en altijd positieve insteek waardeerde ik enorm. Jij bent een van de eerste choline “believers” die mijn werk als specialist en onderzoekster zo compleet heeft gemaakt. Op naar PSMA?

Beste leden van de leescommissie, Prof. dr. ir. J.J.M van der Hoeven, Prof. dr. I.J. de Jong, Dr. C.W. Menken-van der Houven van Oordt, Prof. dr. J.J.M.C.H de la Rosette, Prof. dr. P.L. Jager en Dr. W.V. Vogel, dank voor uw interesse, vertrouwen en tijd die u genomen heeft om dit proefschrift te beoordelen.

Een grote dank aan alle coauteurs van de artikelen verzameld in dit boekje.

Prof. dr. R. Boellaard, beste Ronald, dank voor het privilege om samen met je te mogen werken. Jouw expertise, bijzondere gave om als klinisch fysicus medisch te kunnen denken en schrijven, eindeloze wetenschappelijke ideeën, en vooral vriendelijke manier van zijn, maken onderzoek doen een feest. Ondanks de 183 km tussen het VUmc en UMCG hoop ik op een voorspoedige samenwerking ook in de toekomst.

Prof. dr. A.A. Lammertsma, beste Adriaan, bedankt voor alle hulp en begeleiding over de jaren. Als autoriteit op het gebied van farmacokinetiek, heeft u [¹⁸F]fluoromethylcholine een nieuw leven ingebracht wanneer een ieder sceptisch naar de analyse keek. Niets lijkt u onmogelijk, voor alles heeft u een wetenschappelijke oplossing (zelfs voor de “draak van de zinnen” die ik soms in het Engels kan bouwen). Bedankt!

Dr. A.J.M. van den Eertwagh, beste Fons, dank voor de prettige samenwerking gedurende het gehele promotietraject. Je klinische blik, uitgebreide kennis, scherpe vragen en hulp bij de inclusie van de studie patiënten waardeer ik zeer. Je deur stond altijd voor me open en gelukkig is de afstand van β A naar γ F niet zo groot.

Dr. A.A. Geldof, beste Ab, bedankt voor alle geduld en tijd om de “preklinische” wereld voor me te openen. Boeiend om alle cellijnen in het lab te incuberen, te zien groeien en vooral de aantallen te meten. Jouw expertise en interesse in de nucleaire geneeskunde maakt onze samenwerking sterk.

Dr. I.V. Bijnsdorp, beste Irene, wat ben ik blij om met zo’n gedreven en nauwkeurige onderzoeker te mogen werken. Ik ben je dankbaar voor alle hulp, goede ideeën en scherpe commentaar op ons preklinisch onderzoek. Op naar een nieuw samenwerkingsproject?

Prof. dr. W.R. Gerritsen, beste Winald, bedankt voor de eerste stappen op zoek naar een betrouwbare tracer voor de evaluatie van recidieven van prostaat carcinoom. U kwam altijd met het laatste nieuws van internationale Congressen en gaf me de kans om alle abstracts en “lectures” te screenen. Ondanks uw drukke agenda, lukte het u meestal de beroemde Professor Johann de Bono even te spreken.

Dr. ir. M. Yaqub, beste Maqsood, bedankt voor de fijne samenwerking. Dankzij jouw duidelijke uitleg, blijkt PET/MRI toch niet zo ingewikkeld te zijn als ik dacht.

Drs. M.P. van Kanten, beste Mitchell, dank voor al je hulp, inzet en intensieve werk op het lab. Zelfs op zondag kwam jij de cellijnen controleren om desnoods de experimenten te herhalen. Jij vindt onderzoek leuk en hebt talent hiervoor. Veel succes, het gaat je helemaal lukken.

Appendix

Dr. ir. P. van de Ven, beste Peter, bedankt voor alle hulp bij het schrijven van protocollen en het bedenken van de statistische analyses van onze studies. Wat fijn dat iemand de “ingewikkelde” vragen van de reviewers goed begreep om een duidelijk antwoord te kunnen formuleren.

Drs. G.M. Kramer, beste Gert, dank voor de uitstekende samenwerking. Met jouw kennis, motivatie, scherpe blik, serieuze aanpak, snelle en nauwkeurige manier van denken en doen heb je alle ingrediënten voor succes in huis. “Professor” Kramer het gaat u goed!

Dr. A.A. Vincent, dear Andrew, thank you very much for the nice collaboration. It was a real pleasure to work with you!

Dr. J. Eriksson, dear Jonas, thank you very much for your commitment and help with the production of [¹⁸F]fluoromethylcholine. Tack så mycket!

Prof. dr. A.D. Windhorst, beste Bert, dank voor de prettige samenwerking. Dankzij jou was de productie van [¹⁸F]fluoromethylcholine op alle mogelijke en onmogelijke momenten gereed voor de kliniek en research. Wat geeft dat een goed gevoel!

Prof. dr. N.H. Hendrikse, beste Harry, dank voor jouw deelname aan het team “de choline believers”, vanaf begin tot heden. Samen hebben wij de eerste publicaties over [¹⁸F]fluoromethylcholine doorgenomen, als basis voor een uitdagend onderzoeksproject. Jouw expertise op het gebied van radiofarmacie en interesse om nieuwe tracers voor de kliniek te ontdekken zijn oneindig.

Dr. Lothar Schwarte en dr. Patrick Schober dank voor jullie hulp bij het plaatsen van alle arterielijnen. Het onderzoek was mede door jullie “gouden handen” altijd goed begonnen.

Dr. I.C. Pieters, beste Indra, dank voor het privilege om met zo’n ervaren en dedicated MRI radioloog te mogen werken! Jij nam altijd de tijd om samen de PET/MRI beelden te beoordelen en was kritisch als de opnamen niet volgens het “optimalisatie protocol” verricht waren. Ik hoop je op radiologische congressen te ontmoeten en samen van een kopje “warm water” te mogen genieten.

Drs. R. Reinhard, beste Rinze, dank voor al je tijd die je in onze onderzoeken gestoken hebt. Jij was altijd bereid jouw kennis en expertise op het gebied van MRI prostaat met mij te delen. Wat is dit een mooi voorbeeld van integratie van de Radiologische en Nucleaire werelden!

Mijn dank aan dr. Eline Verwer, dr. Karin Nielsen, drs. Hester Scheffer, drs. Els Boerhout, drs. Aukje van Tilborg en BSc. Daan Noij voor het samen mogen schrijven van veel geciteerde wetenschappelijke publicaties.

Mijn dank aan alle collegae medisch specialisten van de afdeling Medische Oncologie van het VUmc die geholpen hebben met de inclusie van de studie patiënten en die altijd bereid waren om hun kennis en expertise met mij te delen: Prof. dr. Henk Verheul, dr. Jens Voortman, dr. Hans van der Vliet, dr. Marije Vleugel, drs. Liselot Wertenbroek, drs. Mariette Labots en drs. Maurice van der Vorst. Mijn dank gaat ook naar de medische oncologen in het Amstelland Ziekenhuis: dr. Kees van Groeningen en dr. Annette van Zweeden. Last but not least, beste Maartje Klaassen, dank voor alle hulp!

Ik ben mijn dank verschuldigd aan alle collegae en medewerkers van de Urologie afdeling van het VUmc, voor hun gezelligheid, goede adviezen en hulp over jaren. Dr. André Vis, dr. Jakko Nieuwenhuijzen, Jeanette Bossenga, Hoda Al-Itejawi, Yvonne Boom, Ronald Schuurman, bedankt! Een grote dank aan de collegae urologen in het Amstelland ziekenhuis, voor de prettige samenwerking en alle hulp bij de inclusie van de patiënten: dr. Joop Noordzij, dr. Cobi Reisman en dr. Sven Nadorp.

Mijn dank aan mijn opleider in het LUMC, dr. M.P.M. Stokkel. Beste Marcel, mede door jouw enthousiasme en passie voor het vak ben ik vandaag Nucleair geneeskundige. Bedankt voor het vertrouwen en de goede begeleiding over jaren.

Een grote dank aan mijn opleider Interne Geneeskunde in het “TweeSteden Ziekenhuis”, dr. Swan H. Goey, voor de stimulerende omgeving en prettige sfeer waarin ik werd opgeleid. De mooie tijd in Brabant zal ik nooit vergeten.

Drs. Constantin Dragoiescu, drs. Bernies van der Hiel, drs. Imad al Younis, drs. Daphne Rietbergen, drs. Ibrahim Al Butaihi, dr. Liesbeth Salm en alle ex-collegae van het LUMC, dank voor de leuke tijd in Leiden.

Veel collegae van de Afdeling Radiologie en Nucleaire geneeskunde van het VU Medisch Centrum ben ik een dank verschuldigd. Prof. dr. E.F.I. Comans, beste Emile, bedankt voor alles wat ik van je heb mogen leren. Jij bent geboren om professor te zijn en de passie voor PET met anderen te delen. Als geen ander durf jij op basis van de PET beelden het PA verslag in twijfel te brengen, en ja, bij de revisie blijkt er inderdaad een plaveicelcarcinoom te zijn. Dr. P.G. Rajmakers, beste Pieter, bedankt voor de kans om met je te mogen werken. Jij staat altijd klaar voor iedereen en bent bereid je uitgebreide kennis met je collegae te delen. Jij bent expert op elk gebied: van neuro tot cardio en van orthopedie en oncologie tot endocrinologie. Ik ben je dankbaar voor alle leerzame gespreken en goede adviezen! Drs. A van Schie, beste Annelies, bedankt voor alle hulp en tijd om de logistiek op onze afdeling altijd gereed te hebben. Jij bent een voorbeeld van een multitasking arts. Prof. dr. van Berckel, beste Bart, dank voor de fijne samenwerking over de jaren. Onder je leiding krijgt “de Wetenschap” een zeer verdiende plek en staat VUmc Research op het gebied van Alzheimer disease internationaal bekend!

Mijn dank aan alle hardwerkende artsen met wie ik in de loop der jaren de honneurs had om te mogen werken op de Nucleaire afdeling: dr. Ilse Rutten, drs. Nafees Rizvi, drs. Joris Tim, drs. Nils Wagenaar, drs. Mechteld Heijne, dr. Maartje van Rijk, drs. Human Adams, drs. Jim Janssen, drs. Rachel Hezemans, dr. Cristina Mitea, dr. Nelleke Tolboom, dr. Daniëlle van Assema, drs. Benhai Vuong, drs. Erwann Letort en drs. Ben Zwezerijnen. Het is nooit te laat om samen een “werkbezoek” in Italië te plannen om van een “nuclear weekend” in Bologna te genieten.

Al mijn collegae radiologen van de gefuseerde afdeling Radiologie en Nucleaire geneeskunde VUmc wil ik graag bedanken voor de prettige samenwerking, voor hun inzet en expertise. Prof. dr. Kees van Kuijk, dr. Jan Hein van Waesberghe, drs. Ferco Berger, prof. dr. Frederik Barkhof, prof. dr. Jonas Castelijns, dr. Martijn Meijerink, drs. Nazanin Ahmadi, dr. Lilian Meijboom, dr. Joost Bot, dr. Liesbeth Bergers, drs. Janneke vd Bergh, dr. Pim de Graaf, drs. Rutger Lely, drs. Bram vd Meijjs, drs. Esther Sanchez, drs. Cors van Schaik, drs. Jonathan Verbeke, dr. Mike Wattjes en drs. Jan-Paul Klein, bedankt!

Een grote dank aan de physician assistants, alle medisch nucleaire workers en medewerkers van de medische administratie die mij gedurende de jaren geholpen hebben met de logistiek rondom het plannen, verrichten en krijgen van top kwaliteit scans! Esther Bakker, Patricia McCarthy, Saskia Cornelje, Judith van Es, Amina

Elouahmani, Annemiek Stiekema, Femke Jongsma, Elchien Holl, Nasserah Sais, Patty Hudepohl, Robin Hemminga, Nghi Pham, Brendan Irik, Jeroen Wilhelmus, Richard Versteegh, Carmelita Burleson, Kitty Mascini, Tamara Kraal, Claudia Axinia, Marjoke Visser en Vincent Roos, hartelijk dank!

Mijn dank aan Robert Schuit, Henri Greuter, Marissa Rongen en Kevin Takkenkamp voor de prettige samenwerking en de nauwkeurige analyse van de bloed samples. Zonder jullie hulp was [¹⁸F]fluoromethylcholine een onbekende tracer gebleven. Beste Ellie Kemper, bedankt voor je hulp en flexibiliteit op het lab. Beste Henri, alvast bedankt voor de mooie foto's!

De fysici van de afdeling Radiologie en Nucleaire geneeskunde: dr. ir. Arthur van Lingen, dr. ir. Marc Huisman, dr. ir. Floris van Velden, dr. Hans Harms, dr. ir. Mette Stam en Msc. Manfred van der Veld, bedankt voor jullie expertise, alle technische hulp en vooral voor de vele gezellige momenten op 1F.

Beste Cemile Karga, Paul Horstman en Emma Mulder dank voor alle hulp bij de implementatie van de studie protocollen en het uitwerken van de klinische data/ scans. Beste Coreline Burggraaff en Antoinette de Jong dank voor jullie positiviteit en prettige sfeer op 1F.

Mijn dank aan alle specialisten en geweldige medewerkers van de afdelingen Radiologie, Interne geneeskunde, Cardiologie, Chirurgie, Kindergeneeskunde, Longziekten, Neurologie, Oncologie en Orthopedie van het Amstelland ziekenhuis te Amstelveen, met wie ik de privilege heb om te mogen werken.

Een speciale dank aan mijn lieve collegae en ex-kamer/ vleugel genoten: Astrid van der Veldt, Yvonne Jauw en Virginie Frings. Bedankt voor alles wat ik van jullie heb mogen leren, alle steun en voor de gezellige momenten samen. My dears, ik ben zeer trots op jullie!

Het werk als nuclear geneeskundige is veel leuker als de samenwerking met collegae medisch specialisten voorspoedig is. Beste dr. Josée Zijlstra, Prof. dr. Sonja Zweegman, dr. Mariëlle Wondergem, dr. Eveline van Dam, dr. Marelise Eekhoff, dr. Monique van den Tol, bedankt!

Mijn dank aan alle dames op het Secretariaat Radiologie en Nucleaire geneeskunde. Beste Amanda Kroonenberg, zonder je hulp was mijn boekje misschien niet “op tijd” af, maar zeker nooit op het goede adres aangekomen. Je luisterende oor en goede adviezen aan een niet “ervaren” moeder-promovenda hebben mij enorm geholpen. Bedankt! Beste Angelique Mathilda, Caroline Hilferink, Greet Stolker, Letty Drop en Sandra Eliazer, dank voor alle hulp, jullie gezelligheid en spoedige oplossing van alle personeels-gerelateerde zaken.

Veel vrienden en vriendinnen wil ik vandaag bedanken. Lieve Sandra Srbljin, onze vriendschap is begonnen op een nefrologie cursus en is in de loop der jaren mede door de passie voor het vak alleen maar sterker geworden. Jij bent een succesvolle vrouw op alle fronten. Ik heb veel bewondering voor je. Dank voor alle goede adviezen en hulp, nu en in de toekomst.

Lieve Dora Jurisa, 15 jaar geleden zaten wij samen op een cursus Nederlands voor buitenlandse artsen. Sindsdien zij wij vriendinnen geworden en delen wij de passie voor geneeskunde, kunst en culinair genieten. Dank voor alle bijzondere momenten samen.

Lieve Annelies van Dijk en prof. dr. Adrianus de Hoop, bedankt voor jullie vriendschap over de jaren. Jullie steun en wijze lessen hebben onze familie sterker gemaakt.

Lieve Ans van Berkel en Geert Mur, bedankt voor alles wat jullie voor ons betekenen!

Lieve Mimi Tissen en Henk Bonzet, dank voor jullie vriendschap en gastvrijheid. Mimi bedankt voor alle Nederlandse en klinische lessen!

Lieve Emma en Frank Dessens dank voor alle gezellige momenten samen, in Roemenië of thuis in Nederland.

Dear Ute and Paul Hubbes, you have a special place in our heart. Thank you very much for your kindness and friendship! Dear Paul we are very proud to have such a talented future doctor as you in our “family”.

Een grote dank aan mijn lieve paranimfen. Beste Joyce van Dodewaard en Katya Duvivier, bedankt dat jullie op deze bijzondere dag naast mij willen staan. Met twee

sterke vrouwen, gemotiveerde en gepassioneerde medisch specialisten, zoals jullie, voel ik me echt gelukkig.

Mijn dank gaat ook uit naar alle Roemeense kennissen en vrienden uit de Parochie "Sfantul Grigore Teologul" te Schiedam. Parinte dr. Ioan Dura si D-na Presbitera Christina, va multumesc pentru tot ajutorul si sfatul bun.

Lieve Alina Nicolaie, Ana en Olivia Trutescu, ik ben dankbaar dat ik jullie heb mogen ontmoeten. Dank voor alles! (Draga Alina, Ana si Olivia, va multumesc pentru ca existati si pentru ca am avut bucuria sa va intalnesc). Lieve Monica Gomescu, Anca Georgescu, Cristina Bejnariu, Carmen Bolchi, Delia van Rij en Isa Tomescu dank voor jullie vriendschap! (Draga Moni, Anca, Cristina, Carmen, Delia si Isa, va multumesc pentru prietenia voastra). Lieve Dorina Branzei, bedankt voor alles. Jij hebt een bijzondere plek in ons hart en in onze familie. (Draga Dorina, iti multumim pentru tot. Tu ai rezervat un loc special in inima si in familia noastră).

Dear Sibel, Aksu en Urfi Omer thank you for your friendship and all the moments together. I am very proud of you. Dear Sadie Ilse, thank you for all the wise lessons about life. Just keep on smiling, from the heaven where you are.

Lieve Schoonfamilie dank voor alle liefde en goede zorg voor Christian. (Draga fam. Lagersi fam. Zimnicaru, va multumesc pentru toata grijă si dragostea pentru Christian).

Lieve familie in Roemenië, dank voor jullie steun en belangstelling. (Scumpa mea familie din Romania, multumesc pentru cinstea de a-mi fi alaturi. Draga Miri, Cami si Ioana, va multumesc pentru sprijin, incredere si pentru dragostea voastra neconditionata).

Lieve Mama en Papa, zonder jullie was ik hier niet, letterlijk en figuurlijk. Ik ben God en jullie dankbaar voor het geschenken leven, zorgeloze kindertijd, goede opvoeding en mooie jaren thuis. Bedankt voor jullie steun, vertrouwen en eindeloze liefde. Wat ben ik een gelukkig mens met jullie daarbij! (Draga mama si tata, fara voi nu m-as fi aflat astazi aici, atat la propriu cat si la figurat. Multumesc Domnului si voua ca parinti pentru viata pe care mi-ati daruit-o, pentru copilaria fara griji, pentru educatie si pentru frumosii ani petrecuti acasa. Va multumesc pentru ajutor, incredere si nemarginata dragoste. Cat de fericita sunt alaturi de voi!).

Lieve Hansi, mijn man, mijn vriend, mijn privé professor, mijn ingenieur, mijn chauffeur, mijn kok, mijn tuinman, mijn designer, mijn lopende encyclopedie, mijn steun, maar vooral mijn liefde, bedankt! Ik ben je dankbaar voor alle mooie momenten in mijn leven. Te iubesc mult!

Lieve Christian, mijn schat, bedankt dat jij mijn leven compleet hebt gemaakt! Jij bent en blijft een geschenk van God. Kom, laten wij gaan spelen en genieten van het mooie leven!

CURRICULUM VITAE



Daniela-Elena Oprea was born in Brasov, Romania. In 1994 she obtained her High-school diploma at the "Constantin D. Nenitescu" Gymnasium in Brasov. After 6 years of studying Medicine, she obtained in 2000 her Medical Doctor degree from the University of Medicine and Pharmacy Targu-Mures, Romania. Following her heart, in 2001 she moved to the Netherlands. In 2002 she was admitted at the Faculty of Medicine of the Leiden University Medical Center, where she graduated for the second time in December 2004.

She began her specialization in Nuclear Medicine at the Leiden University Medical Center in May 2005, under the supervision of Marcel P. M. Stokkel, MD, PhD. During her specialization she undertook a 1-year placement with the Department of Internal Medicine of "TweeSteden Hospital" in Tilburg, under the supervision of Swan H. Goey, MD, PhD. She completed her specialization in April 2009.

Starting June 2009 she continued her career as Nuclear Medicine physician at the Department of Radiology and Nuclear Medicine of the VU University Medical Center, firstly as a Fellow and, subsequently, from June 2013, as a staff member. This department offered her the optimal environment for pursuing her scientific ambitions through a PhD research on the technical validation of [¹⁸F]fluoromethylcholine PET as a tool towards personalized therapy for metastatic prostate cancer. She undertook this research under the supervision of Professor Otto S. Hoekstra, MD, PhD and Professor Reindert J. A. van Moorselaar, MD, PhD, starting from January 2011.

Her research interests concentrate on the early detection of (recurrent) prostate cancer, implementation of new oncological tracers in clinical practice and monitoring treatment effects in prostate cancer. In this frame, she played a conducive role in the granting of "A study on the pharmacokinetics and repeatability of [¹⁸F]Fluoromethylcholine PET/CT in patients with prostate cancer" project in which she also had a major personal involvement.

She authored 12 Journal publications, as detailed in the Publication list enclosed with this dissertation. Daniela is a member of the European Association of Nuclear Medicine,

the Dutch Association of Nuclear Medicine, the European Society of Radiology, the European Society of Urogenital Radiology and the European Society of Oncologic Imaging.

Her prime ambition is to harmoniously combine patient care, scientific research and transferring her expertise to future doctors. Daniela is happily married to Hansi and they are the proud parents of Christian.

LIST OF PUBLICATIONS

Oprea-Lager DE, Kramer G, van de Ven PM, van den Eertwegh AJ, van Moorselaar RJ, Schober P, Hoekstra OS, Lammertsma AA, Boellaard R. Repeatability of quantitative [¹⁸F]fluoromethylcholine PET/CT studies in prostate cancer. Manuscript accepted for publication in *J Nucl Med*

van Dodewaard-de Jong JM, **Oprea-Lager DE**, Hooft L, de Klerk, JMH, Verheul HMW, Hoekstra OS and van den Eertwegh AJM. Radiopharmaceuticals for palliation of bone pain in patients with castration-resistant prostate cancer metastatic to bone; a systematic review. *European Urology*. 2015 In press doi:10.1016/j.euro.2015.09.005

Oprea-Lager DE, Yaqub M, Pieters IC, Reinhard R, van Moorselaar RJ, van den Eertwegh AJ, Hoekstra OS, Lammertsma AA, Boellaard R. A Clinical and Experimental Comparison of Time of Flight PET/MRI and PET/CT Systems. *Mol Imaging Biol*. 2015;17(3):714–725

Verwer EE, **Oprea-Lager DE**, van den Eertwegh AJ, van Moorselaar RJ, Windhorst AD, Schwarte LA, Hendrikse NH, Schuit RC, Hoekstra OS, Lammertsma AA, Boellaard R. Quantification of ¹⁸F-fluorocholine kinetics in patients with prostate cancer. *J Nucl Med*. 2015;56(3):365–371

Oprea-Lager DE, van Kanten MP, van Moorselaar RJ, van den Eertwegh AJ, van de Ven PM, Bijnsdorp IV, Hoekstra OS, Geldof AA. [¹⁸F]fluoromethylcholine as a chemotherapy response read-out in prostate cancer cells. *Mol Imaging Biol*. 2015;17(3):319–327

Nielsen K, Scheffer HJ, Pieters IC, van Tilborg AA, van Waesberghe JH, **Oprea-Lager DE**, Meijerink MR, Kazemier G, Hoekstra OS, Schreurs HW, Sietses C, Meijer S, Comans EF, van den Tol PM. The use of PET-MRI in the follow-up after radiofrequency- and microwave ablation of colorectal liver metastases. *BMC Med Imaging*. 2014;14:27;doi: 10.1186/1471-2342-14-27

Noij DP, Boerhout EJ, Pieters-van den Bos IC, Comans EF, **Oprea-Lager DE**, Reinhard R, Hoekstra OS, de Bree R, de Graaf P, Castelijns JA. Whole-body-MR imaging including DWIBS in the work-up of patients with head and neck squamous cell carcinoma: a feasibility study. *Eur J Radiol*. 2014;83(7):1144–1151

Oprea-Lager DE, Löfgren J, Raijmakers PG, Law I, van Berckel, van der Laken CJ, Pieters-van den Bos IC, and Kjaer A. Towards multiparametric medical imaging with PET/MRI: current clinical status. *Tijdschr v Nucl Geneesk* 2013;35(4):1160–1171

Yaqub M, **Oprea-Lager DE**, Hofman M and Boellaard R. Methodological aspects of PET/MR imaging. *Tijdschr v Nucl Geneesk* 2013;35(4):1153–1159

Oprea-Lager DE, Bijnsdorp IV, van Moorselaar RJ, van den Eertwegh AJ, Hoekstra OS, Geldof AA. ABCG4 Decreases docetaxel and not cabazitaxel efficacy in prostate cancer cells in vitro. *Anticancer Res*. 2013;33(2):387–391

Oprea-Lager DE, Vincent AD, van Moorselaar RJ, Gerritsen WR, van den Eertwegh AJ, Eriksson J, Boellaard R, Hoekstra OS. Dual-phase PET-CT to differentiate [¹⁸F]Fluoromethylcholine uptake in reactive and malignant lymph nodes in patients with prostate cancer. *PLoS One*. 2012;7(10):e48430

Slot S, **Oprea-Lager DE** and Wondergem MJ. De kunst van het kijken. Uw diagnose? *Ned Tijdschr Hematol* 2012;9: 84–85

Oprea-Lager DE, Sorgdrager BJ, Jukema JW, Scherpertong RW, Ringers J, Coenraad MJ, van Hoek B, Stokkel MP. Clinical value of myocardial perfusion scintigraphy as a screening tool in liver transplant candidates. *Liver Transpl*. 2011;17(3):261–269

